



UNIVERSITY OF TWENTE.

# $\mu$ flow

---

A compact fluorescence detection system that uses a DVD pickup for the optical detection of beads

Maarten Jan Koster

S0112410

Master thesis

May 11, 2011

Electrical Engineering (EEMCS)

BIOS, Lab on a Chip group

Enschede, the Netherlands

**Examination committee:**

Loes Segerink MSc

Dr.ir. Ad Sprenkels

Prof. dr. ir. Albert van den Berg

Prof. dr. ir. Ton van Leeuwen (extern member)

**Document number**

BIOS 03-2011



## **Abstract**

The fertility project started at BIOS, Lab on a Chip group, in 2007, aims at developing a high accuracy point of care semen analyzer that can be used at home, making the semen analysis more comfortable, easier, and cheaper. During a semen analysis the semen quality is to be determined by concentration, motility, morphology and vitality/viability of the sperm cells. At present the concentration and motility can be determined with a microfluidic chip using electrical conductivity measurements. To measure the remaining parameters, new detection methods may be developed and the first results thereof are described in this thesis.

In this thesis, the use of fluorescence detection is described. Using a 'Lab on a Chip' and an optical pickup taken from a DVD player, a fluorescence detection apparatus, the 'μflow' has been designed and built. The optical pickup has a lot of integrated optical components that makes a compact, easy to use and cheap fluorescence detection system possible. A 'Lab on a Chip' consisting of three microfluidic channels and digital marks for position detection has been developed. Automatic guiding the optical pickup to find the three channels was successfully shown using –on chip- digital marks and an automatic focus system. The μflow fluorescence detection capabilities were tested using 6 μm and 2.5 μm fluorescent beads and real-time 2D visualisation of the beads in Labview was demonstrated. Beads were counted and the size, speed, transversal and vertical position of the individual beads in the fluidic channel were determined. The optical resolution is limited by the spot size of the laser and therefore only particles larger than 0.4 μm could be visualized. No experiments were performed using spermatozoa, but it is very likely that spermatozoa can be visualized with the same resolution as beads. If this succeeds for spermatozoa, the μflow would be able to determine the concentration and morphology parameters of the sperm cells (vitality/viability can be assessed using fluorescent dyes). The μflow was built in such a way that in a future project it may also be used for analyzing other biological relevant fluids such as blood.



## Samenvatting

In 2007 is bij BIOS, Lab on a Chip groep, een vruchtbaarheidsproject gestart. Het doel van dit project is het ontwikkelen van een sperma analyse apparaat voor thuisgebruik dat een sperma analyse nauwkeurig, comfortabel en goedkoop kan uitvoeren. Tijdens een analyse moet worden gekeken naar de concentratie, bewegelijkheid, vorm en vitaliteit van de sperma cellen. Momenteel kan de concentratie en beweeglijkheid worden gemeten door middel van een elektrische geleidbaarheids-meting in een microfluidische chip. Voor het meten van de overige parameters kunnen andere detectiemethodes mogelijk uitkomst bieden.

In deze masteropdracht wordt een fluorescentie detectiemethode beschreven. Met behulp van een 'Lab on a Chip' en een optische pickup uit een dvd-speler is een fluorescentie detectie apparaat genaamd ' $\mu$ flow' ontworpen en gebouwd. Een Lab on a Chip bestaande uit drie microfluidische kanalen en digitale markeringen voor positiebepaling is hiervoor ontwikkeld. Omdat de pickup uit vele geïntegreerde optische onderdelen bestaat, is het mogelijk om een compact en goedkoop apparaat te ontwikkelen. Automatische sturing van de pickup zorgt voor een autonome herkenning van de drie kanalen door middel van digitale markeringen en een automatisch focus systeem. Het fluorescentie detectie vermogen van de  $\mu$ flow is getest met behulp van 6  $\mu\text{m}$  en 2,5  $\mu\text{m}$  fluorescerende bolletjes. Deze bolletjes worden in twee dimensies zichtbaar gemaakt in Labview. Het aantal bolletjes kan worden geteld, ook de snelheid, grootte en de verticale/transversale positie van de individuele bolletjes kan worden bepaald. De optische resolutie wordt beperkt door de puntgrootte van de laser, hierdoor kunnen alleen deeltjes groter dan 0,4  $\mu\text{m}$  weergegeven worden. Op dit moment zijn er nog geen experimenten uitgevoerd met sperma cellen, maar het is zeer waarschijnlijk dat sperma cellen met dezelfde nauwkeurigheid kunnen worden weergegeven als de bolletjes. Mocht dezelfde nauwkeurigheid behaald worden met sperma cellen dan zou dit betekenen dat de concentratie en vorm van de sperma cellen gemeten kan worden, vitaliteit kan met behulp van fluorescerende markers zichtbaar gemaakt worden. De  $\mu$ flow is zodanig gebouwd dat in de toekomst ook andere biologisch relevante vloeistoffen zoals bloed geanalyseerd kunnen worden.



# Contents

<b>ABSTRACT .....</b>	<b>3</b>
<b>SAMENVATTING.....</b>	<b>5</b>
<b>TERMINOLOGY.....</b>	<b>9</b>
<b>1 INTRODUCTION.....</b>	<b>11</b>
1.1 BACKGROUND.....	11
1.2 AIM OF THESIS .....	11
1.3 REPORT OUTLINE .....	12
<b>2 THEORY.....</b>	<b>15</b>
2.1 HUMAN SEMEN.....	15
2.1.1 Fertility .....	15
2.1.2 Semen analysis .....	15
2.2 FLUORESCENCE .....	16
2.2.1 Auto fluorescence.....	17
2.3 OPTICAL DETECTION OF PARTICLES AND CELLS INSIDE A MICROFLUIDIC CHANNEL.....	18
2.3.1 Light scattering and light blocking .....	18
2.3.2 Fluorescence.....	19
2.4 $\mu$ FLOW APPROACH .....	20
<b>3 OPTICAL PICKUP.....</b>	<b>21</b>
3.1 PHR-803T OPTICAL PICKUP .....	22
3.2 IDENTIFICATION OPTICAL PARTS .....	22
3.3 OBJECTIVE LENS.....	24
3.4 FOCAL LENGTH .....	25
3.5 RESOLUTION AND FOCAL DEPTH.....	25
3.6 GAUSSIAN BEAM .....	26
<b>4 FOCUS SYSTEM .....</b>	<b>27</b>
4.1 FOCUS DISTANCE MEASUREMENT.....	27
4.2 MOVING LENS.....	28
4.3 PID CONTROL .....	29
4.4 MATLAB SIMULATION.....	30
4.5 MICROCONTROLLER FOCUS CONTROLLER.....	30
<b>5 FLUORESCENCE DETECTION .....</b>	<b>31</b>
5.1 SETUP .....	31
5.2 FLUORESCIN.....	32
5.2.1 Fluorescence power.....	32
5.3 BEADS .....	33
5.4 DYES.....	34
5.4.1 Viability indicator .....	34
5.4.2 Vitality indicator.....	34
5.5 PHOTO DETECTOR.....	35
5.5.1 Photodiode.....	35
5.5.2 Avalanche photodiode.....	35
5.5.3 Photomultiplier.....	36

5.5.4	Fluorescence detector .....	36
5.5.5	Photon detection .....	38
<b>6</b>	<b>FLUIDIC CHIP .....</b>	<b>39</b>
6.1	CHANNEL FINDING .....	40
6.1.1	Digital marks .....	41
6.2	IMPEDANCE SPECTROSCOPY .....	43
<b>7</b>	<b>SOFTWARE.....</b>	<b>45</b>
7.1	LABVIEW GUI .....	45
7.2	MICROCONTROLLER .....	47
7.2.1	Main .....	47
<b>8</b>	<b>ELECTRONICS .....</b>	<b>49</b>
8.1	PDIC .....	49
8.2	VCA DRIVER .....	50
8.3	MICROCONTROLLER AND DAC .....	52
8.4	SLIDE CONTROL .....	52
8.5	MPPC .....	52
8.6	IMPEDANCE SPECTROSCOPY .....	54
<b>9</b>	<b>FUNCTIONAL TESTS.....</b>	<b>55</b>
9.1	ILLUMINATION POWER.....	55
9.2	VOICE COIL ACTUATOR (VCA) .....	55
9.3	PDIC .....	58
<b>10</b>	<b>RESULTS/DISCUSSION .....</b>	<b>59</b>
10.1	FIND CHANNEL .....	59
10.1.1	PDIC-response .....	59
10.1.2	Focus profile.....	61
10.1.3	Channel finding .....	62
10.2	DARK NOISE, ENVIRONMENTAL- AND LEAKING LIGHT.....	64
10.3	BEADS .....	66
10.3.1	Non fluorescent beads .....	69
10.3.2	Fluorescence absorbtion .....	70
10.3.3	Maximum flow speed.....	70
<b>11</b>	<b>CONCLUSION/RECOMMENDATIONS.....</b>	<b>71</b>
11.1	CONCLUSION .....	71
11.2	RECOMMENDATIONS.....	71
	<b>REFERENCES .....</b>	<b>73</b>
	<b>APPENDIX 1 SCHEMATICS.....</b>	<b>76</b>
	<b>APPENDIX 2 PCB'S .....</b>	<b>77</b>
	<b>APPENDIX 3 MECHANICAL DRAWINGS.....</b>	<b>78</b>
	<b>APPENDIX 4 MICROCONTROLLER FLOWCHARTS .....</b>	<b>81</b>
	<b>APPENDIX 5 WIRING .....</b>	<b>89</b>

## Terminology

### *List of Acronyms:*

ADC = Analog to Digital Converter  
AM = Acetoxymethyl  
APD= Avalanche Photodiode  
BD = Blu-ray Disc  
CASA =Computer Assisted Semen Analysis  
CCD = Charge-Coupled Device  
CD = Compact Disc  
DAC = Digital to Analog Converter  
DAQ= Data Acquisition card  
DDS = Direct Digital Synthesis  
DOF = Depth Of Focus  
DVD = Digital Versatile Disc  
FES = Focus Error Signal  
GUI = Graphical User Interface  
HD-DVD = High-Definition/Density DVD  
kcps = kilo counts per seconds  
LASER = Light Amplification by Stimulated Emission of Radiation  
MPPC = Multi Pixel Photon Counter  
NA = Numerical Aperture  
OEM = Original Equipment Manufacturer  
Op-amp = Operational amplifier  
PCB = Printed Circuit Board  
PDE = Photon Detection Efficiency  
PDIC = Position Detector Integrated Circuit  
p.e. = photon energy  
PID = Proportional-Integral-Derivative  
PMT = Photomultiplier Tube  
PN = P-type and N-type  
RFN = negative FES:  $-(A + B+ C+D)$   
RFP = positive FES:  $A + B+ C+D$   
SNR = Signal to Noise Ratio  
SP = Set Point  
USART = Universal Asynchronous Receiver/Transmitter  
VCA = Voice Coil Actuator

### *List of abbreviations:*

$K_d$  = differential gain  
 $K_i$  = integral gain  
 $K_p$  = proportional gain  
 $\mu$ flow = Microflow

### *Constants:*

$h = 6.63 \times 10^{-34}$  [m<sup>2</sup> kg / s] (Planck constant)  
 $v = 3.00 \times 10^8$  [m / s] (speed of light)



# 1 Introduction

## 1.1 Background

Each year, one out of ten couples in the Netherlands remains involuntarily childless [R.J.Raterink 2008]. To find out what the problem is, several tests have to be performed. Often, one of the first tests is determining the fertility of the man by analyzing his semen. This test is relatively easy to perform and non invasive but is accompanied with some difficulties. The man needs to collect semen and bring this within one hour to the hospital. The semen is directly analyzed to determine the quality. Because of large variations between samples this test has to be repeated at least three times, resulting in three visits to the hospital [Segerink 2010]. To make this semen analysis more comfortable, reliable and easier, the test would have to take place in the patient's home environment. This would require a point of care semen analyzer for home use that allows cheap tests with a low variation. For the realization of such an analyzer, the fertility project has been started at BIOS, Lab on a Chip group in 2007. In Segerink [2010] this was achieved by passing spermatozoa through a microchannel with a planar electrode pair that allows the detection of spermatozoa using electrical impedance measurements. It was shown that the change in electrical impedance was related to the size of cells passing the electrodes. This allows distinguishing between spermatozoa and other cells. The concentration of spermatozoa was determined using electrical impedance measurements in combination with a known concentration of beads.

The concentration parameter can now be determined using a Lab on a Chip. However, for reliable sperm quality measurements motility, morphology and vitality/viability of the sperm cells should be taken into account. Most of these parameters can be determined using fluorescent dyes and a thoroughly analysis using a fluorescence microscope. But no automated solution for Lab on a Chip devices reported yet.

## 1.2 Aim of thesis

In this thesis a measurement system for fluorescence detection for Lab on a Chip devices will be developed. A device will be made that can perform fluorescence measurements on a Lab on a Chip device for the characterisation of beads. This device will eventually be used in a point of care semen analyzer and therefore it has to be easy to use, small, cheap and able to carry out quick measurements. The targets of the  $\mu$ flow (Microflow) are:

- Automatic positioning system for finding the on-chip microfluidic channels
- Counting cells/beads
- Position detection of cells/beads inside the microfluidic channel
- Distinguish bead/cell size
- Visualize the morphology of cells/beads
- Asses viability/vitality of cells by using fluorescent dyes
- Combined fluorescence and impedance measurement
- Position detection of cells/beads inside the microfluidic channel by using impedance

### 1.3 Report outline

The theoretical aspects of the thesis are described in chapter 2: human semen and fluorescence are appointed and various techniques for particle detection in microfluidic channels are described. In paragraph 2.4 the  $\mu$ flow design approach is explained. In chapter 3,  $\mu$ flow's optical heart -the optical pickup- is introduced. One of the important features of the  $\mu$ flow, the focus system is described and simulated in chapter 4. The fluorescence detection is explained in chapter 5: Fluorescein, beads and fluorescent dyes are introduced. Next the fluorescence setup is shown and photo detectors are chosen. In chapter 6 the microfluidic chip design is discussed: the channel find algorithm and digital marks are explained, also a new electrodes configuration for impedance spectroscopy is described. The user interface of the  $\mu$ flow and the microcontroller program are described in chapter 7. The electronics and printed circuit board design are described in chapter 8. Functional test of the voice coils, laser diode and photon counter are described in chapter 9. Results and discussion in chapter 10, which starts with results of the channel finding and leaking light experiments. Subsequently, experiments were performed using fluorescent beads. Conclusions and recommendations can be found in chapter 11.

An overview of the  $\mu$ flow with references to the relevant chapters is shown in Figure 1.

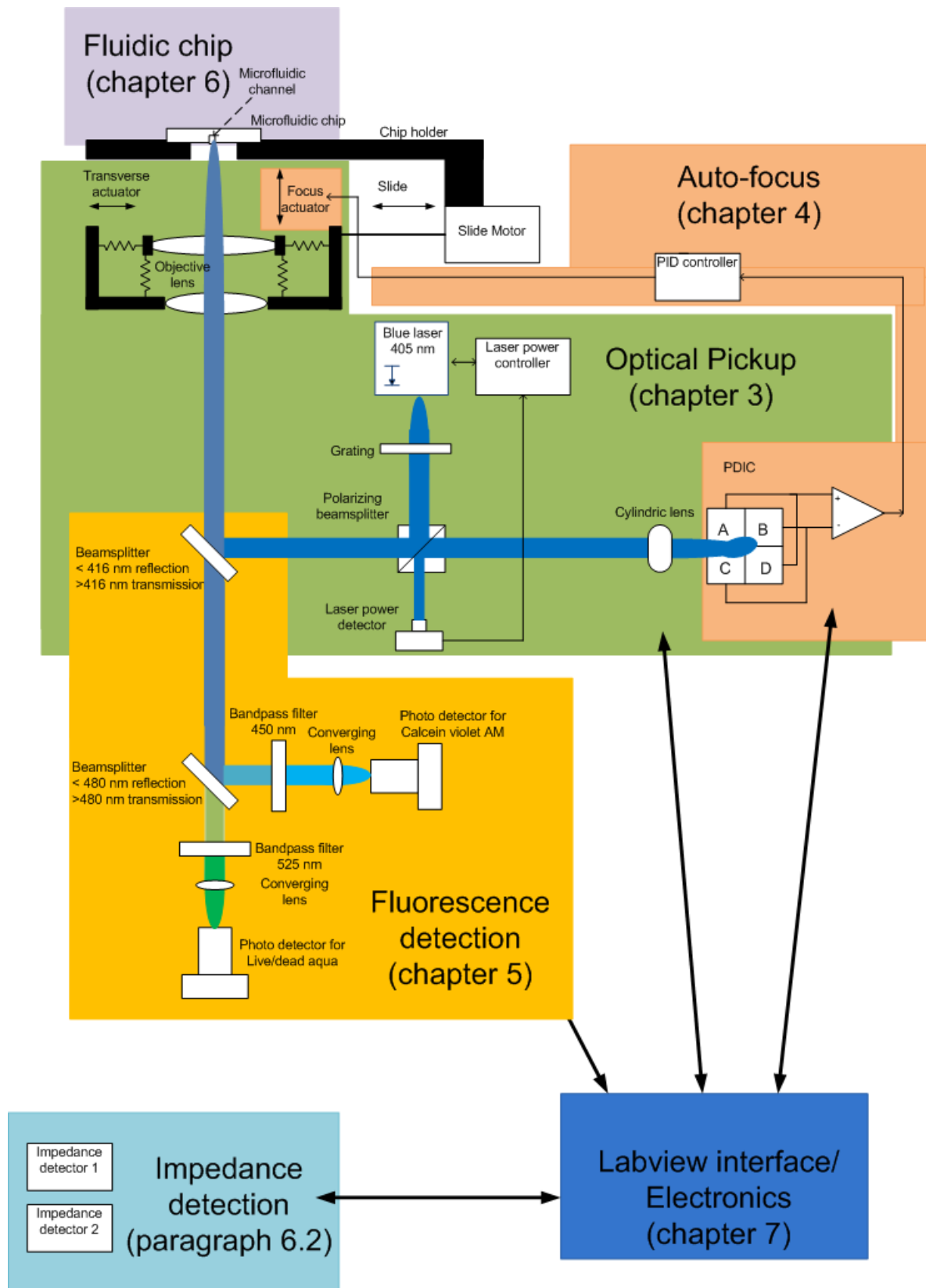


Figure 1 μflow schematic overview



## 2 Theory

The theoretical aspects of the thesis are described in this chapter. First human semen and fertility are appointed, followed by fluorescence. Subsequently various optical techniques for particle and cell detection in a microfluidic channel are presented. In the end of the chapter one approach is chosen.

### 2.1 Human semen

The male reproductive cell is the sperm cell (spermatozoon). Depending on the chromosome (Y or X) it carries, the sperm give rise to male (XY) or female (XX) offspring. A schematic overview of the human sperm cell is shown in Figure 2. The front part is the head which measures 3  $\mu\text{m}$  in diameter and 5  $\mu\text{m}$  in length. The tail is about 50  $\mu\text{m}$  long. Human semen does also consist of various other particles like: ions, sugars and proteins. In fact, for a fertile man the volume percentage of the sperm cells in human semen is only between the 0.1 % and 1 % [Segerink 2010].

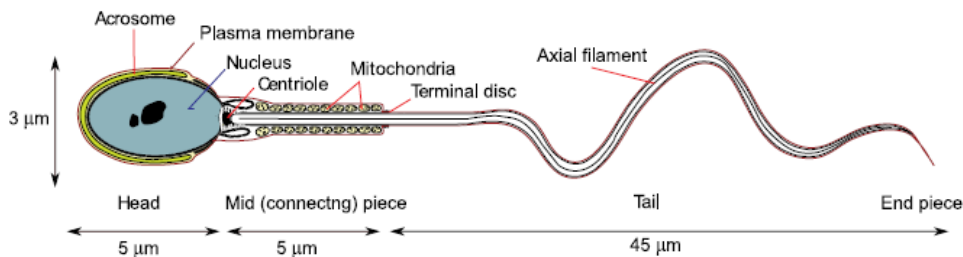


Figure 2 human sperm cell [Villarreal]

#### 2.1.1 Fertility

Sperm quality is determined by: concentration, motility, morphology and vitality of the spermatozoa. Concentration indicates the amount of sperm cells per volume (higher concentrations are better). Motility indicates the amount of motile sperm cells: motile sperm cells can swim faster and result in a higher sperm quality. Morphology is an indicator of the shape of the cell, accounting for defects in the cell (less defects is better). Vitality indicates the percentage of living cells. International guidelines for the quantification of sperm quality have been made by the World Health Organization, the lower reference limits are shown in Table 1.

Table 1 lower reference limits for semen characteristics [WHO 2010]

Parameter	Lower reference limit
Volume	1.5 mL
Concentration (per mL)	$15 \cdot 10^6$
Total motility	40 %
Morphology (normal forms)	4 %
Vitality (live spermatozoa)	58 %

#### 2.1.2 Semen analysis

The semen analysis in a hospital consists of manual counting the sperm cells using a microscope, which is called the “gold standard”. Also the motility, morphology and vitality are determined by counting this way. Most of these analysis are now performed (semi) automatically using a CASA (Computer Assisted Semen Analysis). This system is based on a microscope with image recognition for sperm counting, velocity and shape measurements. Semen can also be analyzed at home using sperm kits. Most of these kits use antibodies for colouring the sperm cells, concentration and motility can be determined [FertilityScore 2009]. Since the results are not analyzed by trained or skilled people, the accuracy and reproducibility of these test is questionable. Another disadvantage is that most of these home-tests only indicate if a certain sperm concentration is present, which gives only limited information.

## 2.2 Fluorescence

The process in which a molecule absorbs light and then emits light at a different (longer) wavelength is called fluorescence. In the biological and life sciences fluorescence is often used as a non-destructive method for analyzing cells. It allows highly sensitive measurements for characterization and distinguishing of (individual) cells. This can be done by labelling the cells with a fluorescent marker called a dye. This dye emits light at a specific wavelength and the cell can be traced. The dye can visualize particular characteristics of a cell, for example: vitality, viability or membrane integrity. This way, fluorescence has the capability to differentiate between two similar sized cells using different dyes. For on-chip semen quality measurements, fluorescent detection could be a promising detection technique. In this paragraph the theory behind fluorescence is explained. The process is explained using a Jablonski energy diagram of a fluorescent dye, shown in Figure 3.

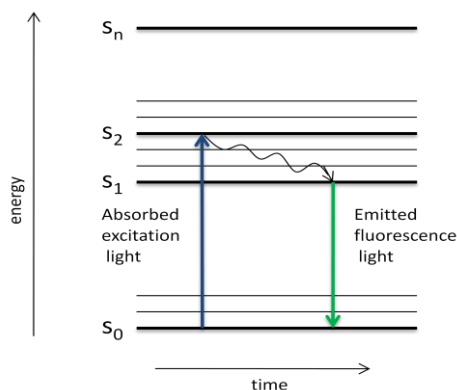


Figure 3 Jablonski energy diagram

The energy diagram shows the various vibrational energy levels that are involved in the fluorescence process of a dye. In the absence of light, the dye is in the ground state ( $s_0$ ). When light with a sufficient energy strikes, a photon will be absorbed and the dye is in an excited state ( $s_2$ ). Vibrational energy is converted to heat and the dye's energy will drop in the lower excited state ( $s_1$ ). The dye will stay in this state for several nanoseconds (this is by far the longest period in the fluorescence process, see time on the x-axis of Figure 3) before emitting a photon and relaxing in the ground state. In Figure 3, the absorption and emission process for one wavelength is shown. However, a normal light source radiates light with a wide spectrum of wavelengths. The dye's absorption of a wide spectrum will generate different absorption transitions that populate different excited states. Each transition has its own probability. This wavelength dependent absorption is shown in Figure 4. From Figure 4 can be seen that the emission spectrum is wavelength dependent too. This is the result of the closely spaced energy levels of the ground state. The probability of each transition shapes the emission spectrum [Olympus 2010].

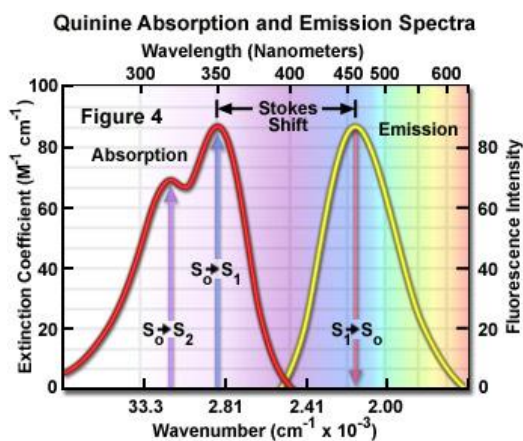


Figure 4 absorption and emission spectrum [Herman 2010]

In Figure 4, a shift in wavelength between the absorption and emission spectrum is shown. This shift in wavelength is called the Stokes shift. This shift is caused by conversion of vibrational energy into heat: the emitted photons have a lower energy (longer wavelength) than the absorbed photon. The difference in photon-energy is equal to the Stokes shift [Olympus 2010].

The process of absorption and emission of photons is not everlasting. Depending on the chemical structure (bonds) of the dye, this process can be repeated several hundreds or thousands times before the dye permanently loses fluorescence, which is called photo bleaching. Overexposure during measurement and exposure of the dye to unwanted light sources should be prevented to minimize photo bleaching. An important parameter of a dye is the efficiency to emit a photon when a photon is absorbed; this is the  $Q_e$  (quantum efficiency) [Olympus 2010]:

$$Q_e = \frac{\text{photons emitted}}{\text{photons absorbed}}$$

### 2.2.1 Auto fluorescence

Fluorescence detection of sperm cells can be implemented using fluorescent dyes attached to the cells. Apart from using fluorescent dyes, the auto fluorescence of the sperm cell could be used as label free fluorescence detection. "Auto fluorescence of sperm cells is particular strong in comparison to other mammalian cells. Most auto fluorescence is coming from various organelles such as mitochondria in the cytoplasm" [Hinterdorfer 2009]. "Acid Phosphatase (AP) is found in high levels in semen and originates from the epithelial cells where it is secreted into the prostate gland". "The level of AP activity is 500 to 1000 times higher in human semen than in any other normal body fluids or secretions" [Gutmann 1941]. Therefore auto fluorescence can be used for differentiating between semen and other normal body fluids. In Stoilovic [1991] the emission and absorption spectra of untreated dry semen were analysed, these spectra are shown in Figure 5. The absorption spectrum of semen was analyzed from 300-480 nm, showing a peak at 400 nm. For two excitation wavelengths (350 nm and 450 nm, see Figure 5), emissions spectra were measured showing peaks at respectively 460 nm and 520 nm.

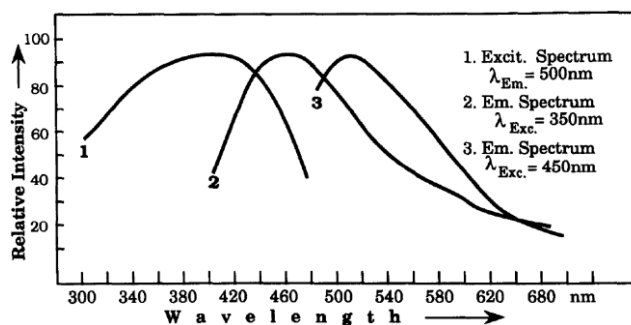


Figure 5 absorption and emission spectra of untreated dry semen [Stoilovic 1991]

For enabling auto fluorescent detection of semen in the  $\mu$ flow, the excitation light source (chapter 3) should be chosen around the absorption peak of 400 nm.

## 2.3 Optical detection of particles and cells inside a microfluidic channel

In the literature several techniques are presented for particle and cell detection in a microfluidic channel using light. This paragraph reviews three techniques: light scattering, light blocking and fluorescence.

### 2.3.1 Light scattering and light blocking

Light scattering and light blocking detectors are often used in applications where particle counting or size recognition is needed. Both techniques are shown in Figure 6 and require a light source for the illumination of the detection volume. When a particle enters the detection volume the scattering or obscuration of light is measured depending on which type of detector is used.

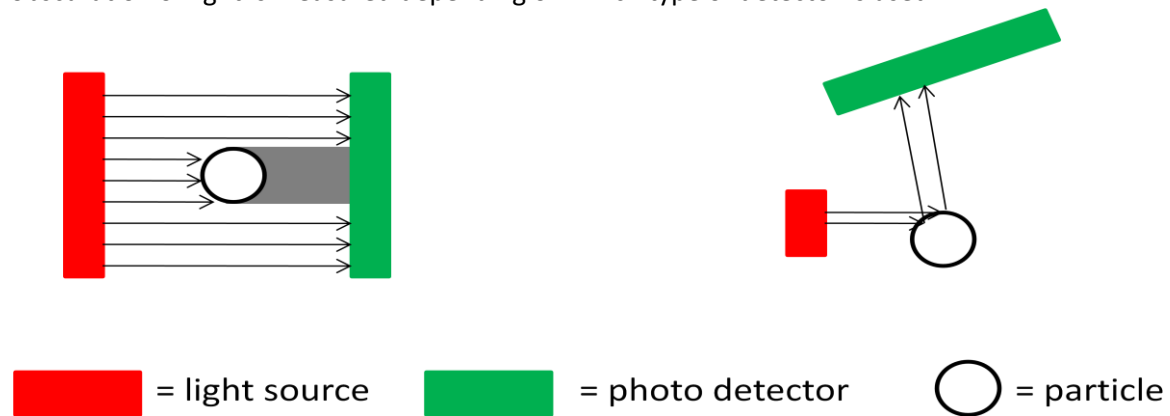


Figure 6 optical detection: light blocking detector (left), light scattering detector (right)

In the light scattering detector the photo detector is positioned at an angle and the reflected light is measured. Bigger particles reflect more light, which makes size recognition possible. In the light blocking detector, the light source is directly focused on the photo detector. A particle in the detection volume will absorb and reflect part of the light away from the photo detector. However, diffuse light inside the blocking detector is reflected resulting in a lower sensitivity compared to the light scattering detector [Zhang 2009]. The sensitivity of both detectors is based on the particle's surface area, not for volume effects as for example measured during impedance spectroscopy. Light blocking detectors are only used for the detection of large particles or concentrated particles however, light scattering detectors could be used for cell and particle detection inside a microchannel [Zhang 2009].

In Kummrow [2009] an on-chip flow-cytometer consisting of side scatter and fluorescence detection was built. The chip consists of a 3D microfluidic structure with integrated optical fibers, mirrors and electrodes and is used for blood cell analysis. Using 2D hydrodynamical focusing the cells are forced into a 5  $\mu\text{m}$  stream with flow rates up to 3 m/s (for high throughput). Cells are characterised by measuring the pulse shape and pulse height of the scattering detectors. This enables them to distinguish between platelets and red blood cells. More advanced parameters were measured using the fluorescence detectors. The combination of scattering and fluorescence detection at extreme high flow rates is promising, however the complex chip design requires in depth knowledge of chip manufacturing and years of research.

Another light scattering detector is shown in Kostner[2007]. A DVD optical pickup is focused on the microfluidic channel (50  $\mu\text{m}$  width) of a glass chip. Hydrodynamical focussing, forces the particles or cells to move across the reflective surface at the bottom of the channel. Discrimination between cells and polystyrene bead was shown. Moreover yeast cells (3-4  $\mu\text{m}$ ) have been detected and counted. The only discrimination parameter is the maximum and minimum of the scattering signal. Since sperm cells have roughly the same dimensions as yeast cells, the setup could potentially be used for

the counting of sperm cells. Cell/bead counting allows for determining the spermatozoa concentration of spermatozoa [Segerink 2010]. Apart from the concentration parameter motility, morphology and vitality of the sperm cannot be determined using light scattering. Because of the low price, compact format and the simple shape selection parameters an optical pickup scattering detector could be integrated next to fluorescence detection (used for determining the other spermatozoa parameters). A reflective layer at the top of the channel is required for the light scattering detector. During the manufacturing of the microfluidic chip this requires an additional mask (compared to Segerink[2010]), the system as proposed by Kostner is therefore not chosen for the  $\mu$ flow.

### 2.3.2 Fluorescence

In Kruger[2002] a miniaturized flow cytometer has been built for counting and sorting cells. The focus of this article is on the integration of active and passive optical components on a disposable chip. Fluorescence excitation was performed by on-chip prism coupling. For the fluorescence detection a band-pass filter and APD (Avalanche Photodiode, paragraph 5.5.2 ) was integrated on-chip. Separation of 6  $\mu$ m beads was shown at a rate of 200 beads/s using external valves and pumps. The integration of many optical parts inside a chip is a great achievement and the results are promising but at the moment this is only possible for experimental purposes.

In Yang[2006] a cell counting/sorting system is presented. A 532 nm green laser is focused inside a microfluidic channel. An APD was used for the fluorescence detection. Counting  $>1 \mu$ m diameter cells at rates up to 120 cells/s was shown with a counting error  $<1.5 \%$ . The size of the system is only  $37 \times 16 \times 18 \text{ cm}^3$ . Hydrodynamical focussing results in a 12.5  $\mu$ m width stream of cells, a micro flow switch with external pumps was used for the sorting. The system sensitivity and counting speed could be sufficient for the  $\mu$ flow; however the system is rather expensive and requires a complex (optical) setup.

In Holmes[2005] dielectrophoretic particle focusing is combined with fluorescence detection. For fluorescence excitation a 633 nm red HeNe laser is used. A PMT (Photomultiplier Tube) is used for the fluorescent detection. Movement of the particles is simultaneously monitored using a high speed CCD (charged coupled device). Vertical and horizontal focusing of the particles is done by four electrodes (two electrodes on top of the channel, two at the bottom). Fluorescent beads in the micrometer range were counted at a rate up to 250 beads/s. Especially the dielectrophoretic particle focusing is interesting for the  $\mu$ flow, since minor modifications to the current chip design (chapter 6) would allow integration of particle focusing.

Fluorescence detection in large diameter channels (300  $\mu$ m) using an optical pickup is described in Shimomura [2008]. An external 532 nm laser is focused inside the microfluidic channel. The laser beam is moved in the vertical and horizontal direction to create a two-dimensional section of a microfluidic channel. For the fluorescence detection a PMT was used. Measurements with different concentrations of Resorufin were performed, a linear response was found for the range of 0.1-100 nM, the detection limit was 800 pM (chip to chip reproducibility 2.1 %). Another application where an optical pickup is used is in [Yim 2008]. The mixing pattern of two fluids is visualized using fluorescent dyes, A resolution of 1  $\mu$ m was archived, combined with good results found for sensitivity and reproducibility.

In Zhu[2010] a cell phone camera was used in combination with only a cost-effective colour filter, lens and illumination led's. A spatial resolution of 10  $\mu$ m was achieved with additional digital imaging processing.

## 2.4 $\mu$ flow approach

In paragraph 2.3.2 several approaches for the fluorescence detection of particles and cells inside a microfluidic channel have been presented. Some approaches result in a difficult optical setup that is both spacious and expensive [Kruger 2002], [Yang 2006]. Because of the limited amount of time to spend on this thesis and the need for a compact fluorescence detection system, another approach is necessary. To meet at the time pressure (part of) a ready-made optical system must be used. In this chapter the optical pickup approach and the cell phone camera of Zhu[2010] are analyzed in more depth. Eventually one option is chosen.

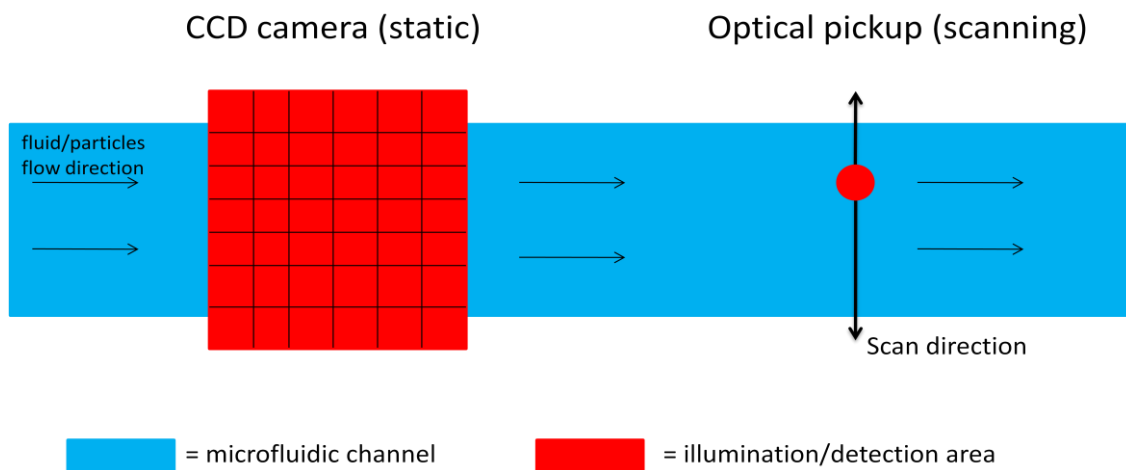


**Figure 7 fluorescence detection in microfluidic channel: multiple pixels (left), single pixel (right)**

In Zhu[2010] a cell phone camera was used in combination with only a cost-effective colour filter/lens and illumination led's. The fluorescent stained cells are excited using a led light source. The led illuminates a large area of the microfluidic channel, the fluorescent emission from the entire area is collected by a CCD, shown in Figure 7 (left side). An image is captured after a certain time. Signal intensities from the individual pixels are converted into a digital image. A CCD can acquire a two dimensional image of the fluorescence light, which allows cell-shape recognition. However, the photo detectors inside the CCD are not designed for the detection of weak fluorescence light. The low sensitivity will therefore cause a loss of fluorescence information. In Zhu[2010] a spatial resolution of 10  $\mu\text{m}$  was achieved with additional digital imaging processing. This is not enough for the detection of sperm cells. A higher resolution is possible using a more advanced CCD or better optics. The CCD camera option requires a high quality camera and a relative simple experimental setup. The focus will shift to image processing: finding smart algorithms for cell recognition and identification.

Another option is to use an optical pickup from a DVD or CD player. In this approach a laser beam is scanned back and forth across the width of the microchannel. The excited area is representing one single pixel, see Figure 7 (right side). Using hydrodynamical focussing there is also the option to keep the laser beam static above the channel. By modifying the optical pickup, measurements with high sensitivity can be performed because the objective lens has a high NA (Numerical Aperture) and a beam diameter  $< 1 \mu\text{m}$ . The optical pickup has also the possibility to control the focus automatically. In combination with a transversal movement using voice coils this ensures high throughput measurements. The optical pickup sensitivity can be increased by adding a more sensitive photo detector with a small form factor [Kummrow 2009], [Yang 2006]. The optical pickup option does not focus on image processing like it is the case of Zhu[2010] and requires a more broad set of skills. Because of the many advantages listed above, the optical pickup was eventually chosen from the two options.

### 3 Optical pickup

The optical pickup is  $\mu$ flow's optical heart because it incorporates the most (important) optical features. In this chapter the principle of reading an optical disc is explained first. Subsequently the PHR-803T optical pickup is introduced and the optical parts are explained.

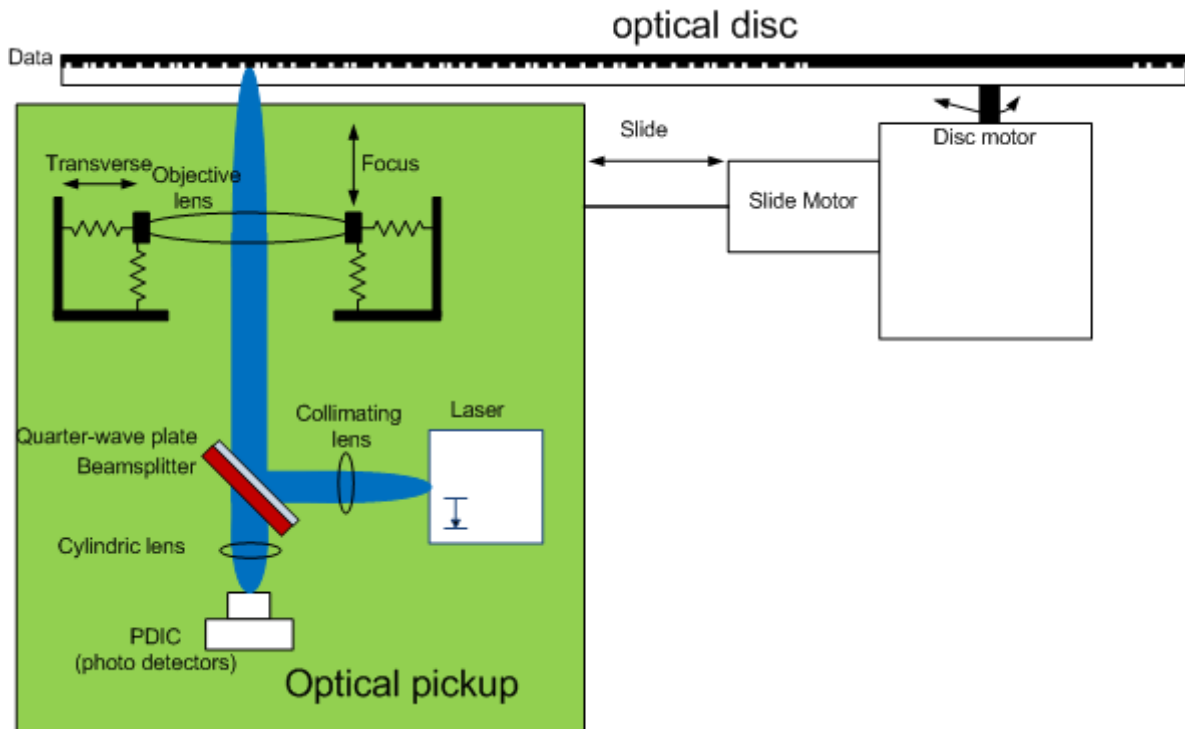


Figure 8 reading an optical disc

In Figure 8 the general reading principle of an optical disc (CD or DVD) is shown. A light beam is emitted by a laser diode and will first meet a collimating lens that creates a parallel beam. The polarizing beamsplitter reflects the beam and the quarter-wave plate creates a quarter-wavelength phase shift (only the shifted light will later be transmitted to the photo detectors). The beam is then focused on the data layer of the optical disc using the objective lens. Light is reflected back from the data layer and will pass through the objective lens onto the quarter-wave plate. The polarizing beamsplitter transmits the beam and an astigmatic lens (lens with two focal points) is focussing the beam at the photodiodes inside the PDIC (Position Detector Integrated Circuit). Photodiodes convert the optical data into electric pulses [Odgaard 2004].

For robust data transfer the distance between data layer of the optical disc and the objective should be kept constant and equal to the focal length of the objective lens. This is done by the focus system described in chapter 4. The focal length of the objective lens is changed by moving the lens in the vertical direction using a VCA (Voice Coil Actuator). Besides vertical displacements, the objective can also be moved in the transversal direction. This allows access to data nearby, since the data on an optical disc is positioned in several thousands of circular tracks. The working range of the transverse-actuator ( $< 1$  mm) is only a few hundred tracks, for large transversal displacements a slide motor changes the position of the entire optical pickup.

### 3.1 PHR-803T optical pickup

The first distinction in between optical pickups is which optical format is supported: CD (Compact Disc), DVD (Digital Versatile Disc), HD-DVD (High Definition/Density DVD) or BD (Blu-ray Disc). For detecting auto fluorescence of semen (paragraph 2.2.1) a blue laser diode is required and only HD-DVD and BD optical pickups are equipped with this one. A blue laser can also archive higher resolutions because the wavelength of the light is smaller compared to the red and infrared laser diodes used in respectively DVD and CD formats. Comparing HD-DVD and BD, the HD-DVD format is preferred because it provides a larger working distance compared to BD (paragraph 3.2), resulting in a simpler setup. Besides the HD-DVD format, optical pickups are often backwards compatible with DVD and CD. These multiple format optical pickups are preferred for use in the  $\mu$ flow because they incorporate multiple laser wavelengths. The more wavelengths are available the more different dyes can be used. Another important aspect is the obtainability: most optical pickups are produced for several years and will eventually become discarded. Therefore, the preference is given to a new and widely available optical pickup model.

For the  $\mu$ flow, the PHR-803T optical pickup (Figure 9 and Figure 10) was chosen because it supports multiple formats including HD-DVD, incorporates autofocus, is easy to obtain and costs only 10 dollars. The PHR-803T is also used in the HD-DVD drive of the XBOX-360 game console. The supported formats are: CD, DVD and HD-DVD.

### 3.2 Identification optical parts

Unfortunately optical pickups are OEM (Original Equipment Manufacturer) devices and therefore undocumented. All information is classified and unobtainable, and the PHR-803T was no exception. Before the optical pickup could be used in the  $\mu$ flow all the parts had to be identified first. After days of reverse engineering, all parts could finally be identified. For example: to identify the PDIC, the optical pickup was inspected under a microscope: the part number was visible on the silicon wafer through the glazed window of the PDIC. The optical components of the PHR-803T pickup are numbered in Figure 9 and Figure 10 and a schematic overview is shown in Figure 11.

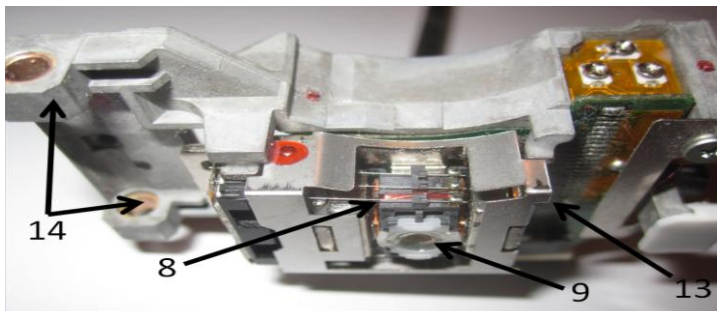


Figure 9 PHR-803T optical pickup side view: voice coil actuator (8), objective lens (9), laser power control (13) and slide connection (14)

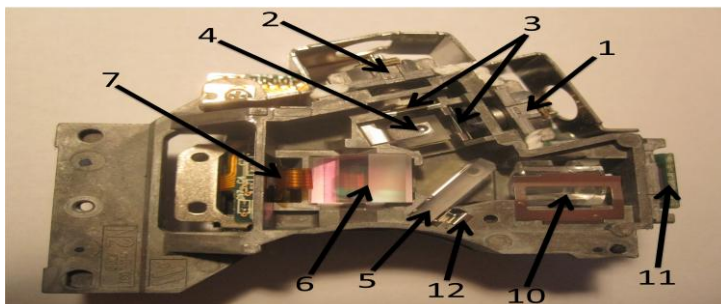


Figure 10 PHR-803T optical pickup bottom view: laser diode 405 nm (1), laser diode 660 nm and 780 nm (2), diffraction grating (3), beamsplitter (4,5), mirror (6), waveform aberration corrector (7), astigmatic lens (10), PDIC (11) and laser power detector (12)

For the HD-DVD format a 405 nm ultraviolet laser beam is emitted by the laser diode (1). For the DVD and CD format, respectively a 660 nm red laser beam and a 780 nm infrared laser beam are emitted by the dual emission laser diode (2). The laser beam will first meet diffraction grating<sup>1</sup> (3). The beams of the two laser diodes are then multiplexed in a polarizing beamsplitter (4). Afterwards the laser beam is reflected by a second polarizing beamsplitter (5) and a mirror (6). It is eventually passed through a waveform aberration corrector<sup>2</sup>(7) and focused on the data layer of the optical disk using a two lenses objective. Notable fact is that no collimating lens is used for collimating the laser beam, as a result much of the laser power is wasted. Most likely this was done to reduce costs.

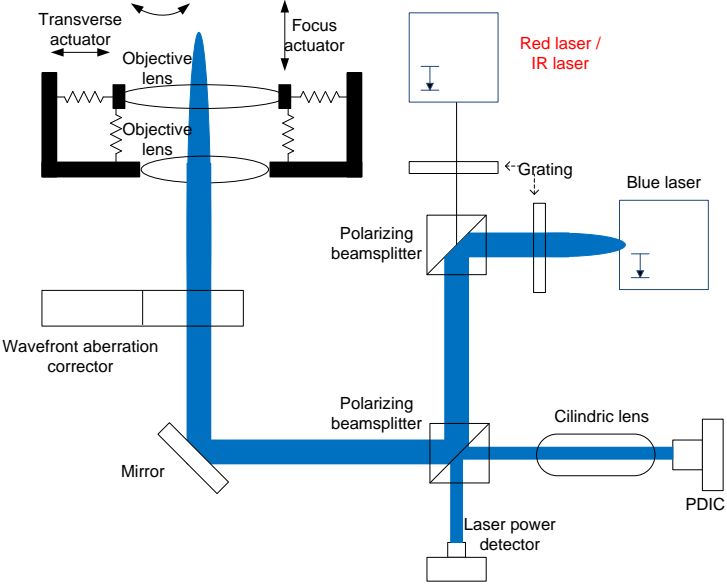


Figure 11 schematic overview of: PHR-803T optical pickup

Specifications of the PHR-803T are not available, however this multiple format optical pickup should work conform the standards of both CD, DVD and HD-DVD format. In Table 2, these standards are shown.

Table 2 standardized optical formats

	CD	DVD	HD-DVD	(BD)
$\lambda$ [nm]	780	660	405	405
NA	0.45	0.6	0.65	0.85

<sup>1</sup> The diffraction grating creates sub-beams from the main beam. Using the method called ‘twin-spot radial detection’ the optical pickup can recognize the radial position and find the data tracks. The  $\mu$ flow uses only the main beam.

<sup>2</sup> In between the mirror and objective a wavefront aberration corrector is placed. This is a miniature LCD screen that allows for correction of the wavefront. This results in a better focused beam. Wavefront correction is not necessary in the  $\mu$ flow, therefore the LCD screen will not be used. Moreover there is no information on how to control the LCD.

The wavelength  $\lambda$  corresponds to the colour of the laser diode. The NA (numerical aperture) represents the resolving power of the objective lens and is defined as[Wikipedia 2009]:

$$NA = \sin \theta$$

Where  $\theta$  is the maximum angle at which the objective lens can accept light. In Figure 12 a schematic drawing is shown, where F is the focal point, f the focal length and D the lens diameter.

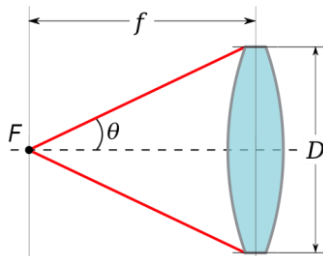


Figure 12 NA of a lens [Wikipedia 2009]

### 3.3 Objective lens

Supporting three different NA's at three different wavelengths requires a complex objective lens design; this design is shown in Figure 13.

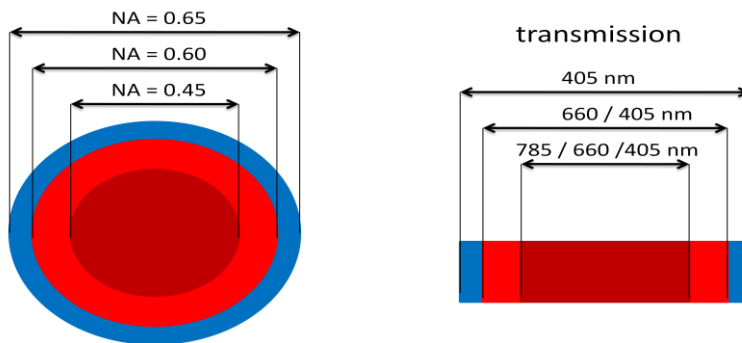


Figure 13 objective lens top view (left), side view (right)

The objective lens has a wavelength selective diameter; it consists of three interference filters. The inner and middle interference filters are separated at a diameter corresponding to a NA of 0.45 for transmitting 785 nm light (CD-format). The middle and outer interference filters are separated at a diameter corresponding to a NA of 0.6 for transmitting 660 nm light (DVD-format). The outer diameter (measuring 4mm) corresponds to a NA of 0.65 for transmitting 405 nm light (HD-DVD-format)[Katayama 2008]. The actual objective lens of the PHR-803T consists of two separate lenses, shown in Figure 11 (the two lenses combined give the objective lens as shown in Figure 13). The lower lens is fixed; the upper lens can be moved using voice coil actuators. Vertical movements of the upper lens are used for focussing and transversal movements for track finding can be made. Also the tilt of the upper lens can be adjusted.

### 3.4 Focal length

The distance between the objective lens and the data layer of the optical disk is ideally equal to the focal length of the objective lens (at this point the data-layer of the disk is in focus). The focal length  $f$  of the objective lens can be found using Figure 12 and the NA equation (paragraph 3.2):

$$f = \frac{D}{2 \cdot \tan(\sin^{-1} NA)}$$

For the HD-DVD format the resulting focal length is 2.3 mm. If we would extrapolate this for a BD-format optical pickup (with a lens diameter of 4 mm) the focal length is only 1.2 mm. This small focal length of the BD-format is why this format is not chosen in the  $\mu$ flow. Besides that in the  $\mu$ flow the distance to the channel from the bottom of the microfluidic chip is 500  $\mu$ m (chapter 6), an additional distance of 1 mm (chapter 6) is caused by the chip holder, meaning that a BD-format optical pickup cannot be placed at all. For the PHR-803T HD-DVD-format optical pickup 0.8 mm of space is left.

### 3.5 Resolution and focal depth

For an optical disk player, the smallest optical spot size that can be visualized in theory is determined by the diffraction limit (DL)[Olympus 2009]:

$$DL = 0.61 \cdot \frac{\lambda}{NA}$$

The small wavelength and high NA of the HD-DVD format result in a diffraction limit of 0.4  $\mu$ m. This resolution allows the  $\mu$ flow to visualize even the smallest cells without any problem. Unfortunately, a trade off between resolution and DOF (Depth of Focus) exists: a high resolution leads to a small DOF. DOF is the range of distance from the focal point of the lens in which the image produced by the lens has a certain sharpness [Olympus 2009]. In the HD-DVD-format the DOF is small, meaning that for reliable data reading from the disk, the data layer should be close to the focal point of the lens. Inside an optical disk player the optical disk rotates at several thousand rotations per minute, for a reliable data transfer the position of the objective lens is adjusted constantly. The need for precise and fast corrections requires a sophisticated autofocus mechanism; this is explained in chapter 4.

The importance of DOF for the  $\mu$ flow is explained next. For simplicity the fluorescent particles inside the microfluidic channel of the  $\mu$ flow are represented as a point source of fluorescence light. If the particles are at the focal length of the objective lens, the particles are in focus and maximal fluorescence signal is received by the objective lens. However, in the situation where the particles are at a distance unequal to the focal length, the fluorescent signal is much weaker because much of the light is diffracted away from the focal point of the objective lens.

### 3.6 Gaussian beam

The laser inside the optical pickup generates a Gaussian light distribution [Wikipedia 2009]. Near the focal point a Gaussian beam has a characteristic hourglass shape, shown in Figure 14.

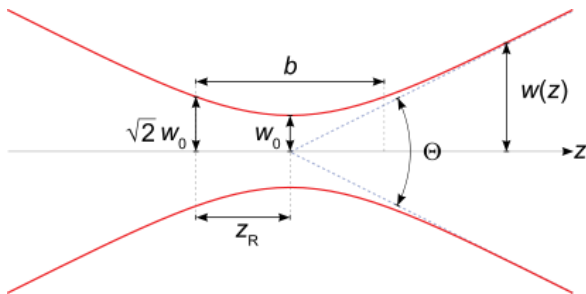


Figure 14 Gaussian beam[Wikipedia 2009]

Where  $Z_R$  is the Rayleigh length: distance from the beam focal point ( $W_0 =$  waist) where the radius is increased with  $\sqrt{2}$  and the area of the cross section is doubled, the optical intensity drops to  $\frac{1}{e^2} \approx 13.5\%$  of the value at the focal point [Wikipedia 2009].

$$Z_R = \frac{\pi W_0^2}{\lambda}$$

The radius of the beam at distance  $z$  from the waist/ focal point is [Wikipedia 2009]:

$$W(z) = W_0 \sqrt{1 + \left(\frac{z}{Z_R}\right)^2}$$

This can be rewritten for  $Z(w)$  :

$$Z(w) = Z_R \sqrt{\left(\frac{w}{W_0}\right)^2 - 1}$$

The calculated specifications for the PHR-803T optical pickup and a BD-format optical pickup example are shown in Table 3

Table 3 PHR 803T optical pickup specification and BD optical pickup example

	CD	DVD	HD-DVD	(BD)
$\lambda$ [nm]	780	660	405	405
NA	0.45	0.6	0.65	0.85
$\theta$ [°]	27	37	41	58
D [mm]			4	4
F [mm]			2.3	1.2
Space left for optical pickup In $\mu$ flow [mm]			0.8	-0.3
Smallest spot size [ $\mu$ m]	1.1	0.7	0.4	0.3
Rayleigh length [ $\mu$ m]	$\pm 4.9$	$\pm 2.3$	$\pm 1.2$	$\pm 0.7$

## 4 Focus system

This chapter deals with the focus system. First the individual parts of the focus system are described. Subsequently a voice coil model is elaborated and simulated in Matlab. Next, the complete focus system including a PID (proportional-integral-derivative) controller is simulated in Matlab. At the end of the chapter the implementation of the PID controller in a microcontroller is described.

For robust data transfer, the distance between the data layer of the optical disc and the objective should be kept constant and equal to the focal length of the objective lens (paragraph 3.5). However, during the reading of an optical disk, the distance between the data layer and objective lens will become disturbed. This disturbance is due to the rotating disk, external vibrations or surface defects (scratches, fingerprints, etc). An optical disc player uses a focus system to suppress these disturbances, hereby keeping the data layer continuously within the depth of focus (paragraph 3.5). In the  $\mu$ flow the focus system of the optical pickup is used to find the channels and digital marks (paragraph 6.1). When the particles are correctly focused, optimal detection of their fluorescence by the objective lens is guaranteed. It has to be mentioned that the detection of the objective lens only partly determines the fluorescence detection ability of the  $\mu$ flow. The fluorescence detection limit of the  $\mu$ flow as a whole is determined by the SNR (Signal-to-Noise Ratio):

$$SNR = \frac{P_{signal}}{P_{noise}}$$

Where  $P_{signal}$  is the average received fluorescence power and  $P_{noise}$  is the average noise power; the SNR is depended on the bandwidth.

### 4.1 Focus distance measurement

Focus distance measurement in the optical pickup is performed using the astigmatic principle. The astigmatic principle uses a cylindrical lens (Figure 15) in front of the photo detectors of the PDIC (Figure 8). This lens has two focal points: one in front and one behind the photo detectors of the PDIC.

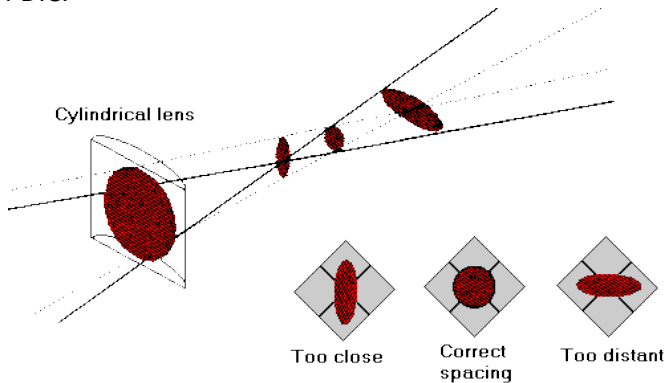


Figure 15 astigmatic principle [John 1993]

The photo detectors inside the PDIC have a four-quadrant configuration. The beam spot will produce a circular shape if an object is at the focal length of the objective lens. The cylindrical lens is designed in such a way that this point occurs in between the two focal points of the cylindrical lens. If the object is not at the focal length of the objective lens, the beam spot will have an elliptic shape, the aspect ratio of this ellipse changes as the objective distance increases from the focal length of the objective lens [Odgaard 2004]. This is indicated by the FES (focus error signal), given by [Odgaard 2004]:

$$FES = (B + D) - (A + C)$$

Where A, B, C and D are voltages corresponding to the incident light on the PDIC photo detectors A,B,C and D. The linear range and gain of the FES are determined in paragraph 10.1.1: the linear range corresponds to  $6.8 \mu\text{m}$ , the gain in the linear range is  $0.27 \text{ V}/\mu\text{m}$ . The FES is also shown in Figure 16.

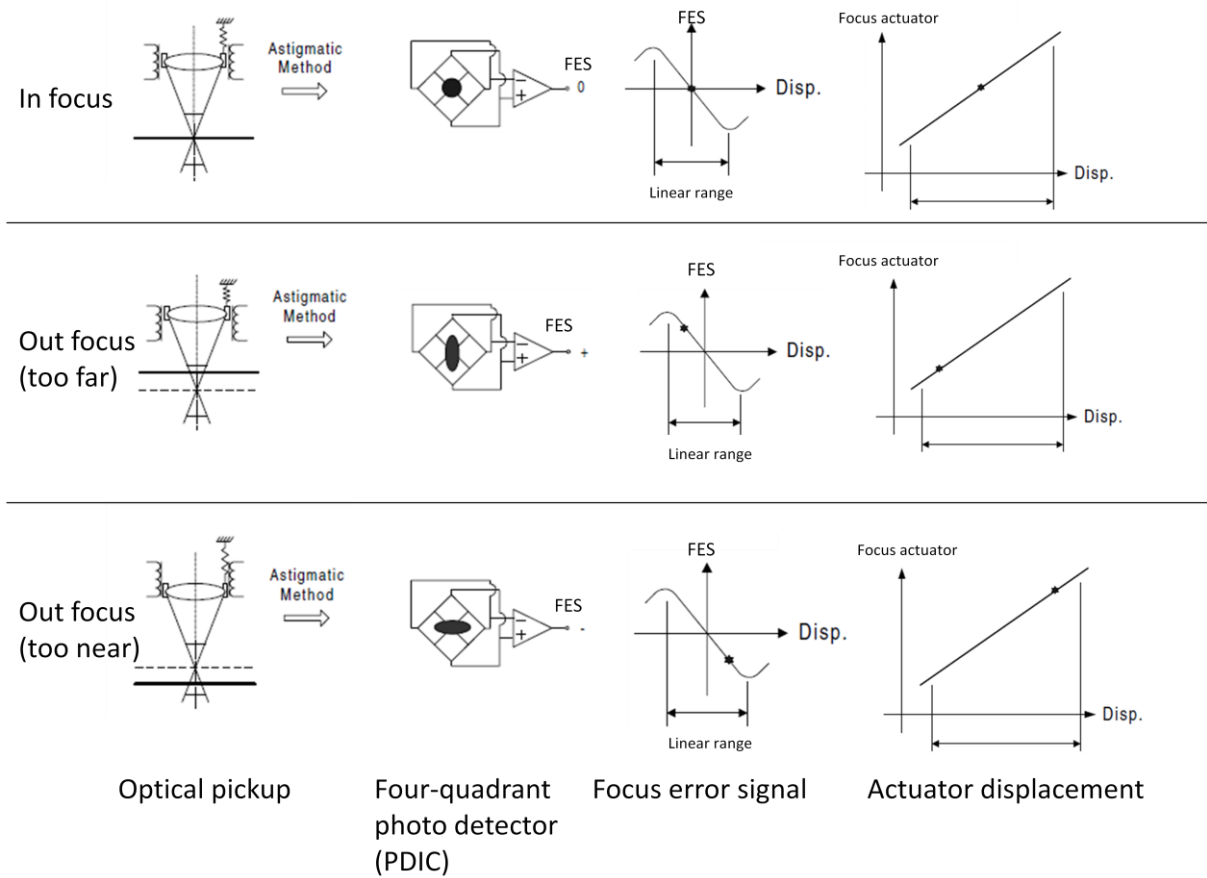


Figure 16 auto focus [Fan 2001]

## 4.2 Moving lens

The objective lens should be moved along the vertical axis (focus axis) to adjust the FES to zero (Figure 16). The objective lens is moved by the focus VCA which is a voltage controlled electromagnetic voice coil. The moving objective lens is connected to a damper with four springs, shown in Figure 17. Where  $m$  is the moving lens mass [kg],  $k$  the spring constant [N/m],  $C$  the viscous damping coefficient [N s/m],  $f(t)$  is the electromagnetic force of the voice coil actuator [N] and  $x(t)$  the displacement [m] of the objective lens. The moving lens system can be modelled as a second order dynamic system, the general form of a second order transfer function is [Torng 2006]:

$$L(s) = \frac{X(s)}{F(s)} = K \frac{\omega_n^2}{s^2 + 2\zeta\omega_n s + \omega_n^2}$$

Where  $K$  is the DC gain,  $\omega_n$  is the natural frequency and  $\zeta$  is the damping ratio.

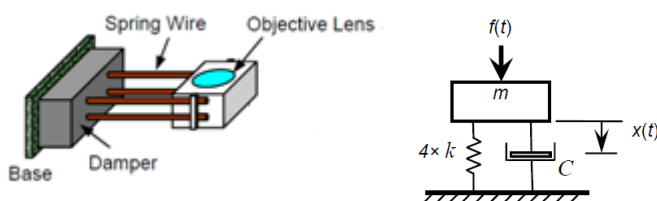


Figure 17 moving lens (left), dynamic model (right) [Torng 2006]

Inserting the mass of the objective lens, spring constant and viscous damping coefficient in the transfer function [Torng 2006]:

$$L(s) = \frac{X(s)}{F(s)} = \frac{1/m}{s^2 + (C/m)s + 4(k/m)}$$

The transfer function for both the focus and transverse actuator has been calculated in paragraph 9.2. From the transfer function the spring constant and viscous damping coefficients were determined.

### 4.3 PID control

The focus distance measurement and VCA are integrated in a feedback loop. An electronic controller determines the characteristics of the loop (bandwidth, gain, phase margin). In Figure 18 the complete focus system is schematically shown.

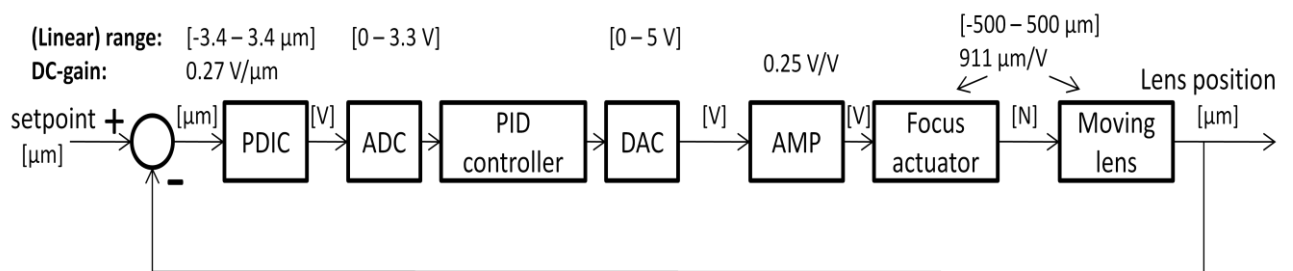


Figure 18 schematic overview of the focus system with transfer parameters

A PID controller was chosen because this controller can be simulated and tuned in Matlab(R2009b). The PID controller is implemented using a microcontroller and therefore an analog-to-digital converter (ADC) and a digital-to-analog converter (DAC) are needed for the data conversion. The output of the PID controller is amplified before it drives the focus VCA. The FES from the PDIC is subtracted from the desired focus error (setpoint = 0) and processed by the PID controller.

The PID controller consists of three different blocks (shown in Figure 19). The proportional control amplifies the current error signal with  $K_p$  (proportional gain). There will always be a steady state error if only a proportional controller is used. To reduce the steady state error an Integral control part is added. This controller reduces the steady state error to zero.

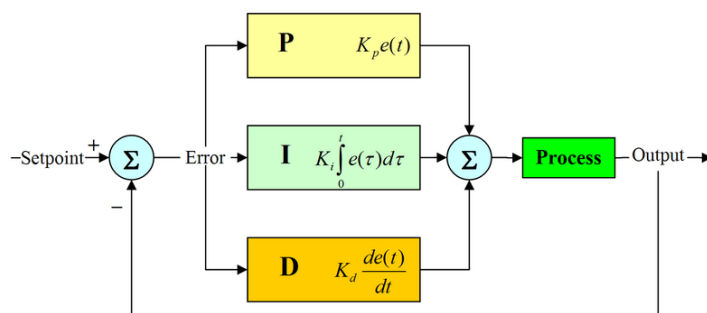


Figure 19 PID controller [Wikipedia 2006]

The output of the PID controller is the sum of proportional, integral and differential part [Wikipedia 2006]:

$$u(t) = K_p e(t) + K_i \int_0^t e(\tau) d\tau + K_d \frac{d}{dt} e(t)$$

#### 4.4 Matlab Simulation

The transfer function of the total focus system was determined using the transfer functions of the individual blocks: moving lens (paragraph 4.2), VCA driver (paragraph 8.2) PDIC amplifier (paragraph 8.1), PDIC (paragraph 10.1.1). All the transfer parameters are listed in Figure 18. The low-pass filter behind the PDIC results in a low bandwidth of the complete system. The automatic PID tuning function of Matlab recommends using an integral controller ( $K_i = 0.51$ ). In Matlab the frequency response of the focus system including the integral controller was simulated, the step response ( $10 \mu\text{m}$  focus VCA displacement) was simulated in Matlab and is shown in Figure 20. The shape of response corresponds to a stable 2<sup>nd</sup> order system. The system has a 13 dB gain margin (calculated by Matlab)

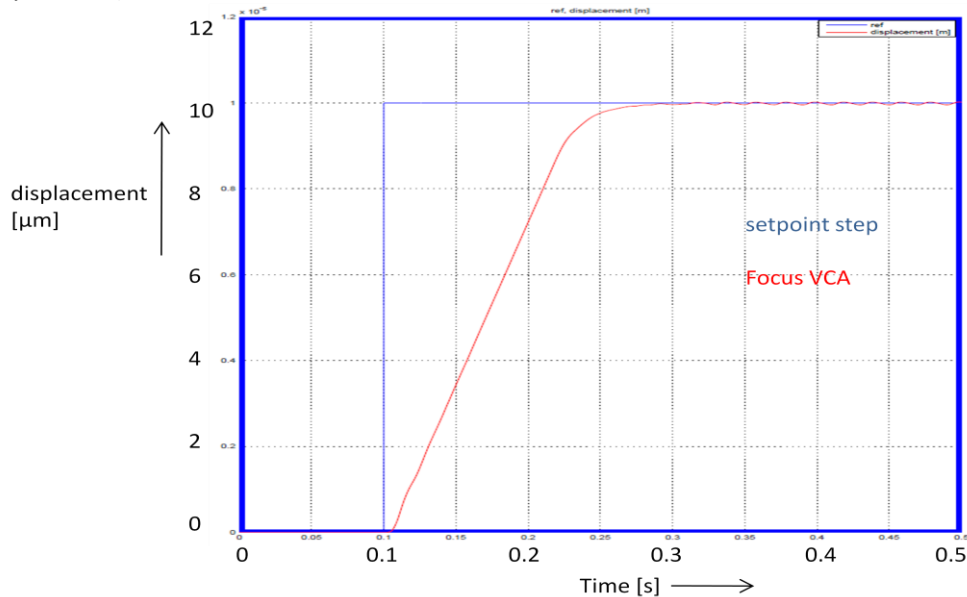


Figure 20 focus system response ( $10 \mu\text{m}$  step)

#### 4.5 Microcontroller focus controller

The focus controller is implemented in a floating point microcontroller. The controller consists of two parts. The first part is looking for a PDIC-FES maximum to position the laser within the linear range of the PDIC focus distance measurement, the PDIC-FES is shown in Figure 21(1).

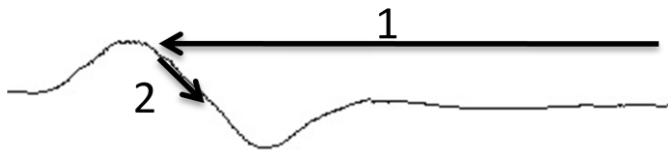


Figure 21 Microcontroller focus controller (PDIC-FES is shown)

When the PDIC-FES linear range is found, the integral controller -tuned by Matlab- takes over (Figure 21 (2)). The PID controller is implemented using the following algorithm (only integral part is used)[Braunl 2008]:

$$U_n = U_{n-1} + K_p(e_n - e_{n-1}) + K_i \frac{(e_n + e_{n-1})}{2} + K_d(e_n - 2e_{n-1} + e_{n-2})$$

## 5 Fluorescence detection

In this chapter the fluorescence detection of the  $\mu$ flow is discussed. First the fluorescence setup is shown. Next two different dyes, Fluorescein and fluorescent beads are introduced. The emitted fluorescent light is calculated and suitable photo detectors are chosen.

### 5.1 Setup

The fluorescence detection is schematically shown in Figure 22. The laser diode (405 nm) excites the fluorescent particles inside the microfluidic channel. Fluorescent light emitted from the microfluidic channel ( $> 416$  nm) is transmitted by the first beamsplitter (Thorlabs MD416). A second beamsplitter (Thorlabs 480) splits the two fluorescence wavelengths: 450 nm is reflected and 525 nm light is transmitted. The reflected light passes a 450 nm bandpass filter (Thorlabs FB450-40), the passband is 40 nm, outside the passband the light transmission is  $< 0.001$  %. After the bandpass filter the light is converged by a Plano-Convex lens (Edmund Sciences NT47-872-INK), an antireflection coating provides  $< 0.4$  % reflectance. The focal spot of the lens is aligned at the active light sensitive areas of the photo detector (paragraph 5.5). The light that is transmitted by the second beamsplitter passes a 525 nm bandpass filter (Thorlabs MF525-39), the passband is 39 nm. After the bandpass filter the light is converged by a Plano-Convex lens (Edmund Sciences NT47-872-INK).

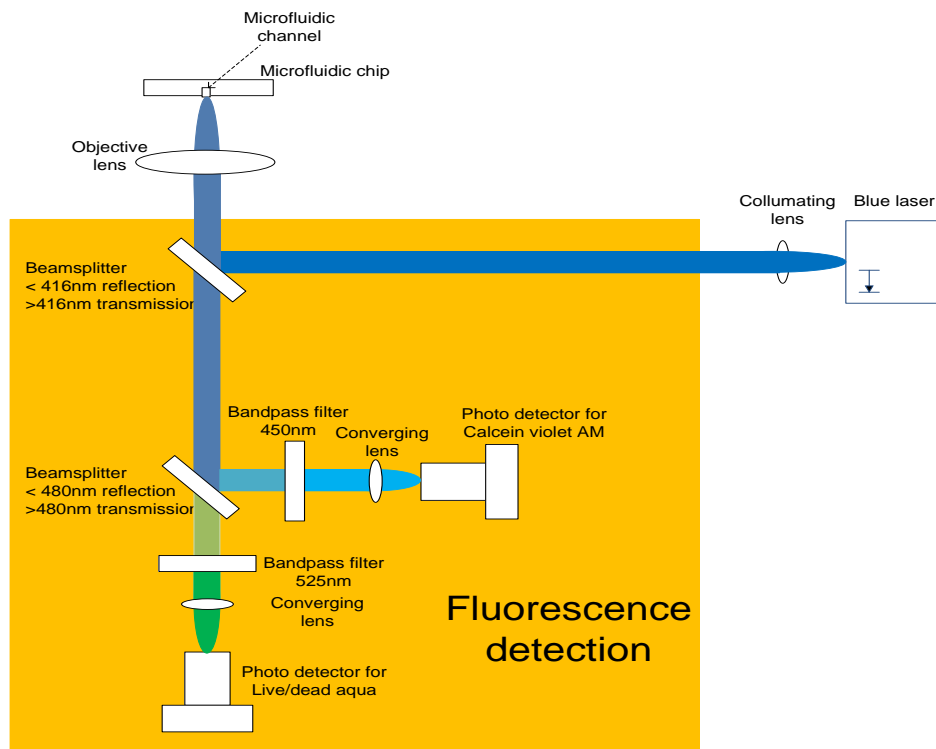


Figure 22 fluorescence detection

## 5.2 Fluorescein

The first fluorescent experiments of the  $\mu$ flow are performed using Fluorescein sodium salt F6377 [Sigma-Aldrich]. Fluorescein is used as a fluorescent tracer, with an emission of 521 nm [Corkan 1998]. Fluorescein is dissolved in ethanol and the  $Q_e$  is really sensitive to pH.

### 5.2.1 Fluorescence power

The absorption (A) of light in a liquid is described by Lambert Beer [Banerjee 2008]:

$$A = \varepsilon(\lambda)lk = \ln \frac{P_0}{P_t}$$

Where  $\varepsilon(\lambda)$  is the molar absorptivity, (l) the cuvette length, (k) the volume concentration, ( $P_0$ ) the excitation power and ( $P_t$ ) the transmitted power.

The emitted fluorescence power is [Banerjee 2008]:

$$P_e(\lambda) = Q_e(\lambda) \cdot P_a(\lambda) = Q_e(\lambda) \cdot (P_0 - P_t(\lambda)) = Q_e(\lambda) \cdot P_0(1 - e^{-\varepsilon(\lambda)lk})$$

Where ( $Q_e$ ) is the quantum efficiency of the liquid ( $P_a$ ) is the absorbed power ( $P_0$ ) is the excitation power, ( $P_t$ ) is the transmitted power.

Fluorescein  $\varepsilon(525 \text{ nm}) = 18211 [\text{M}^{-1}\text{cm}^{-1}]$ ,  $Q_e = 0.8$  [Corkan 1998],  $l = 1.2 \text{ } \mu\text{m}$  (Rayleigh length of laser beam, paragraph 3.5), excitation power 1.5 mW (paragraph 10.1.1).

$$P_e(525 \text{ nm}, k = 1 \cdot 10^{-3}) = 0.8 \cdot 1.5 \cdot 10^{-3} (1 - e^{-18211 \cdot 1.2 \cdot 10^{-4} \cdot 1 \cdot 10^{-3}}) = 2.62 \text{ } \mu\text{W}$$

$$P_e(525 \text{ nm}, k = 1 \cdot 10^{-5}) = 0.8 \cdot 1.5 \cdot 10^{-3} (1 - e^{-18211 \cdot 1.2 \cdot 10^{-4} \cdot 1 \cdot 10^{-5}}) = 26.2 \text{ nW}$$

$$P_e(525 \text{ nm}, k = 1 \cdot 10^{-7}) = 0.8 \cdot 1.5 \cdot 10^{-3} (1 - e^{-18211 \cdot 1.2 \cdot 10^{-4} \cdot 1 \cdot 10^{-7}}) = 0.262 \text{ nW}$$

Not all the power will be received by the photo detector. Light will be attenuated by the optical parts in between the microfluidic channel and the photo detector. The light is first attenuated by the Borofloat glass of the microfluidic chip. The transmission of the Borofloat is 90 % (Figure 23).

Transmission [%]

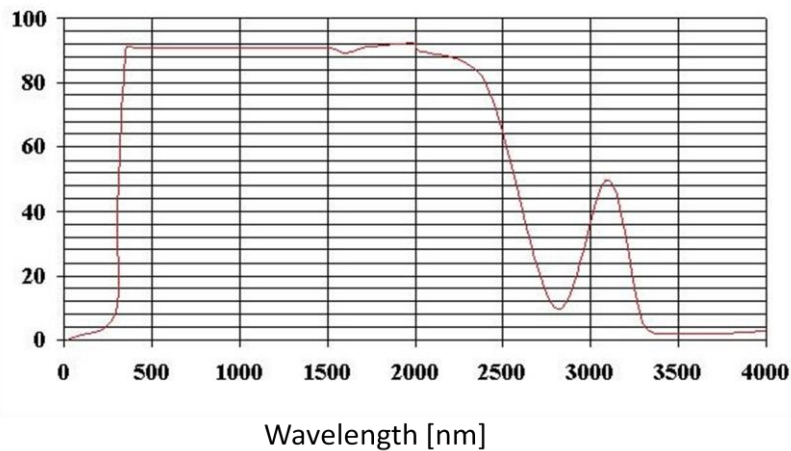


Figure 23 Borofloat transmission [Valleydesign]

The emitted light is radiated in all directions, therefore the light captured by the objective lens will depend on the distance of the lens to the channel and the size of the lens. The distance of the lens to the channel is equal to the focal length and was calculated in paragraph 3.4. The high NA of the objective lens results in a relative low attenuation:

$$A_{objective\ lens} = \frac{\text{lens area}}{\text{spherical light distribution at focus distance}} = \frac{\pi r_{lens}^2}{4\pi r_{focus}^2} = 0.18$$

After the objective lens, the light will have to pass one (or two) beamsplitter, a bandpass filter and a converging lens. Both the beamsplitters have a 90 % transmission, the bandpass filter will transmit > 90 % of the light within the passband and transmit only < 0.001 % of the light outside the passband. The total attenuation for the 525nm passband and the 405 nm laser band are calculated below.

$$A(\lambda) = A_{borofloat}(\lambda) \cdot A_{objective\ lens}(\lambda) \cdot A_{beamsplitter\ (2X)}(\lambda) \cdot A_{bandpass\ filter}(\lambda)$$

$$A(525\ nm) = 0.9 \cdot 0.18 \cdot 0.9 \cdot 0.9 \cdot 0.9 = 0.12$$

$$A(405\ nm) = 0.90 \cdot 0.18 \cdot 0.1 \cdot 0.1 \cdot 1 \cdot 10^{-5} = 1.6 \cdot 10^{-8}$$

The power at the photo detector ( $P_D$ ) is:

$$P_d(\lambda) = P_e(\lambda) \cdot A(\lambda)$$

For different Fluorescein concentrations the 525 nm fluorescence light at the fluorescence photo detector is calculated:

$$P_d(525\ nm, k = 1 \cdot 10^{-3}) = 2.62 \cdot 10^{-6} \cdot 0.12 = 314\ nW$$

$$P_d(525\ nm, k = 1 \cdot 10^{-5}) = 26.2 \cdot 10^{-9} \cdot 0.12 = 3.14\ nW$$

$$P_d(525\ nm, k = 1 \cdot 10^{-7}) = 262 \cdot 10^{-12} \cdot 0.12 = 31.4\ pW$$

The 405 nm laser power leaking into the fluorescence photo detector is:

$$P_d(405\ nm) = 1.5 \cdot 10^{-3} \cdot 1.6 \cdot 10^{-8} = 2.4 \cdot 10^{-11}\ W = 24\ pW$$

Since the photo detector noise (paragraph 5.5) is neglectable compared to the leaking light noise: the leaking light restricts  $\mu$ flow's limit of detection to  $k = 1 \cdot 10^{-7}$ , this concentration results in  $SNR = 1.3$  (only leaking light contribution). For a lower limit of detection the 405 nm leaking light has to be filtered by an additional lowpass filter (placed after the first beamsplitter).

### 5.3 Beads

Handling cells and dyes can be difficult and time consuming. Because a limited time is available for experiments, fluorescent polystyrene beads are used first. The same photon detectors and optic filters will be used throughout all experiments, this requires the emission spectrum of the beads to be similar to the dyes (paragraph 5.4). The diameter of the bead should be comparable to the stained cells. Eventually two different diameter beads with an emission of 460 nm were chosen. The two different sizes (2.5  $\mu$ m and 6  $\mu$ m) can mimic the difference between spermatozoa and larger cells and allows size recognition experiments.

The two beads specifications are listed below [Invitrogen 2001]:

- P12825 PeakFlow cytometry reference beads 2.5  $\mu\text{m}$  diameter, 3 mL,  $1.2 \cdot 10^8$  beads/mL
- P12826 PeakFlow cytometry reference beads 6  $\mu\text{m}$  diameter, 3 mL,  $1.7 \cdot 10^7$  beads/mL

## 5.4 Dyes

For the fluorescent detection of cells, the cells have to be labelled with a fluorescent dye. In the  $\mu\text{flow}$  a 405 nm violet laser is used. This wavelength is relatively new and therefore only a limited amount of dyes is available. The company Invitrogen offers two violet excited dyes that can be used for the combined detection of viability and vitality of cells. These dyes do not required fixed cells.

### 5.4.1 Viability indicator

The L34957 LIVE/DEAD Fixable Aqua Dead Cell dye kit [Invitrogen 2009] can be used for viability measures (membrane integrity). This dye kit uses a violet excitable dead cell dye with an emission of 526 nm. The fluorescent dye labels dead cells more brightly than living cells because the dye stains the cytoplasm of the cells that have lost membrane integrity (Figure 24).

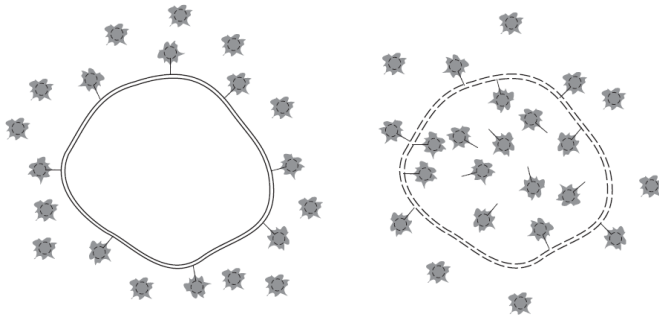


**Figure 24 principle of LIVE/DEAD Fixable Dead Cell dye kit. The dye only interacts on surface of living cells and yields low fluorescent (left). Dye reacts throughout volume of cell with compromised membrane, yielding highly fluorescent (right) [Invitrogen 2009].**

### 5.4.2 Vitality indicator

The C34858 CellTrace calcein violet, AM (Acetoxymethyl) [Invitrogen 2006] can measure the enzyme activity of cells and is an indicator of vitality. This dye kit uses a violet excitable AM dye with an emission of 440 nm. The AM dye can indicate the level of intercellular esterase activity of a cell. This is determined by the enzymatic conversion of the non fluorescent AM ester to a fluorescent dye that is retained in the cell. Vital cells are yielding highly fluorescent because of their high intracellular esterase activity.

The combination of the two dyes creates a robust violet excited live/dead assay. Viability and vitality of cells can be detected using only one violet laser.

## 5.5 Photo detector

A photo detector is capable of converting light into an electric current. The three most common photo detectors are: the photodiode, APD and the PMT.

### 5.5.1 Photodiode

The photodiode is a light sensitive semiconductor PN (P-type and N-type) junction. When light energy greater than the semiconductor material's bandgap strikes the junction, it excites electrons and generates holes. In contrast to the avalanche photodiode (paragraph 5.5.2) and photomultiplier (paragraph 5.5.3) the photodiode has no internal gain. For the detection of low intensity light an external amplification (op-amp) is needed. This amplification adds noise and therefore photodiodes are only used for high intensity light levels where limited external amplification is needed. In the  $\mu$ flow photodiodes are used in the PDIC for focus distance measurements and channel recognition since these applications operate at high intensity light levels. For fluorescence detection, extremely low light levels have to be detected (paragraph 5.2.1), at these light levels the photodiode and amplifier performances result in unwanted low SNR's (Figure 25). Therefore, photodiodes are not suitable for fluorescence detection [Kauffman 2000],[Kauffman 2005].

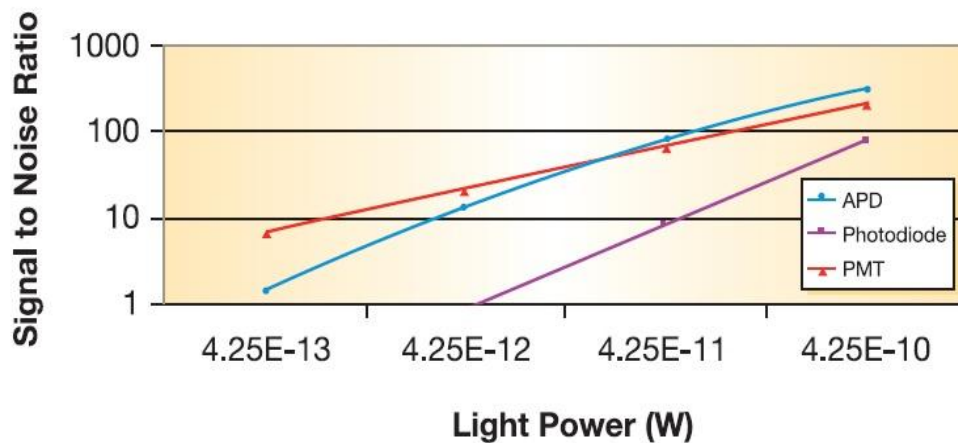


Figure 25 photo detectors SNR for different light powers, bandwidth 2 KHz (SNR of complete system including external op-amp amplification) [Kauffman 2005]

### 5.5.2 Avalanche photodiode

An APD consists just like a photodiode (paragraph 5.5.1) of a light sensitive semiconductor PN junction. By placing a reverse voltage on the PN junction, electrons are accelerated. Each time an electron collides with the crystal lattice an electron-hole pair is generated, this is called 'avalanching'. The avalanche effect amplifies the initial signal by a factor  $> 50$  [Kauffman 2000]. The avalanching effect creates more noise compared to a photodiode but less compared to an external amplifier. Therefore APD is used for low light levels where a photodiode in combination with an external amplifier produces too much noise. The use of an APD in the fluorescence detector of the  $\mu$ flow will result in a higher SNR compared to a photodiode (Figure 25). For extreme low light levels (photon counting) the APD's SNR is slightly lower compared to a PMT (paragraph 5.5.2), for intermediate light levels the APD's SNR can be higher compared to a PMT. Because of the high SNR at low light levels an APD would be suitable for fluorescence detection in the  $\mu$ flow [Kauffman 2000],[Kauffman 2005].

### 5.5.3 Photomultiplier

For extreme sensitive light detection, a PMT can be used. The PMT is a vacuum tube that generates electron-hole pairs on light exposure. Plates inside the tube accelerate the electrons almost noise free, which results in an internal gain  $> 10^5$ . The PMT has a high dynamic range and high SNR's for extreme weak light (Figure 25), however the quantum efficiency  $< 20\%$ , is low compared to (avalanche) photodiodes (quantum efficiency  $< 80\%$ ). Because of the large size, high price and the need for sensitive handling, the PMT is not suitable for the  $\mu$ flow [Kauffman 2000].

Recently, new semiconductor photomultipliers have been developed. Compared to the PMT these devices have a higher quantum efficiency, smaller size, lower operating voltages and lower prices. The company Hamamatsu offers a MPPC (Multi Pixel Photon Counter). This is a semiconductor photomultiplier made of multiple APD's that are operated at a reverse voltage higher than the breakdown voltage resulting in gains  $> 10^5$ . The APD's are arranged in a matrix of 100 (pixels), each pixel outputs a pulse when it detects one photon. The MPPC output signal is the sum of all the individual pixel signals. This semiconductor photomultiplier is at many points superior compared to an APD (Table 4) and is therefore chosen as fluorescence detector in the  $\mu$ flow[Hamamatsu].

### 5.5.4 Fluorescence detector

For the fluorescence detector a semiconductor photomultiplier was chosen: Hamamatsu S10362-11-100U. Specifications are shown in Table 4. For comparison and backup purposes an APD was bought: EG & G VACTEC C30902EH (Farnell: 1182339). This APD was bought because it was easy obtainable from the Farnell assortment. Specifications of both the MPPC and APC are shown in Table 4.

**Table 4 comparison of APD and semiconductor photomultiplier**

	Avalanche photodiode C30902EH	semiconductor photomultiplier S10362-11-100U
Wavelength (peak sensitivity) [nm]	830	440
Spectral response [nm]		320 – 900
PDE (Photon Detection Efficiency) [%]		45 (440 nm)
Fill factor [%]	100	61,5
Sensitivity	77 A/W	
Internal gain	$\approx 100$	240.000
Active area [mm <sup>2</sup> ]	0.2 (0.5 mm diameter, round shape)	1 (1 mm x 1 mm, squared shape)
Bandwidth [MHz]	800	10
Dark noise	15 nA	800 kcps (0.5 p.e.)
Operating voltage [V]	200	70
Package	TO-18 (5.3 mm can)	TO-18 (5.3 mm can)
Price [euro]	128	96

The peak sensitivity of the MPPC is closer to the wavelengths used for fluorescence detection in the  $\mu$ flow. Because of the high internal gain of the MPPC the sensitivity is more than 100 times higher compared to the APD and therefore less external amplification is required. Another important aspect is the active area of the sensor. The small active area of the APD makes alignment of the detector really difficult. APD's with a large active area are available but prices are proportional to the active area. The MPPC has a five times larger active surface and a lower price compared to the APD. Bandwidth of both detectors is more than sufficient. Both the MPPC and the APD require a high voltage supply for the reverse bias voltage.

The output signal of the MPPC is the sum of all the 100 APD pixels. When a photon is incident on one of the APD pixels a current pulse is generated. This current pulse is converted to a voltage pulse by a transimpedance amplifier (current to voltage amplifier). The shape and pulse height are the same for

every incident photon. By comparing the pulse with a threshold value of 50 % of the pulse height (notated as 0.5 p.e photon energy), the amount of incident photons can be counted with a comparator, these counts are usually notated as kcps (kilo counts per seconds). The pulse time is about 100 ns, during this time the MPPC pixels are not sensitive for any other incident photons. In case more than one of the APD pixels receives a photon instantaneously, the pulse height will increase proportional to the amount of activated pixels[Hamamatsu].

Just like any other semiconductor the MPPC generates noise due to thermal excitation, this noise is amplified by the reverse voltage. The MPPC cannot discriminate between pulses produced by photons or thermal noise. In Table 4 the thermal noise is called dark noise and is for the MPPC defined as the amount of pulses produced by thermal excitation. For higher light levels the dark noise can be reduced by choosing a higher comparator threshold of 1.5 or 2.5 p.e. At these comparator levels - that respectively count two or three activated pixels - dark noise is very unlikely and therefore the dark count will be lower. Dark noise measurement at different comparator thresholds are shown in paragraph 10.2. Dark noise can be further reduced by choosing a longer time span over which the photons are counted[Hamamatsu].

To speed up the experiments a MPPC module C10507-11-100U was bought. This module consists of: a MPPC photodiode, current to voltage converter, comparator circuit, high voltage power supply, temperature compensation circuit, counter and USB interface (Figure 26).

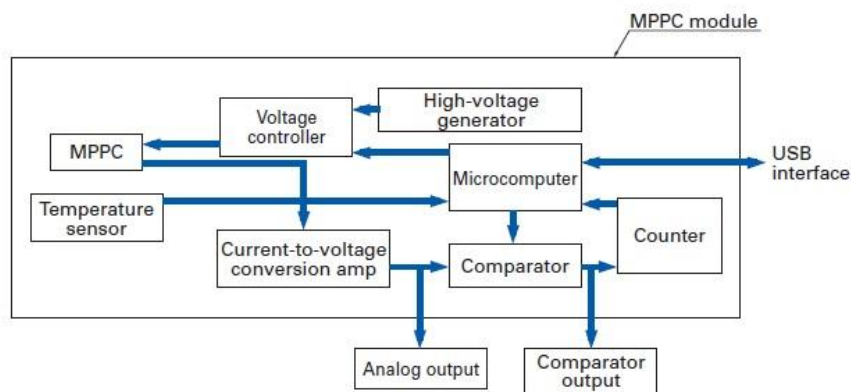


**Figure 26 MPPC module [Hamamatsu]**

The pulses generated by the MPPC are converted to a voltage by the transimpedance (current to voltage) amplifier. The voltage pulses are amplified, and the comparator compares the pulse height with a threshold voltage corresponding to one (two or three) incident photons. The amount of incident photons is counted and the counter values are sent to a computer via a USB interface. The MPPC gain is temperature and voltage dependent: when the temperature raises the gain at a fixed bias voltage decreases. To obtain a stable gain, the MPPC module is monitoring the temperature and adjusting the bias voltage continuously. The downside of this module is that it does not operate on Windows 7 and the module cannot be connected directly to a Labview program. The only way to connect the module to Labview is to use the digital counter output of the module. This digital output outputs the digital pulses from the comparator and can be connected to the Labview DAQ of the  $\mu$ flow (paragraph 7.1).

Besides the MPPC module, electronics for operating two MPPC's are built. These electronics are incorporated on the  $\mu$ flow's PCB (paragraph 8.5) and consist of: a transimpedance amplifier, voltage amplifier, comparator and counter. These electronics allow simultaneous detection at two fluorescence wavelengths.

### 5.5.5 Photon detection

The energy of a photon ( $e$ ) depends on the Planck constant  $h$  [ $\text{m}^2 \text{kg} / \text{s}$ ], speed of light  $c$  [ $\text{m}/\text{s}$ ] and the wavelength  $\lambda$  [ $\text{nm}$ ] [Wikipedia 2010].

$$e = \frac{hc}{\lambda}$$

The total number of incident photons at the MPPC ( $n_d$ ):

$$n_{i\_MPPC}(\lambda) = \frac{P_d(\lambda) \cdot \lambda}{hc} \text{ [photons/s]}$$

For a Fluorescein concentration of  $k = 1 \cdot 10^{-7} M$  (paragraph 5.2.1) the total number of incident photons at the MPPC:

$$n_{i\_MPPC}(525 \text{ nm}, k = 1 \cdot 10^{-7} M) = \frac{31.4 \cdot 10^{-12} \cdot 525 \cdot 10^{-9}}{6.63 \cdot 10^{-34} \cdot 3.00 \cdot 10^8} = 82.9 \cdot 10^6 \text{ photons/s}$$

The PDE (Table 4) indicates what percentage of the incident photons is detected by the MPPC. Each detected photon will result in one photon count:

$$n_{det\_MPPC}(525 \text{ nm}, k = 1 \cdot 10^{-7} M) = P_d \cdot n_{i\_MPPC} = 0.45 \cdot 82.9 \cdot 10^6 = 37.3 \text{ Mcps}$$

## 6 Fluidic chip

This chapter starts with an overview of the fluidic chip design. Next the channel find algorithm and digital marks are explained. At the end of the chapter the electrode configurations for the impedance detectors are discussed.

The fluidic chip design is based on the design described in Segerink[2010]. In Segerink[2010] three microfluidic channels were isotropically etched in a 500  $\mu\text{m}$  Borofloat glass substrate. The dimensions of the channels (18  $\mu\text{m}$  depth and 38  $\mu\text{m}$  in width) were chosen such that channel volume was as small as possible without clogging of particles [Segerink 2010]. Six holes for the inlets and outlets of the channels were powder blasted in the same substrate. For the impedance detection, planar platinum electrodes (200 nm thick and 20  $\mu\text{m}$  in width) were sputtered on a second 500  $\mu\text{m}$  Borofloat glass substrate; the two substrates were bonded together. Because the  $\mu\text{flow}$  will have to analyse beads with dimensions similar to spermatozoa, the microfluidic channel dimensions are chosen equal to those used in Segerink[2010]. Also the six inlets/outlet and electrodes connections are similar to [Segerink 2010], which allows using the same chipholder. However the design used in Segerink[2010] was optimized for impedance spectroscopy measurements, the  $\mu\text{flow}$  fluidic chip should allow for (automatic) fluorescence measurements. The fluidic chip design is therefore modified. For the automatic positioning of the optical pickup, digital marks are added to the chip (Figure 27); the digital marks are explained in paragraph 6.1.1. Since the electrodes mask had to be changed for the digital marks, this provided the opportunity for experimenting with a new electrodes configuration for impedance spectroscopy. The new electrodes configuration is explained in paragraph 6.2.

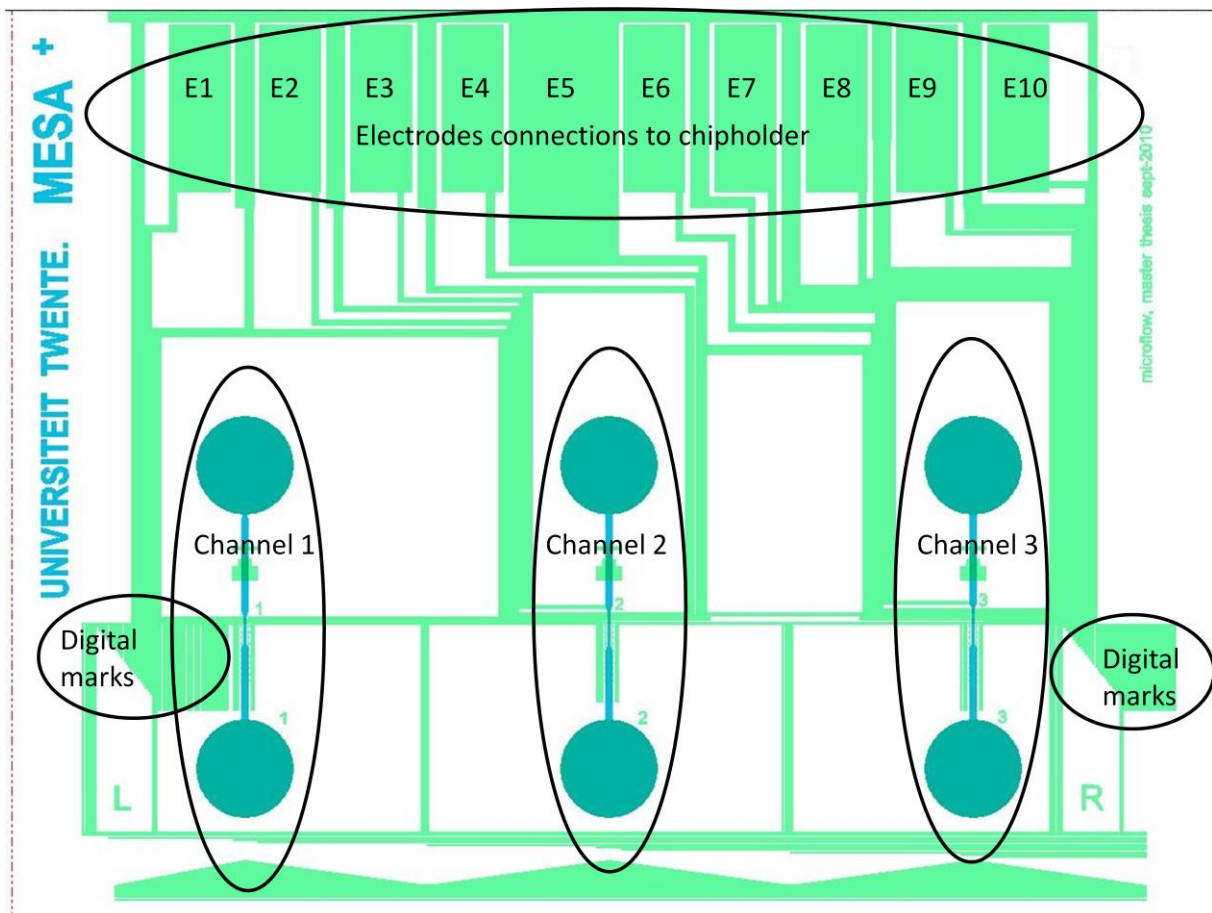


Figure 27 overview of the  $\mu\text{flow}$  fluidic chip

## 6.1 Channel finding

For the automatic positioning of the laser beam in the centre of one of the three fluidic channels a channel finding routine (Figure 28) is performed by the microcontroller. In this routine the laser is first focused on the digital mark layer (1). When the digital marks are in focus the slider moves the optical pickup/ laser across the chip surface. While moving, digital marks give the microcontroller information about the laser position relative to the chip (2). At some point a digital mark that indicates the beginning of a fluidic channel is detected (3). The optical pickup is stopped and will now be positioned somewhere between the start and end mark of the fluidic channel. The exact position of the laser is unknown since the stop time cannot be determined very accurately. For accurate positioning of the laser at the centre of the fluidic channel (4), the transverse VCA is used. First the laser is moved backwards by the transverse VCA until the channel start mark is recognized again. The transversal position and the vertical focus of this start mark are stored in the microcontroller's memory and send to Labview (paragraph 7.1). The laser is moved forward until the channel stop mark is recognized. The transversal position and the vertical focus of this stop mark are stored in the microcontroller's memory and send to the Labview program. The transversal and focus position of both the stop and start mark is known, therefore the centre position of the fluidic channel can be calculated by the microcontroller and the laser is moved into this position.

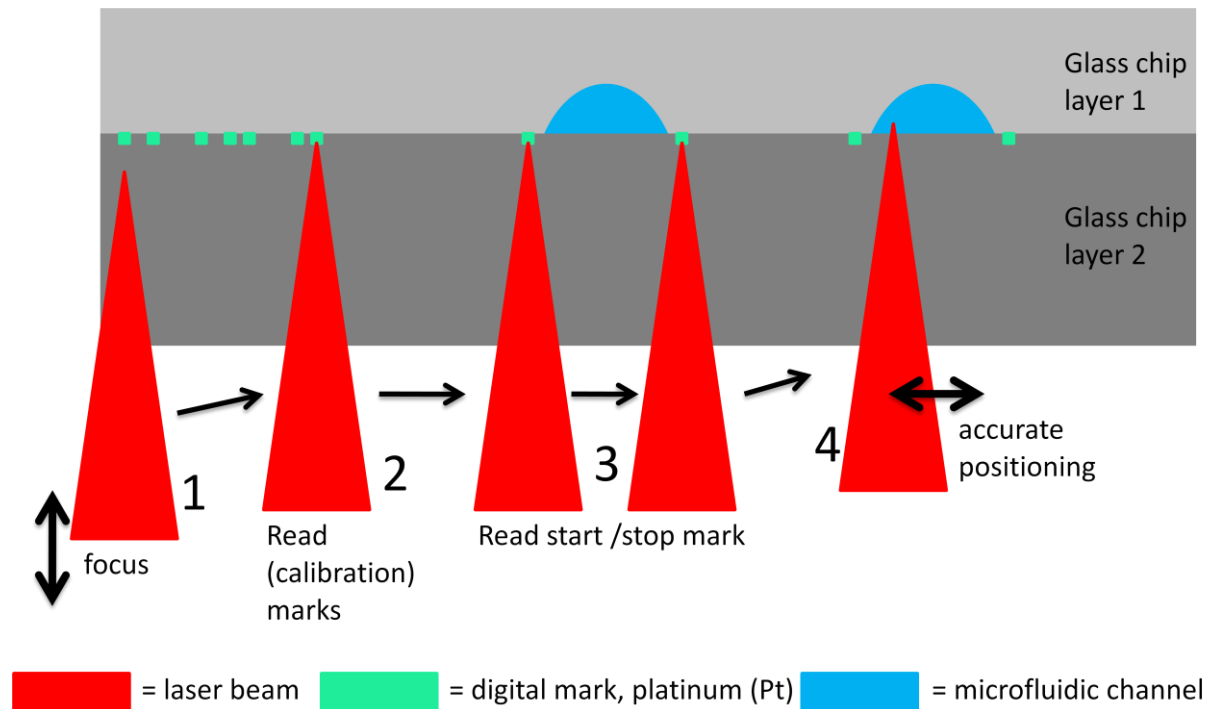


Figure 28 channel finding routine

6.1.1 Digital marks

Digital marks are used for the automatic positioning of the laser beam in the centre of the fluidic channel and to perform some automatic measurements. A digital mark is made of reflective platinum sputtered on the fluidic chip (this sputtered layer is also used for the impedance spectroscopy electrodes). When the laser passes across a digital mark, the reflected light is received by the PDIC.

A large variety of marks is placed on the fluidic chip. When the laser beam is moved across the fluidic chip, the marks that are shown in Figure 29 will be recognized.

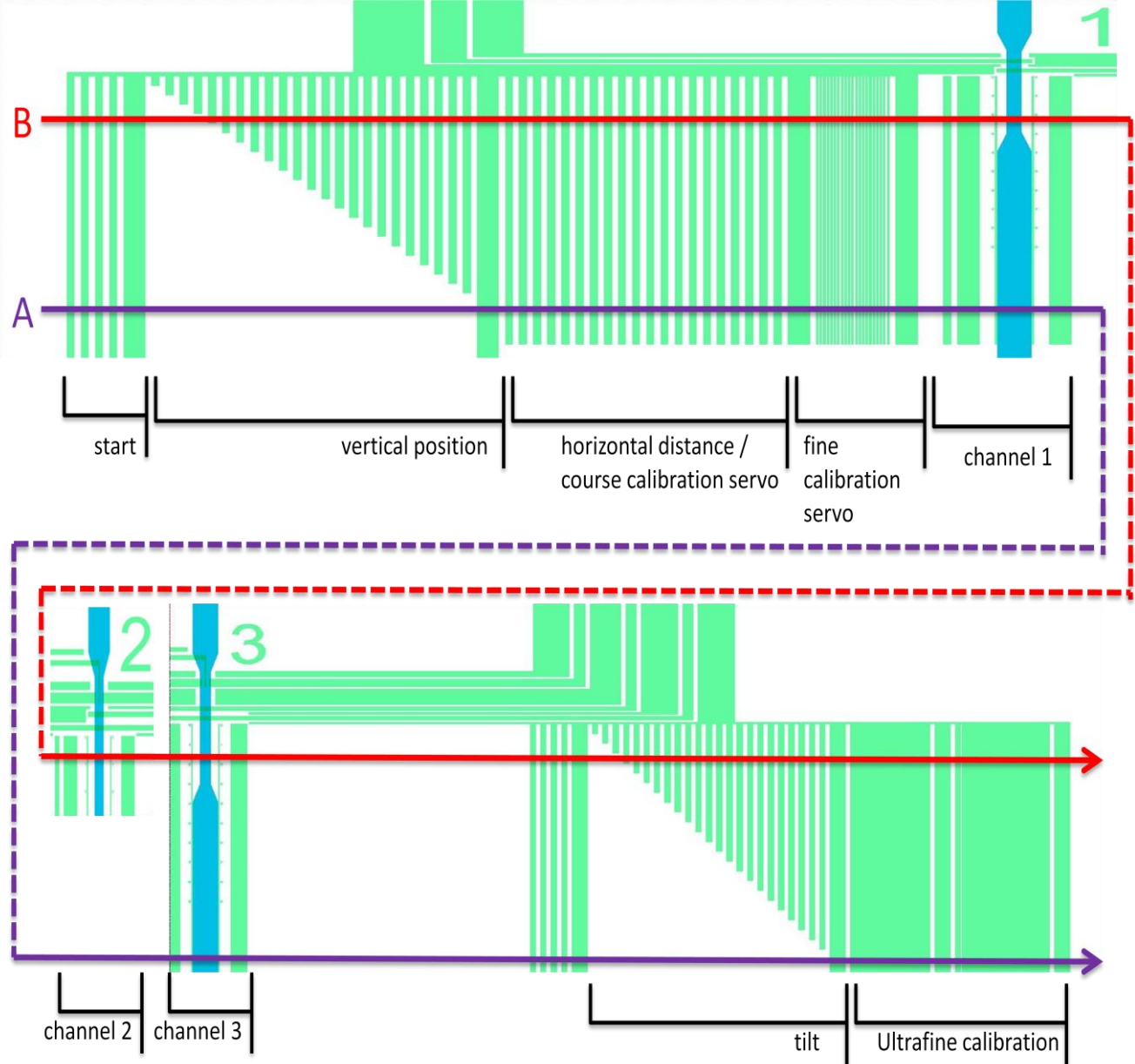


Figure 29 digital marks

## **Start**

The first mark is the 'start mark'; this mark consists of five reflective areas (4x 20  $\mu\text{m}$  and 1x 60 $\mu\text{m}$  in width). When the 'start mark' is recognized, the position of the laser relative to the fluidic chip is known. Differentiation between small and wider strokes is done by determination of the pulse time: the wider stroke produces a pulse lasting three times longer than a small stroke.

## **Vertical position**

The 'vertical position mark' gives information about the vertical position of the laser. When the laser passes the 'vertical position mark', the number of short pulses before a long pulse is counted. The amount of short pulses corresponds to the vertical distance relative to the impedance measurement area. When the laser moves at vertical position B (Figure 29), 19 short pulses are counted. In total 23 pulses could be counted when the laser was positioned next to the impedance detection area. Each count < 23 means that the laser is positioned 50  $\mu\text{m}$  further away from the impedance area. Nineteen counts (laser position B) corresponds to a distance of  $(23-19)*50 \mu\text{m} = 200 \mu\text{m}$  from the impedance detector. In the range of 18 to 23 counts the fluidic channel is 38  $\mu\text{m}$  in width. In the range 0 to 16 the fluidic channel is 100  $\mu\text{m}$  in width.

## **Horizontal distance calibration / course calibration servo**

From the start to the end of the 'horizontal distance mark', a distance of 880  $\mu\text{m}$  is covered. The amount of steps for the slide stepper motor to travel this distance is counted. This can be converted to  $\mu\text{m}/\text{motor step}$  to measure the horizontal displacement of the slider. This mark is also used for the course calibration of the servo. In the middle of the 'course calibration servo mark' the laser can be stopped. In this position the course calibrated of the servo is started: a microcontroller routine monitors the PDIC intensity (optical counting of 20  $\mu\text{m}$  spaced strokes) as a function of the transverse VCA control signal. This calibration can be used for optimizing the fluidic channel scanning by determining the linear range and gain of the transverse VCA.

## **Fine calibration servo**

The fine calibration of the servo makes use of the same principle as the course calibration. The calibration pattern is principally identical but contains reflective areas of only 5  $\mu\text{m}$  in width.

## **Fluidic channel**

The 'channel 1 start mark' consists of one short pulse and one long pulse, marking the point 100  $\mu\text{m}$  from the middle of fluidic channel one. Fluidic channel two and three 'start marks' consist of respectively two and three short pulses in combination with a long pulse.

## **Tilt**

This mark is identical to the 'vertical position mark' described earlier. The vertical position is compared to the first vertical measurement. If these measurements are identical, the fluidic chip tilt < 100  $\mu\text{m}$ .

## **Ultrafine calibration servo**

Next to the 'tilt detection mark', two 'ultrafine calibration marks' are located. These are identical to the 'fine calibration servo mark', but the reflective areas are respectively 2  $\mu\text{m}$  and 1  $\mu\text{m}$  in width. This section is only used for test purposes because the strokes are too small for the lithographic/etch process.

## 6.2 Impedance spectroscopy

Since the electrodes mask had to be changed for the digital marks, there was some room left for experimenting with a new electrodes configuration for impedance spectroscopy. In Segerink[2010] impedance measurements are performed using two electrodes. Since no differential measurement is performed, sensitive electronics (lock-in amplifier) have to be used. By using a reference impedance measurement using a differential measurement setup [Gawad 2001] the sensitivity could be improved. By using the configuration in Gawad[2001] the detector volume is doubled. For high semen concentrations this results in unreliable sperm count because the chance that more than one cell is present in the detector volume is significant. A possible solution is to perform the differential impedance measurement in the channel width (Figure 30). Electrodes E2 and E4 are driven with a differential AC voltage. By adding a measurement electrode E3 in between E2 and E4 this is acting as a voltage divider. When no particles are present in the channel the two impedances will be equal and the measurement electrode will be 0 V. When the resistance changes, because a particle passes, a voltage is measured. By measuring the voltage sign, the transversal position of particles can be determined. However, in this configuration the electrodes are spaced close to each other, which results in a small measurement volume (small part of the channel is covered) and the frequency response of the electrodes is shifted to higher frequencies.

Besides the differential measurements a two electrodes impedance measurements [Segerink 2010] was incorporated on the chip (Figure 30). This combination of two detectors allows for standard testing using the two electrodes setup and transversal position detection using the differential setup. In channel 3 these two impedance measurements are spaced further away to minimize interference.

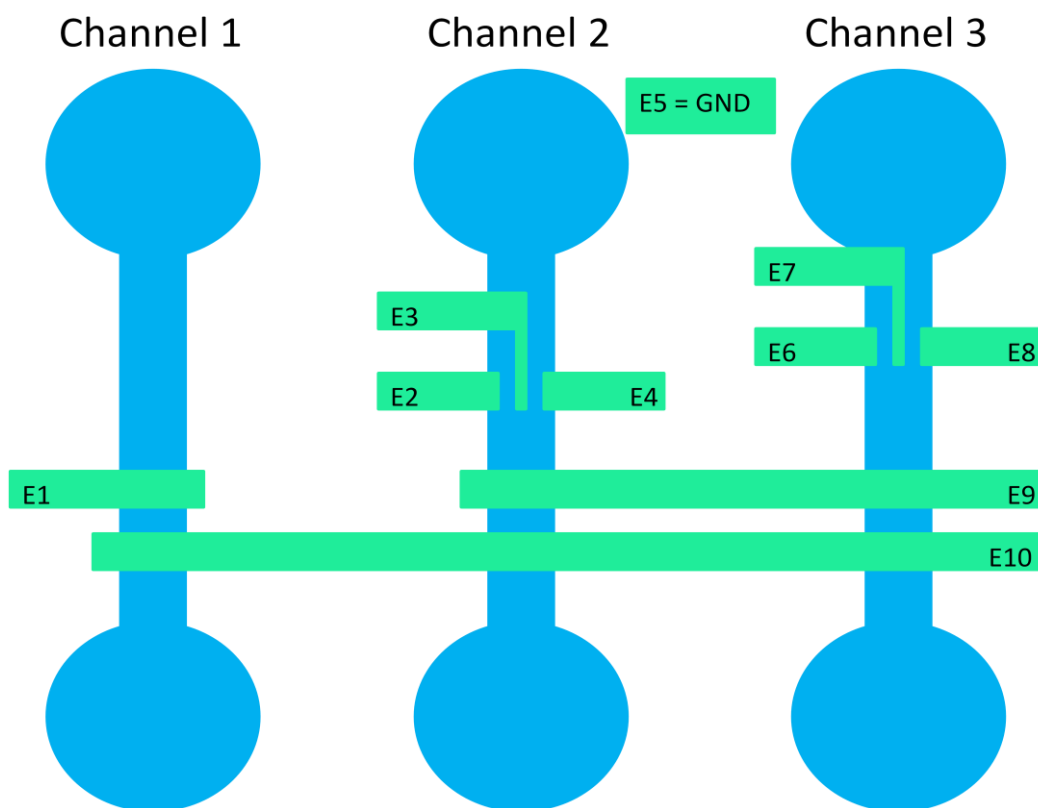


Figure 30 electrodes configuration

To reduce parasitic capacitance between the electrodes a grounding electrode is placed in between most of the electrodes Figure 28 (grounding between electrodes is not shown in Figure 30)



## 7 Software

The software part of the  $\mu$ flow consists of a Labview GUI (graphical user interface) and a microcontroller program.

### 7.1 Labview GUI

The GUI of the  $\mu$ flow is build in Labview (2010 SP1). The GUI provides control of the complete  $\mu$ flow and measurements are displayed in real time. Two physical devices are controlled by the GUI: the microcontroller (located on the  $\mu$ flow PCB) and the DAQ (data acquisition card), both devices are shown in Figure 31.

Most of the optical pickup functionalities, slider, PDIC and the fluorescence/impedance detectors, are controlled and configured by the microcontroller. These functionalities require fast timing which cannot be provided by the DAQ. The DAQ is used for data acquisition of the fluorescence/impedance detectors and generates waveforms for channel scanning.

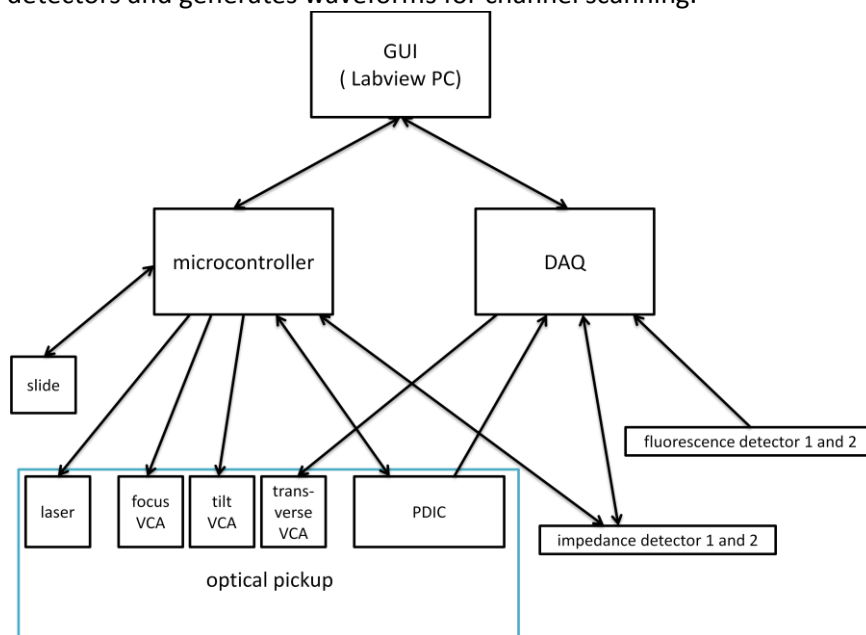


Figure 31 GUI control diagram

Before fluorescence measurements can be started, the find channel routine has to position the laser at the centre of a microfluidic channel. This is all controlled by the microcontroller GUI (Figure 32). Focus profile, channel finding and measurement are three separated blocks in the microcontroller GUI. These three microcontroller routines can be started by pressing the button at the top of the blocks. Parameters can be controlled by the knobs and sliders. Indicators visualize transversal position and the vertical focus of the recognized digital marks.

The functionalities of the microcontroller GUI are described using Figure 32.

- A : start button for focus profile routine
- B: com port selection for the USB to serial converter
- C: shows the transversal position and the vertical focus of the focus point at the start and end of the chip (focus profile)
- D: shows the vertical distance between the laser and the impedance measurement area (paragraph 6.1.1). This functionality is not working yet.
- E: configuration parameters for the auto focus system (chapter 4). PDIC gain set the gain of the PDIC (paragraph 8.1).
- F: fluidic channel selection (channels 4-7 are test modes)

- G: shows the transversal position and the vertical focus of the focus point at the start and end of the channel (channel positioning)
- H: laser power and colour
- I: configuration parameters of the digital mark recognition.
- J: bandwidth of the two MPPC's and the scaling factor to convert the photon count to a DAC voltage.
- K: p.e. selection for the two MPPC's
- L: programmable gain amplifier for the impedance detectors.

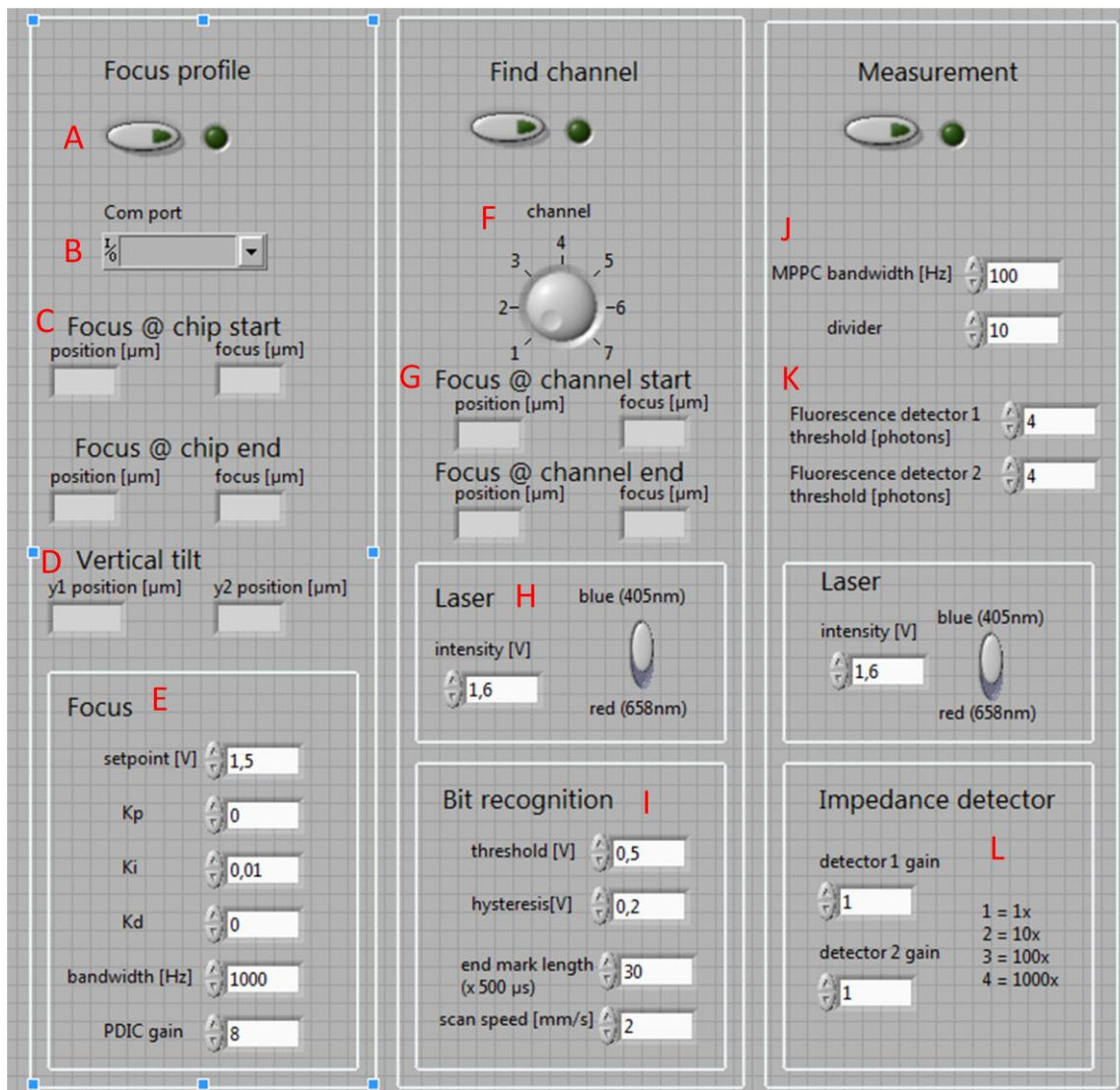


Figure 32 microcontroller GUI

The waveform GUI (Figure 33) controls the waveform generation of the DAQ. Waveform mode 1 (Figure 33: left) allows scanning in one direction (transverse or focus). Waveform mode 2 (Figure 33: right) allows scanning in two directions (transverse and focus simultaneously). For the transverse direction a sinus waveform is generated, for the focus a staircase with a step time equal to half of the transverse period. This allows a two dimensional slide through of the microfluidic channel.

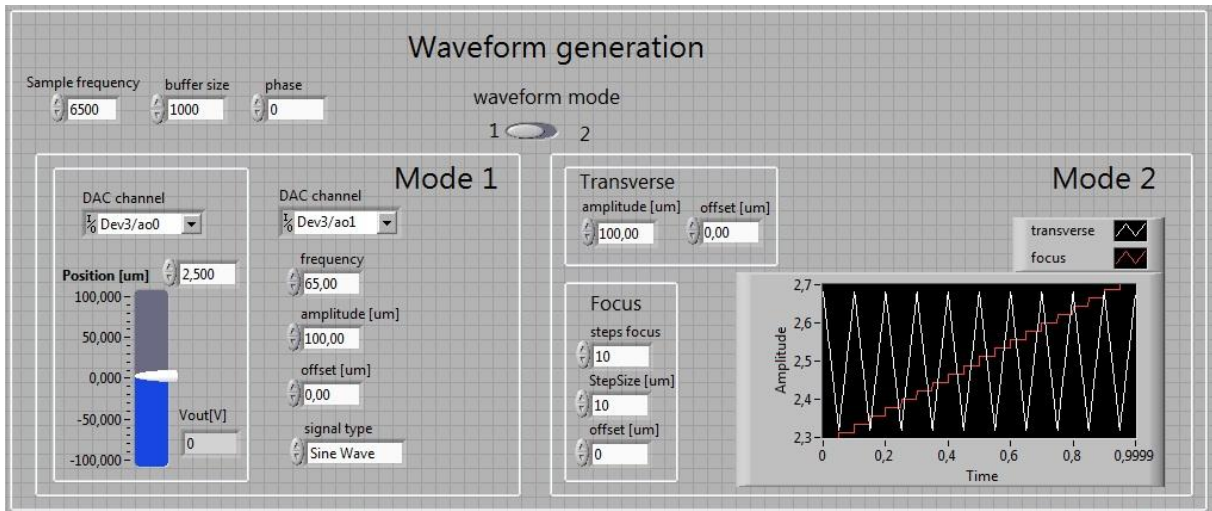


Figure 33 waveform generation GUI, scanning in one direction(left), scanning in two directions (right)

The sampling of the fluorescence/impedance detectors and the PDIC is also performed by the DAQ. All signals except for the fluorescence detectors are sampled using ADC's, for the fluorescence detector, digital counters for the photo counting are sampled. Visualisation is performed using standard graphs or using intensity graphs. Intensity graphs show the fluorescence during a measurement at each point inside the fluidic channel. This allows for easy visualisation of particles inside the channel. A 2D image of the fluidic channel (using waveform mode 2) can also be visualized by an intensity graph.

## 7.2 Microcontroller

Most of the  $\mu$ flow microcontroller program is shown in appendix 4. In this paragraph only the main flowchart is described, some terms are explained first:

- Macro = subprogram of the main program
- USART (Universal asynchronous receiver/transmitter) = receiver/transmitter for the USB communication between the microcontroller and Labview GUI
- Interrupt = program is paused by external trigger such as the USART

### 7.2.1 Main

The  $\mu$ flow program starts at the begin mark in the main flowchart, shown in Figure 34. First the  $\mu$ flow functionalities are disabled and the DAC voltage outputs are initialized by the initialize macro. The USART is enabled and produces an interrupt when a string that contains the  $\mu$ flow settings is sent by Labview. When no interrupt is produced update=0 and mode=default (0x30). When Labview sends a string with  $\mu$ flow settings, the update variable becomes high and the string is received and stored in the microcontroller memory. An acknowledge string is sent back to Labview to confirm that all data is transferred correctly (in Labview a green indicator will now lighten up). Depending on the settings that have just been sent from the Labview program, the microcontroller will start: focus profile (mode 0x31), find channel (mode 0x32) or measurement (mode 0x33). Normally a focus profile is required before a fluidic channel can be found therefore the focus profile routine (mode 0x31) will be explained first. During focus profile the DAC voltages, PID/laser/gain parameters are updated in the load findchannel macro. Subsequently the focus profile macro is started; this macro finds the focus profile of the fluidic chip and sends the data (transversal position and the vertical focus of the two focus points) back to Labview.

When the focus profile routine is finished, a channel can be selected in Labview. The channel information is sent to the microcontroller and the find channel routine (mode 0x32) is started by the microcontroller. The DAC voltages and other parameters are updated first in the load findchannel macro. Subsequently the find channel macro is started, which will position the laser in the centre of the selected fluidic channel (transversal position and the vertical focus of the start/end focus points is sent back to Labview).

When the laser is positioned in the centre of the fluidic channel, a fluorescent measurement can be started by Labview. Data for the fluorescence measurement is sent to the microcontroller and the fluorescence measurement routine (mode 0x33) is started by the microcontroller. First the laser intensity and MPPC update ration/gain are updated by the load fluorescence macro. Afterwards the MPPC measurement is started by the MPPC macro.

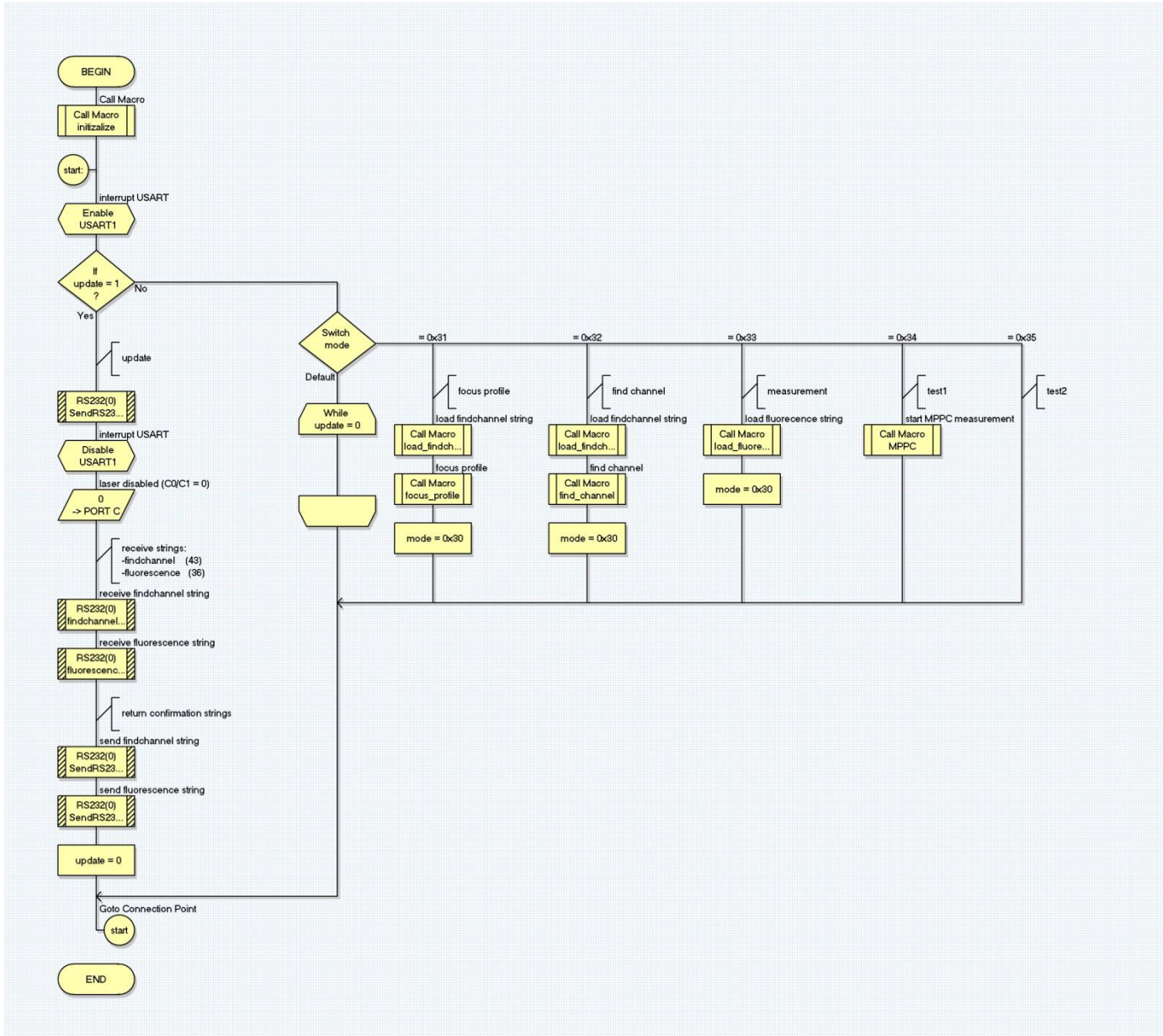


Figure 34 main flowchart

## 8 Electronics

In this chapter the electronics are described. The electronics are incorporated on a PCB (printed circuit board). The final PCB design is shown in Figure 35. Before this PCB was tested a first and second design (Figure 68, 74) were developed. The PCB design and all the schematics in this chapter have been created using the PCB design software EAGLE. The final PCB -shown in Figure 35- is divided into four parts: the main PCB (left side), two identical PCB's for the MPPC's and transimpedance amplifiers (1) and one PCB for the impedance spectroscopy electrodes (7). Manufacturing and cutting one large PCB reduces cost and development time.

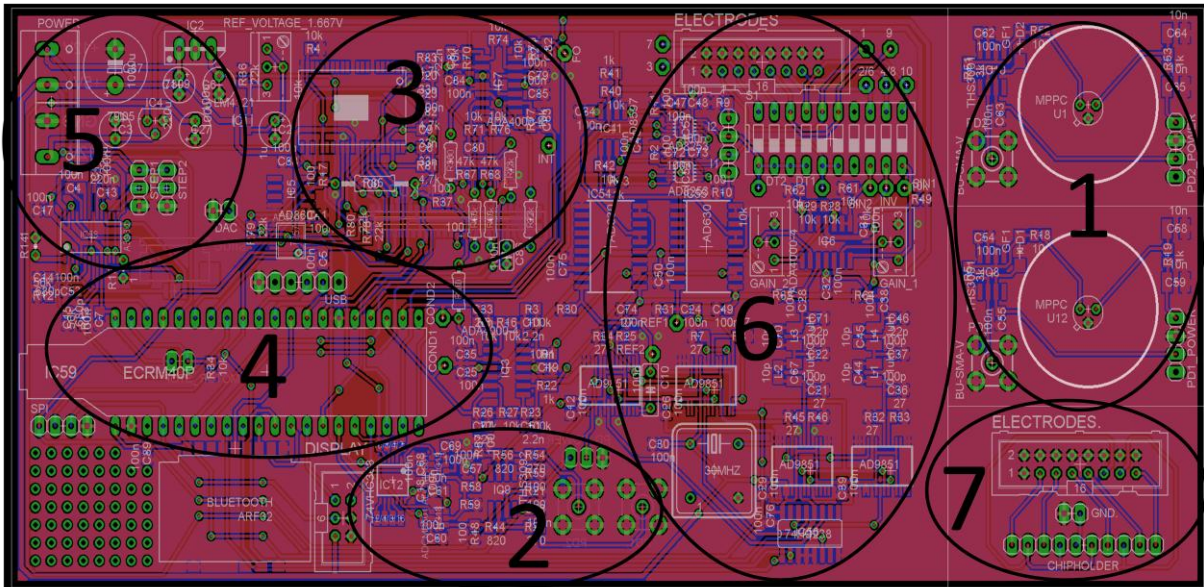


Figure 35 final PCB: MPPC's and transimpedance amplifiers (1), MPPC amplifiers, comparators and dividers (2), optical pickup interface and VCA drivers (3), microcontroller, DAC and USB (4), power supply and slide motor driver (5), DDS and impedance detectors (6), connector for impedance spectroscopy electrodes (7)

### 8.1 PDIC

The PDIC is a triple wavelength photo detector IC with integrated amplifiers and control circuit. Its 20 photo detectors are optimized for the detection of 405 nm, 650 nm and 780 nm wavelengths. In the  $\mu$ flow only the 405 nm detection is used. The gain of the internal detectors is controlled by two digital lines (SW1 and SW2). The sensitivity and bandwidth for the different gain modes are specified in Figure 36.

HD-DVD / Blu-Ray® / DVD Mode (SW0 = H) Detector-Pattern 1														
Gain Mode			A, B, C, D				E, F, G, H				RFP / RFN			
No	SW1	SW2	Sens. [mV/uW]		BW [MHz]		Sens. [mV/uW]		BW [MHz]		Sens. [mV/uW]		BW [MHz]	
			405nm	650nm	min.	typ.	405nm	650nm	min.	Typ.	405nm	650nm	min.	typ.
1	L	M	0.23	0.45	80	100	0.56	1.125	60	80	0.15	0.3	110	120
2	L	M	0.45	0.9	80	100	1.125	2.25	60	80	0.3	0.6	110	120
4	M	L	0.9	1.8	80	100	2.25	4.5	60	80	0.6	1.2	110	120
8	M	M	1.8	3.6	80	100	4.5	9	60	80	1.2	2.4	110	120
16	M	H	3.6	7.2	80	100	9	18	60	80	2.4	4.8	110	120
32	H	L	7.2	14.4	80	100	18	36	45	60	4.8	9.6	90	110
64	H	M	14.4	28.8	65	80	36	72	30	50	9.6	19.2	70	90
128	H	H	28.8	57.6	45	55	72	144	20	35	19.2	38.4	45	55

Figure 36 PDIC sensitivity and bandwidth at different internal gains (Melexis 2007)

In this figure the A,B,C and D detectors are used for the focus error signal. The RFP and RFN output are used for the intensity/data signal and are defined as:  $RFP = A + B + C + D$ ,  $RFN = -(A + B + C + D)$ .

The maximum output range of the intensity output (RFP-RFN) was found in the datasheet of the PDIC [Melexis 2007],  $RFP - RFN = [0 \text{ V} \dots 3 \text{ V}]$ . Because the ADC has a range  $[0 \dots 3.3\text{V}]$  an amplification of 1.1x will cover the complete range of the ADC. For the channel find algorithm the PDIC intensity should recognize digital marks. These marks are  $20 \mu\text{m}$  in width and have to be read at a slider speed of  $2 \text{ mm/s}$ , a lowpass filter with a cutoff frequency of  $100 \text{ Hz}$  filters the high frequency noise. The resulting differential to single converter is shown in Figure 37.

The focus error signal (FES) was amplified 4x (Figure 37), resulting in an output signal range of  $[-5 \text{ V} \dots 5\text{V}]$ . In the next amplifier stage the signal is DC shifted and amplified to the ADC range  $[0 \dots 3.3\text{V}]$ . A zenerdiode of  $3.3\text{V}$  protects the ADC for over voltages. At an operation speed of  $2 \text{ mm/s}$ , the focus error signal should integrate over  $40 \mu\text{m}$ . The focus error signal is therefore lowpass filtered with a cutoff frequency of  $50 \text{ Hz}$ .

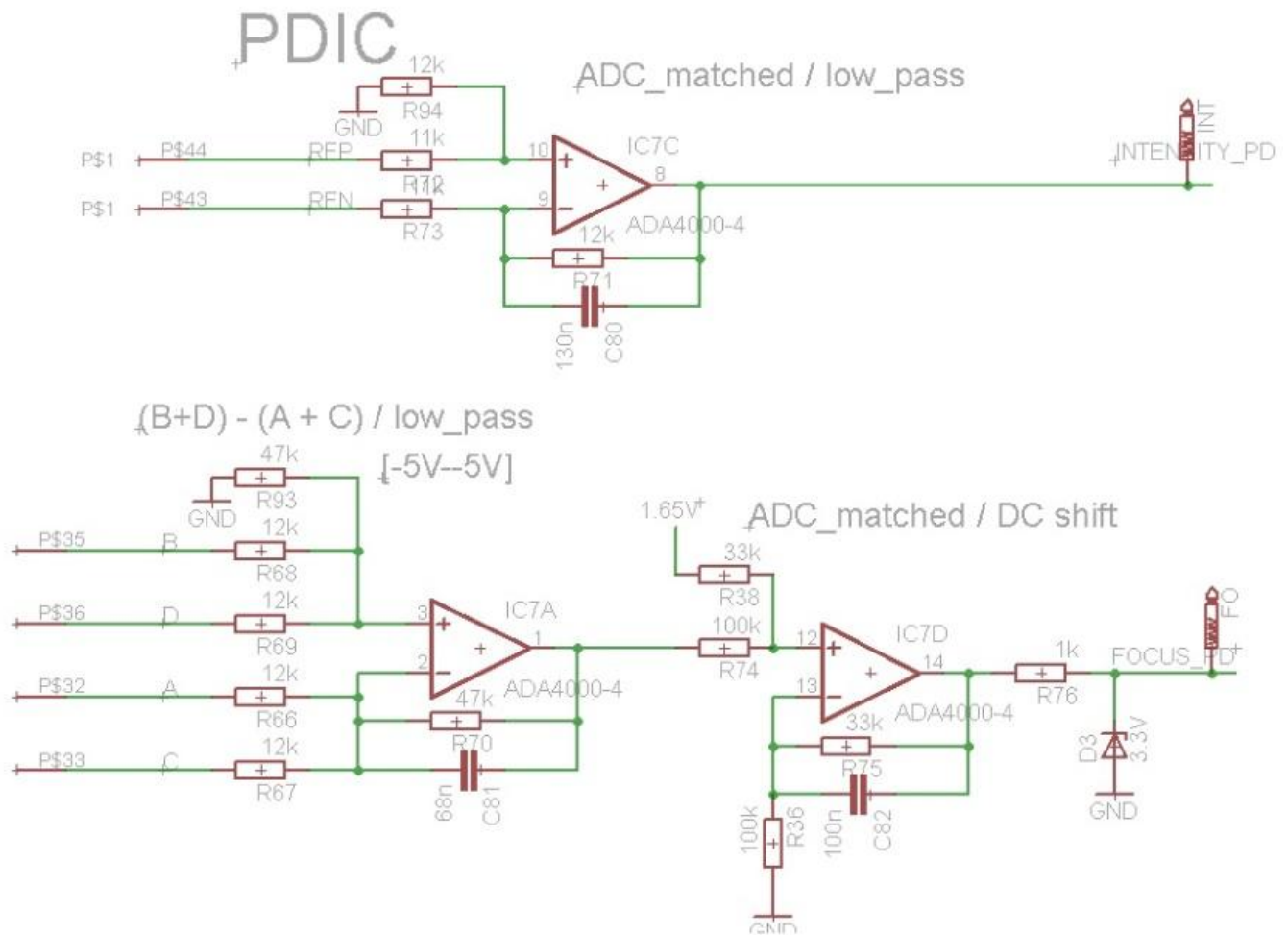


Figure 37 PDIC electronic interface, intensity (upper part), FES (lower part)

## 8.2 VCA driver

For driving the focus-,transverse- and tilt VCA's a high power amplifier is needed. To reduce the complexity of the PCB an IC with build in power amplifiers was preferred. For this purpose the IC used for the VCA driving inside the optical pickup player was reused, in fact an identical and new IC was ordered. This IC (R2S3028) has the required three integrated power amplifiers, however datasheets were almost unobtainable. The available data is shown in Figure 38.

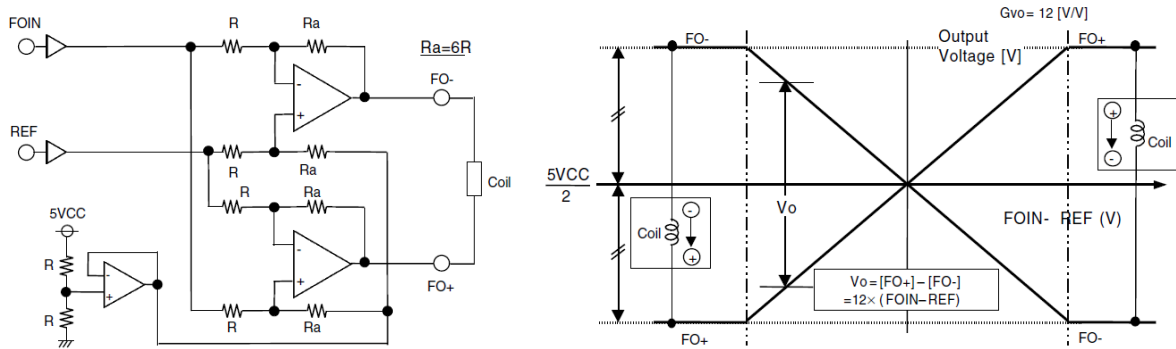


Figure 38 VCA driver schematic (left), transverse function (right) [Renesas 2003]

The desired range for the voice coil actuators is  $\approx 1\text{mm}$ . This range requires a VCA driving voltage of  $\approx 1\text{V}$  (paragraph 9.2). However from Figure 38 can be seen that the internal gain is  $12\text{ V/V}$  while the DAC which is the input of the VCA driver has a range of  $5\text{ V}$ . For the highest VCA resolution, the complete DAC range should be used; therefore the signal of the DAC is attenuated first.

The calculation of the attenuation circuit (Figure 39) is based on the focus actuator.

The focus actuator gain =  $911\ \mu\text{m/V}$  (paragraph 9.2).

Amplification =  $12 * 1 / (1 + 47) = 0.25$  (attenuation is  $4\times$ )

Resulting gain =  $227\ \mu\text{m/V}$

Besides the DAC, also the Labview DAQ card can control the VCA driver (Figure 39). This results in a combined control of the  $\mu\text{flow}$  DAC ( $\mu\text{flow}$  microcontroller) and the DAQ (Labview).

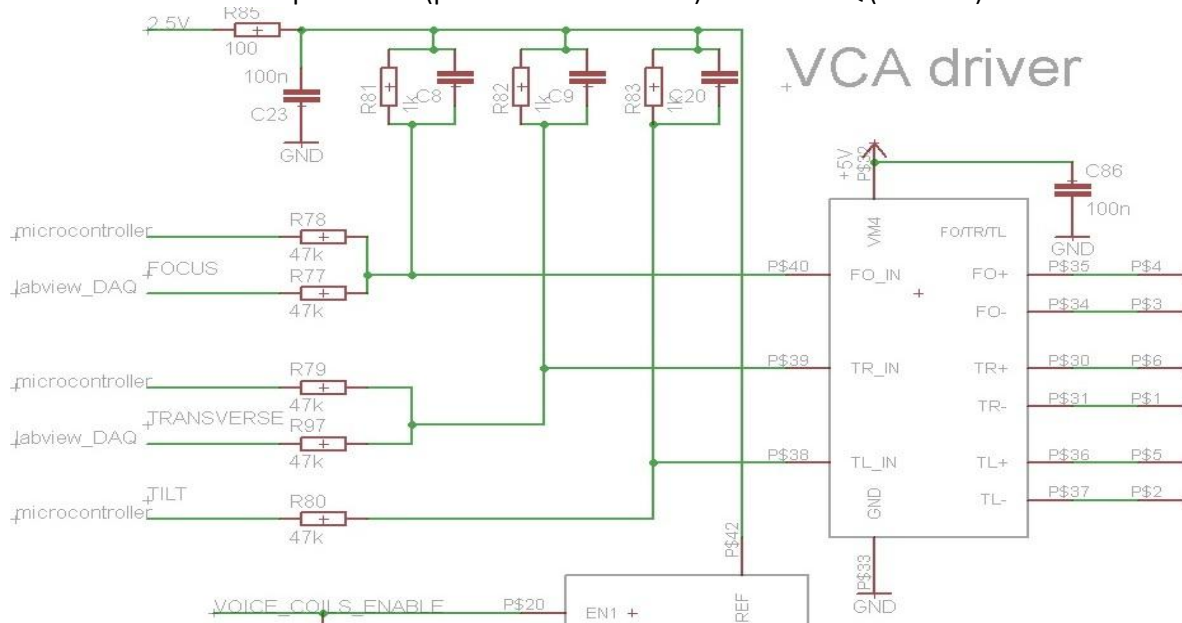


Figure 39 VCA driver interface

Driving the focus actuator:

$V_{\text{control}} = 0\text{V}$  objective lens goes up in vertical direction

$V_{\text{control}} = 2.5\text{V}$  objective lens in centre position

$V_{\text{control}} = 5\text{V}$  objective lens goes down in vertical direction

Driving the transverse actuator:

$V_{\text{control}} = 0\text{V}$  objective lens to end of chip direction

$V_{\text{control}} = 2.5\text{V}$  objective lens in centre position

$V_{\text{control}} = 5\text{V}$  objective lens to start of chip direction

The tilt actuator is not used at the moment.

### 8.3 Microcontroller and DAC

Most of the optical pickup functionalities, slider, PDIC and the fluorescence/impedance detectors are controlled and configured by the microcontroller. Because limited time is available for writing a microcontroller program, the visual programming language Flowcode (paragraph 7.2) by MatrixMultimedia is used. This company does also supply microcontroller development boards that have an integrated USB interface for easy data transfer. Since the  $\mu\text{flow}$  routines requires advanced floating point measurements and high speed operation, the fastest available development board was chosen: the ECIO ARM [MatrixMultimedia 2010]. This development board is based on a 32 bit ARM7 processor AT91SAM7S128 [ATMEL 2010]. The microcontroller development board is placed on the  $\mu\text{flow}$  PCB (Figure 35).

Because the microcontroller cannot generate accurate analog output signals (only PWM outputs) a DAC (digital to analog converter) is needed. For this purpose the AD5668 DAC was chosen. This DAC is programmable using a serial interface, which saves I/O lines on the microcontroller (vacant I/O's are badly needed for other purposes). Eight DAC channels available for: focus VCA, transverse VCA, MPPC1 threshold, MPPC2 threshold, MPPC1 output, MPPC2 output and reference voltages. Moreover AD5668 internal 2.5V voltage reference is used for the VCA driver biasing. The settling time of 2.5  $\mu\text{s}$  and 16bit accuracy are sufficient.

### 8.4 Slide control

For large displacements  $> 1$  mm the optical pickup slides across a rail using a stepper motor. For high accuracy positioning of the optical pickup a special stepper motor driver is needed. For this purpose the A3980 micro stepping driver is chosen because it allows micro stepping: each stepping sequence is divided into 64 micro steps. This reduces vibrations and allows accurate displacements. Because no information was available about the slider and stepper motor, the optical pickup displacement per micro step was determined experimentally. For an optical pickup displacement of 30mm, 3200 microsteps were needed. This results in 9.4 $\mu\text{m}$  / micro step.

The stepper motor requires 320 micro steps for one revolution, at each revolution the optical pickup moves  $\approx 3$  mm.

### 8.5 MPPC

The two MPPC's are supplied using the high voltage of the MPPC module (paragraph 5.5.4), this module supplies a 70 V reverse bias (temperature compensated). The current pulses produced by the MPPC are converted to a voltage by the THS3001 transimpedance amplifier. The gain of this amplifier is defined by the feedback resistor R5, Figure 40 (left). This transimpedance amplifier is mounted on a separate PCB close to the MPPC to reduce noise. A coax cable connects the output of the transimpedance amplifier to the main PCB. At the main PCB the signal is amplified using a voltage amplifier with a gain of 3. The output of the voltage amplifier is connected to a comparator which compares the pulses with a reference voltage corresponding to 0.5/1.5/2.5/3.5 p.e. (photon energy) The generated pulses are only 5 ns long [Hamamatsu]this short pulse could be problematic for the digital counters of the microcontroller. Therefore digital dividers with a selectable division ratio of 2,4,8 or 16 are placed after the comparators. After which two 32-bits counters of the microcontroller count the pulses in a certain time interval.

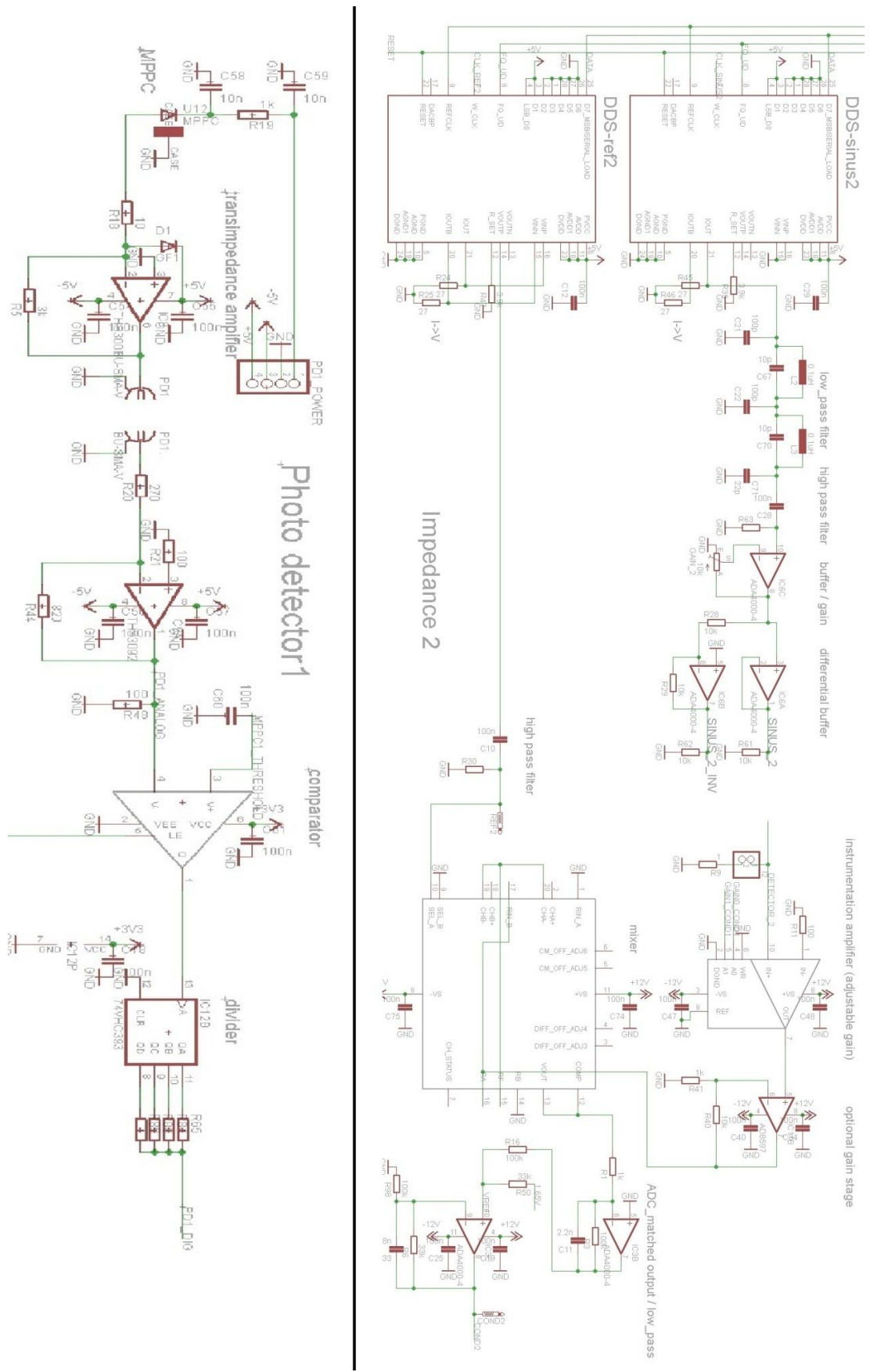


Figure 40 MPPC fluorescence detector electronics (left), impedance spectroscopy electronics (right)

## 8.6 Impedance spectroscopy

In Segerink[2010] a measurements frequency of 96 KHz was used since a resistive plateau of the electrode configurations was present at this frequency and cells are acting as insulating particles for frequencies  $> 1$  MHz. Apart from the electrodes configuration used in Segerink[2010], a new electrodes configuration with smaller electrodes will be tested, it is expected that for smaller electrodes a higher measurement frequency is required. Therefore the new electrode configuration requires an adjustable frequency generator with a differential output signal. A standard frequency generator could be used for this purpose but this option is difficult to miniaturize. A compact solution is to use a dedicated frequency synthesizer IC. For this purpose the AD9851 DDS (Direct Digital Synthesis) IC is chosen. This IC generates a 10 bit sinus using a wavetable, frequency and phase are adjustable. The DDS signal is filtered by a bandstop filter for removing the 180 MHz digital clock and filtered by a high pass filter for removing offset, both filters are shown in Figure 40 (right) and were simulated in LTspice IV. The filtered DDS signal is amplified to a single or differential output for respectively the single and differential impedance measurements.

For the impedance detection in the two electrodes configuration the measurement current is converted to a voltage by resistor R9 in Figure 40 (right). In the three electrodes (new) configuration, the output voltage is directly converted by the instrumentation amplifier. The gain of this amplifier (1x, 10x, 100x or 1000x) can be digital adjusted by the microcontroller. A second (optional) amplifier amplifies the signal 10x before the lock in amplifier multiplies the signal with a reference signal. The reference signal is produced by a second DDS IC, this IC generates the same measurement frequency - the phase however can be adjusted. The output of the lock-in amplifier is filtered and a level shifter produces an output of [0-3.3 V] for the microcontroller ADC.

The impedance detector and frequency generator is build in twofold, the detectors can be used at different frequencies.

## 9 Functional tests

In this chapter some functional tests are performed with the optical pickup. First the illumination power of the laser is measured; afterwards the VCA's are characterized and the PDIC response at the bottom of the channel is analyzed.

### 9.1 Illumination power

For estimating the fluorescence absorption of particles/fluids, the illumination power of the laser has to be known first. In the following test the illumination power of the laser is measured at the output of the objective lens. In Figure 41 the illumination power of the 405 nm and 660 nm lasers are measured as a function of the driving voltages. The 660 nm laser diode stopped working at illumination powers  $> 350 \mu\text{W}$ .

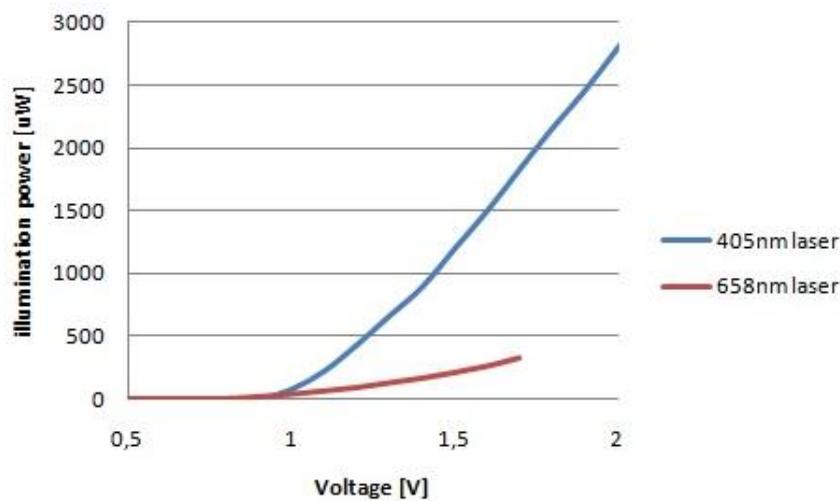


Figure 41 laser illumination power, measured after objective lens

### 9.2 Voice coil actuator (VCA)

By using a laser Doppler vibrometer the vibration amplitude and frequency of a surface can be measured by extracting the Doppler shift of a laser beam directed on that surface [Wikipedia 2011]. The frequency response of the focus and transverse VCA was measured using such a laser Doppler vibrometer. The magnitude and phase responses are shown in Figure 42 and Figure 43.

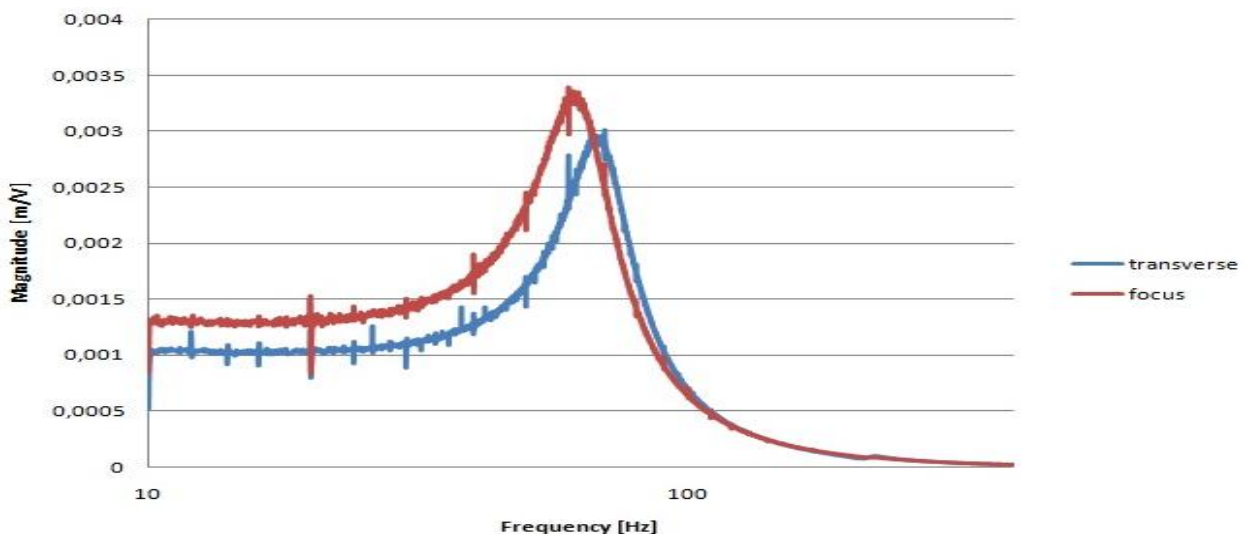


Figure 42 VCA transfer function, magnitude (Polytec MSA-500 Micro System Analyser laser Doppler vibrometer)

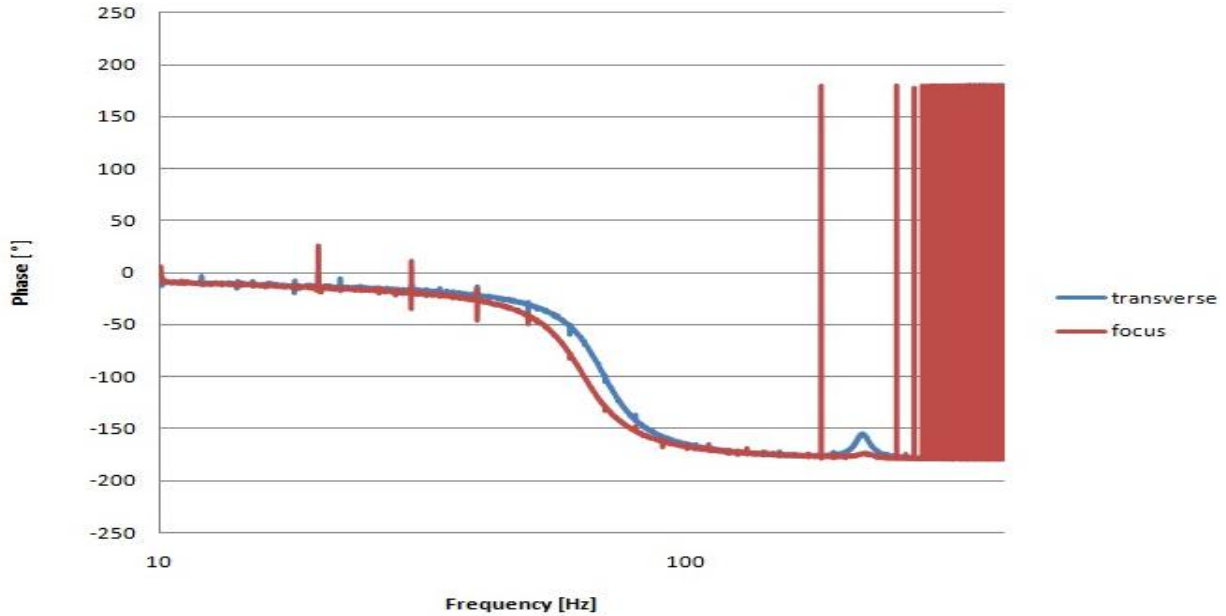


Figure 43 VCA transfer function, phase (Polytec MSA-500 Micro System Analyser laser Doppler vibrometer)

The phase plot indicates the order of the system, a phase shift of  $180^\circ$  shows that a system is at least a second order. Both VCA responses are therefore at least second order systems. The strange behaviour of the focus-VCA phase response for frequencies  $> 180$  Hz is probably caused by the low magnitude of the signal. Increasing the measurement resolution could possibly solve the strange behaviour.

The natural frequency ( $\omega_n$ ) of second order system is the frequency at  $-90^\circ$  phase shift and corresponds to the maximum power of the system.

$$\omega_{n\_transverse} = 428.0 \text{ [rad/s]} \quad (68 \text{ Hz})$$

$$\omega_{n\_focus} = 389.8 \text{ [rad/s]} \quad (64 \text{ Hz})$$

To determine the damping coefficient of the system, the two frequencies where the power is half of the maximum power ( $-3\text{dB}$ ) have to be found first. In the magnitude plot, these points can be found at  $\frac{1}{\sqrt{2}}$  of the maximum. The damping coefficient is then calculated using:

$$\zeta = \frac{\omega_{-3dB\_1} - \omega_{-3dB\_2}}{2\omega_n}$$

$$\zeta_{transverse} = 0.150$$

$$\zeta_{focus} = 0.165$$

The VCA displacement curve was created using a 5 Hz sinus (1Vpp). The acquired data was divided by a phase shifted sinus, resulting in a displacement curve shown in Figure 44. From the displacement curve the DC gain is determined:

$$A_{transverse} = 911 \cdot 10^{-6} \text{ [m/V]}$$

$$A_{focus} = 910 \cdot 10^{-6} \text{ [m/V]}$$

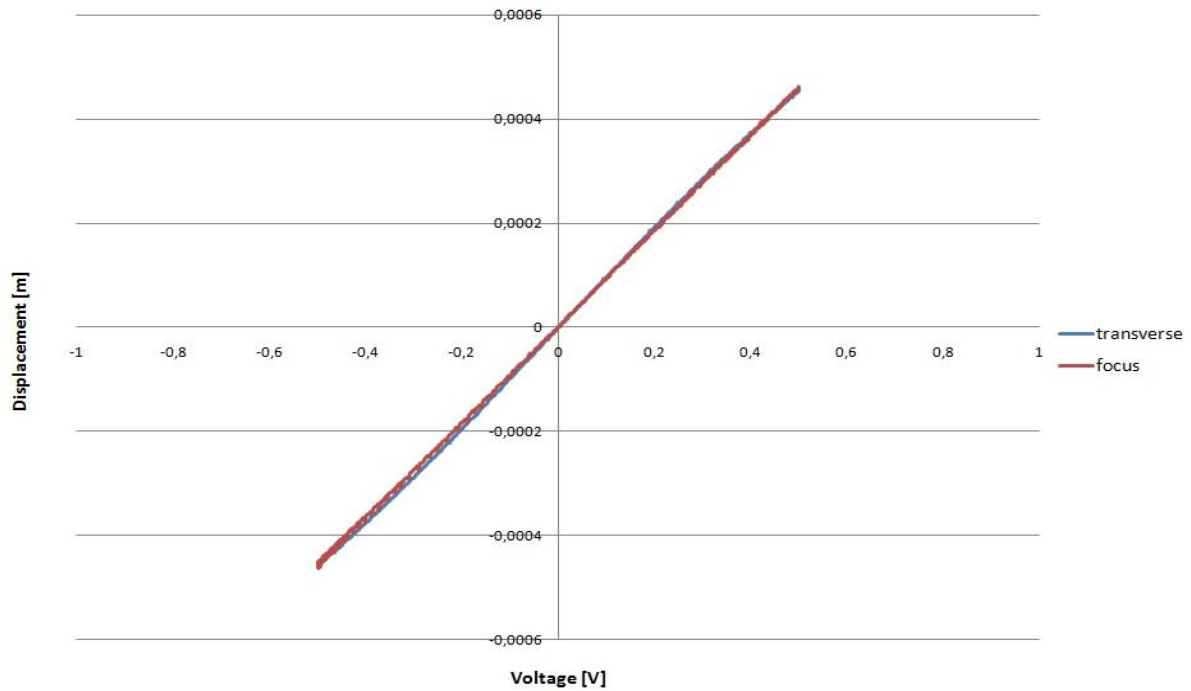


Figure 44 VCA displacement (Polytec MSA-500 Micro System Analyser laser Doppler vibrometer)

The transfer functions of the objective-lens:

$$L_{transverse}[m/V] = \frac{X(s)}{F(s)} = K \frac{\omega_n^2}{s^2 + 2\zeta\omega_n s + \omega_n^2} = \frac{166,91}{s^2 + 128,41s + 183220}$$

$$L_{focus}[m/V] = \frac{X(s)}{F(s)} = \frac{138,24}{s^2 + 128,62s + 151909}$$

A Bode diagram of the focus transfer function was made using Matlab and is shown in Figure 45.

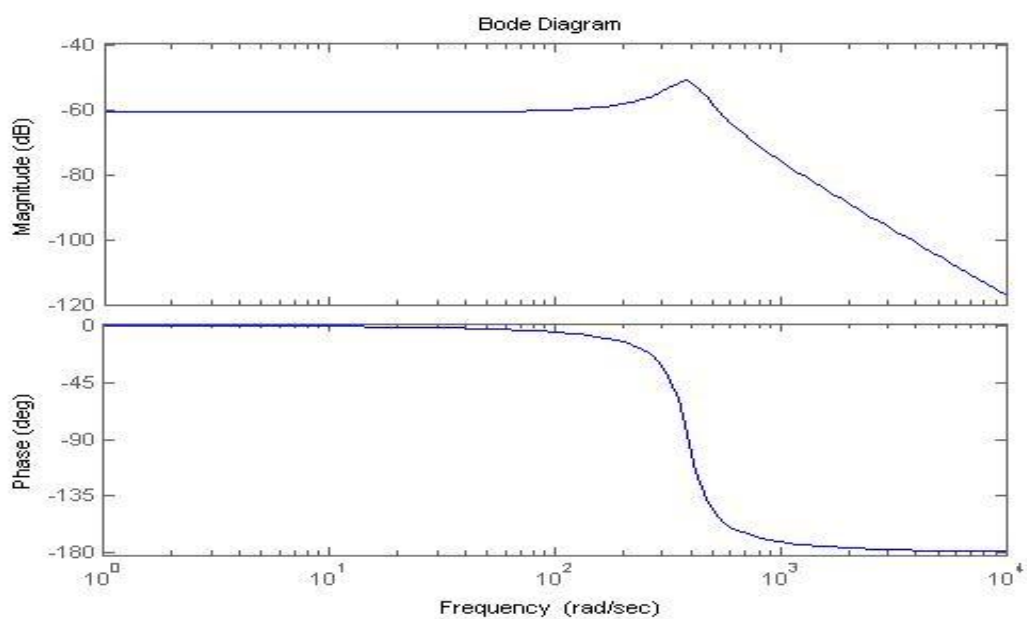


Figure 45 focus VCA/lens bode plot

The objective lens including the four springs was weighted on a scale:  
 $m = 0.23 \cdot 10^{-3} [kg]$

In paragraph 4.2 the damper viscosity is defined as:

$$C = 2\zeta m \omega_n [N m/s^2]$$

$$C_{\text{transverse}} = 29.5 \cdot 10^{-3} [N s/m]$$

$$C_{\text{focus}} = 30.3 \cdot 10^{-3} [N s/m]$$

In paragraph 4.2 the spring constant is defined as:

$$k = \frac{1}{4} m \omega_n^2 [N/m]$$

$$k_{\text{transverse}} = 10.53 [N/m]$$

$$k_{\text{transverse}} = 9.15 [N/m]$$

### 9.3 PDIC

In Figure 51 the PDIC-FES is monitored at the bottom of the fluidic channel (border between channel and Borofloat). Because of reflections at this border the PDIC-FES is able to find the focus point without help of any reflective mark (paragraph 10.1.1). However the response is very weak and often not reliable as a result of noise. A similar response was unfortunately not visible for the Borofloat/Borofloat border at other places on the chip. Therefore a continuous autofocus cannot be used. As an alternative the focus is measured at start and end on the chip using a linear focus profile routine (paragraph 10.1.1).

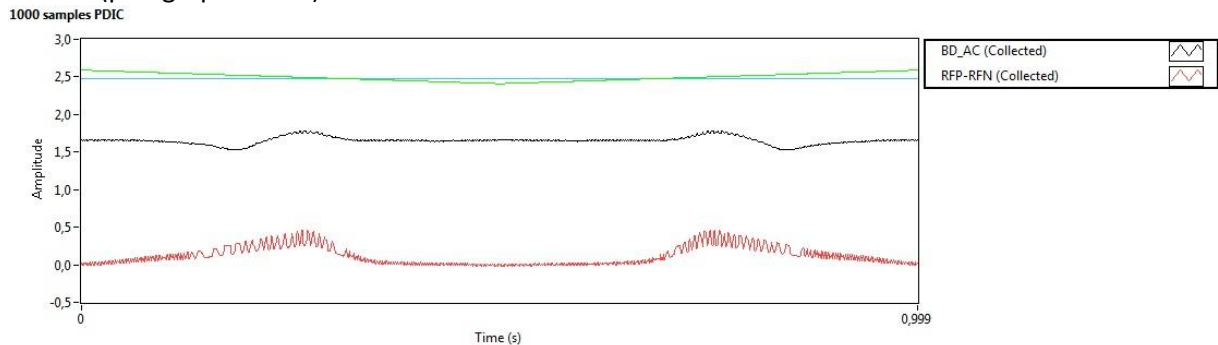


**Figure 46 PDIC-FES and PDIC-intensity response, for 50  $\mu\text{m}$  vertical-displacement (1 Hz triangle), 1.5 mW laser centred at bottom of channel (border between channel and Borofloat)**

## 10 Results/discussion

In this chapter  $\mu$ flow's experimental results are shown and discussed. Experiments for the channel find functionality are described first. At the end of the chapter experiments with fluorescent beads are discussed.

### 10.1 Find channel

The automatic channel finding routine and auto focus are optimized using the experiments described in this paragraph. Experiments are performed using the measurement setup shown in Figure 47.

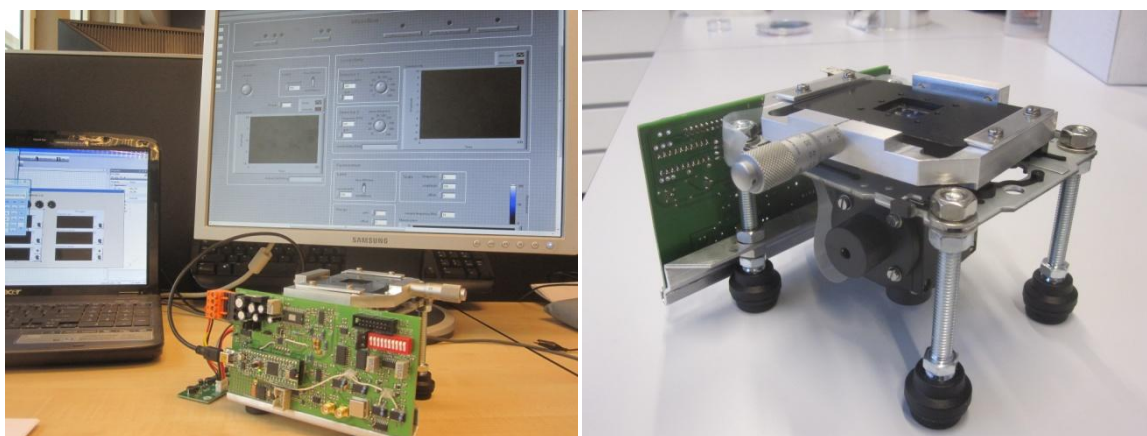


Figure 47 measurement setup

The experiments and  $\mu$ flow settings are controlled by the Labview user interface on a laptop (Windows 7). The Labview program controls the  $\mu$ flow microcontroller PCB and the Labview DAQ. A microfluidic chip is positioned inside the chipholder. For the find channel experiments the fluorescence detector is disabled.

#### 10.1.1 PDIC-response

The PDIC-FES has to be characterized for a Matlab simulation of the focus system (chapter 4). Moreover the PDIC-FES and PDIC-intensity have to be characterized for the automatic channel finding routine performed by the microcontroller (paragraph 6.1). For these characterizations, the laser is focused on a digital mark (reflective surface) of the microfluidic chip. The vertical position of the laser is varied  $50 \mu\text{m}$  ( $\pm 25 \mu\text{m}$  out of focus) by the focus VCA. In Figure 48, 49 and Figure 50 this is done for three different laser illumination powers. The PDIC-FES is shown as BD\_AC (red) and PDIC-intensity is shown as RFP-RFN (black), the triangular excitation is visible in green.

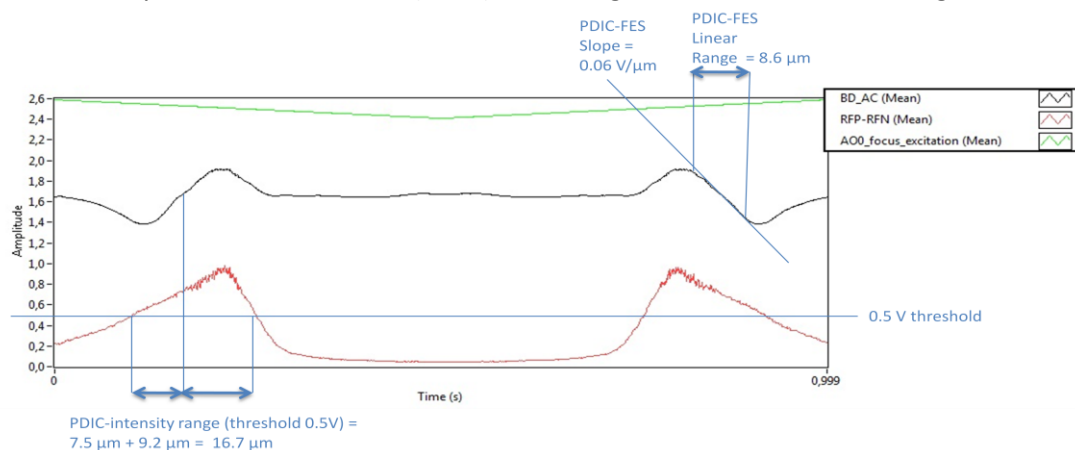
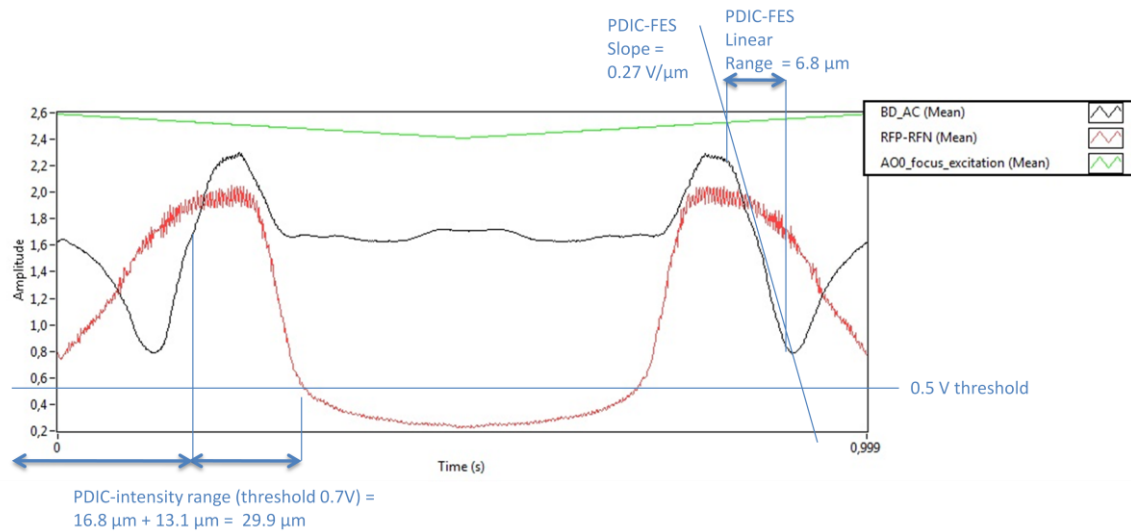
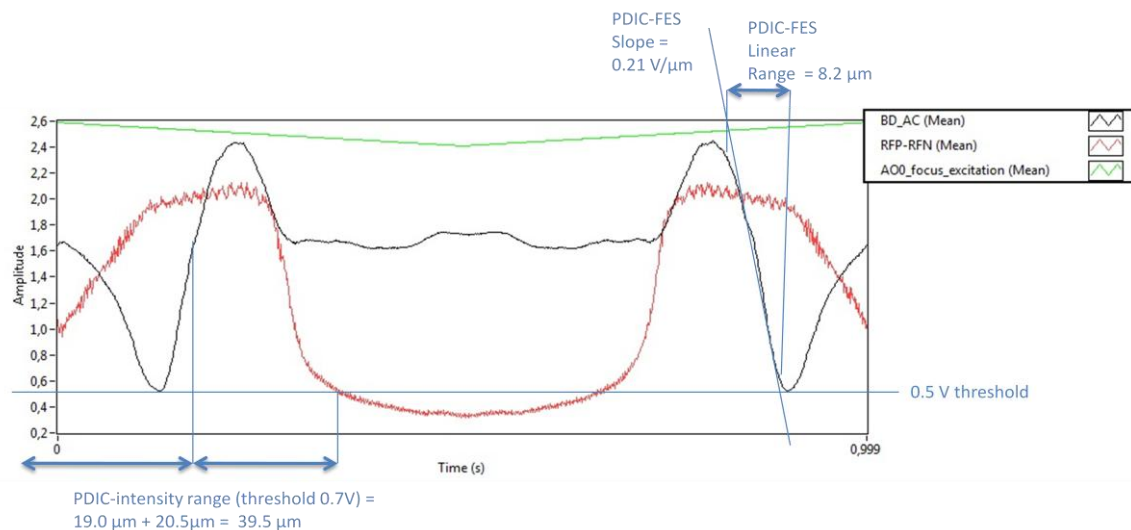


Figure 48 PDIC-FES and PDIC-intensity response, for  $50 \mu\text{m}$  vertical-displacement (1 Hz triangle) 0.4 mW laser



**Figure 49 PDIC-FES and PDIC-intensity response, for 50  $\mu\text{m}$  vertical-displacement (1 Hz triangle) 1.5 mW laser**



**Figure 50 PDIC-FES and PDIC-intensity response, for 50  $\mu\text{m}$  vertical-displacement (1 Hz triangle) 2.2 mW laser power**

During digital mark detection the PDIC-intensity is compared with a threshold voltage. This threshold should be chosen higher than the noise at the PDIC-intensity. Unfortunately, the PDIC-intensity amplitude gets smaller if the digital mark is out of focus. Since the laser beam will get out of focus during the process of reading marks (paragraph 10.1.2), a focus error tolerance is needed. This tolerance is defined as the distance from the focus point where the PDIC-intensity has an amplitude  $>$  threshold  $>$  noise. By using a high laser illumination power the PDIC-FES amplitude will be higher. A too high illumination power will shorten the lifetime of the laser diode. By choosing a laser illumination power of 1.5 mW a tolerance of 29.9  $\mu\text{m}$  is obtained (Figure 49) and the PDIC-FES gain is higher compared to an illumination power of 2.2 mW (Figure 50). The linear range of 6.8  $\mu\text{m}$  proves to be sufficient for the focus profile routine (paragraph 10.1.2).

The PDIC-FES linear range and gain are used in the Matlab simulation of the focus system, calculated using Figure 49.

### 10.1.2 Focus profile

In this experiment the optical pickup slides across the complete microfluidic chip, ideally all the digital marks are recognized after the optical pickup reaches the end of the chip. However the chip is normally tilted 50-100  $\mu\text{m}$  in the vertical direction, this is more than the focus error tolerance of 29  $\mu\text{m}$ . It is therefore expected that not all the digital marks will be recognized if only one point on the chip is used for measuring the FES. In Figure 51 the FES is measured at the start of the fluidic chip. Using only one focus point the focal error increases when the laser moves towards the end of the fluidic chip. As a result the PDIC-intensity becomes lower, at the point where PDIC-intensity  $< 0.5$  V, the digital mark detection will not recognize the marks anymore.

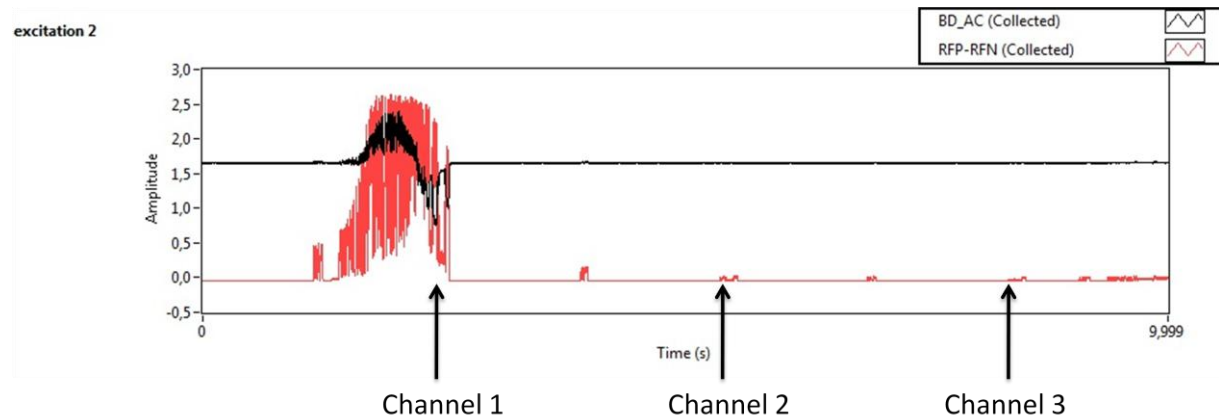


Figure 51 reading digital mark of the complete fluidic chip using only one autofocus point at the start of the chip, scan speed 2 mm/s

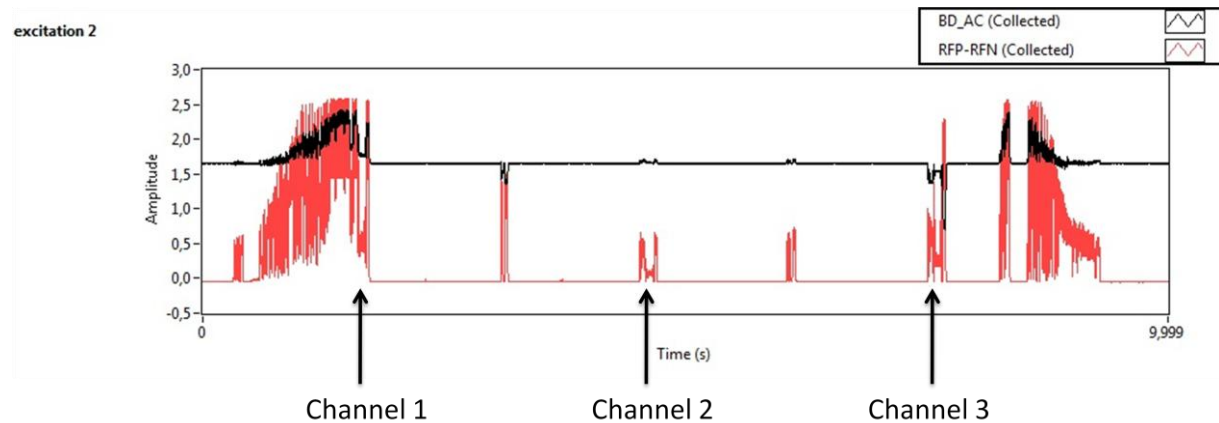


Figure 52 slide reading digital mark of the complete fluidic chip using two autofocus points (linear focus profile), scan speed 2 mm/s

Using a focus point at the beginning and end of the chip (combined with a linear focus profile in between the two focus points), the digital mark detection is improved. As shown in Figure 52 the PDIC-intensity amplitude remains more constant and the digital mark detection works for digital the complete chip although digital marks around channel 2 are detected with some difficulties. To improve the detection around channel 2, the bending of the slider rails because of the fluorescence detector weight should be taken into account. Because of time issues this has not been integrated yet.

### 10.1.3 Channel finding

During the focus profile routine, information of the two focus point is automatically transmitted to the Labview GUI (Figure 53). The transversal position and the vertical focus of the focus point at the start and end of the chip are visualized. From Figure 53 can be seen that the transversal position between the start and end focus point ( $24139 \mu\text{m} - 8666 \mu\text{m} = 15473 \mu\text{m}$ ). The tilt of the chip ( $564.5 \mu\text{m} - 516.9 \mu\text{m} = 47.6 \mu\text{m}$ ). Testing different chips, the tilt varies from 40-100  $\mu\text{m}$ .



Figure 53 Labview measurements: focus profile (left), find channel (right),

After a successful focus profile routine a fluidic channel can be found using the channel find routine. For example, if we want to position the laser beam at the centre of channel one: The slider first moves the optical pickup (Figure 54 (1)) past channel 1 to position A. The slider is moved backwards (2) until the digital marks B is recognized. The slider moves further (3) and is stopped somewhere in between the marks C and D. At this point the transverse-VCA moves the laser back (4) to mark C to find out at which transversal distance the optical pickup has stopped from mark C. For an additional verification of the optical pickup position is moved forward (4) until mark D is recognized. The transversal position and focus of mark C and D is transmitted to the Labview program (Figure 53). From Figure 53 can be seen that the transversal distance between mark C and D ( $594.2 \mu\text{m} - 496.6 \mu\text{m} = 97.6 \mu\text{m}$ ). This is close to the 100  $\mu\text{m}$  of the fluidic chip mask. This difference could be the result of the transverse-VCA calibration using a different optical pickup (paragraph 9.2). More measurements have to be performed (using more optical pickups) to determine the spread of the transversal-VCA gain between optical pickups.

Because the distance between C and D is the only distance of 100  $\mu\text{m}$  in the neighbourhood of the channel, this is also a confirmation that the laser is positioned in between C and D. Besides the transversal position, the vertical focus of mark C and D was measured end sent to the Labview GUI. The tilt between mark C and D ( $563.4 \mu\text{m} - 562.7 \mu\text{m} = 0.7 \mu\text{m}$ ), which is expected since the two point are near each other. Moreover the vertical focus is close to the vertical focus found at the start of the chip ( $564.5 \mu\text{m}$ ) by the focus profile routine. Using the data of the marks C and D, the microcontroller can position the laser in the middle of the fluidic channel.

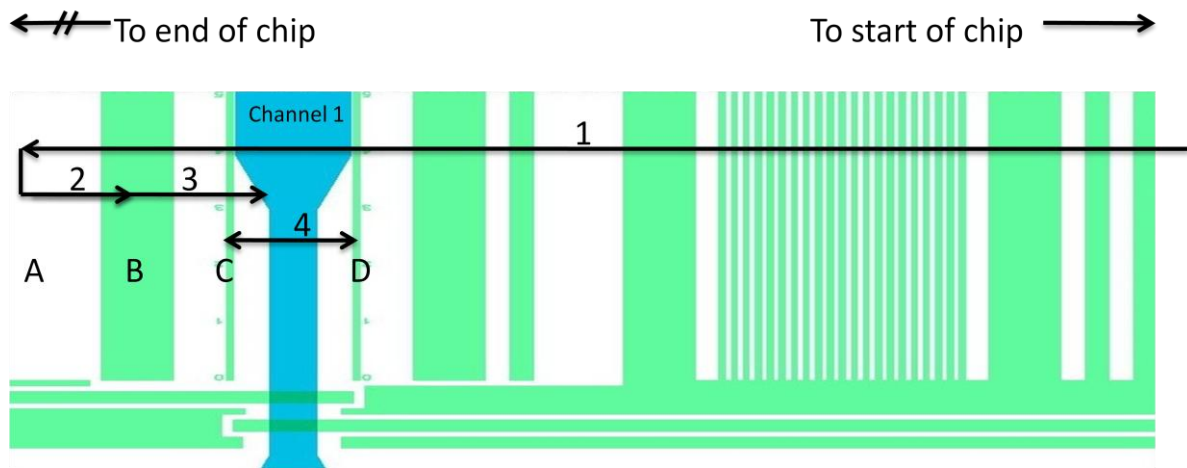


Figure 54 fluidic chip mask around channel 1 (figure is mirrored compared to Figure 29!)

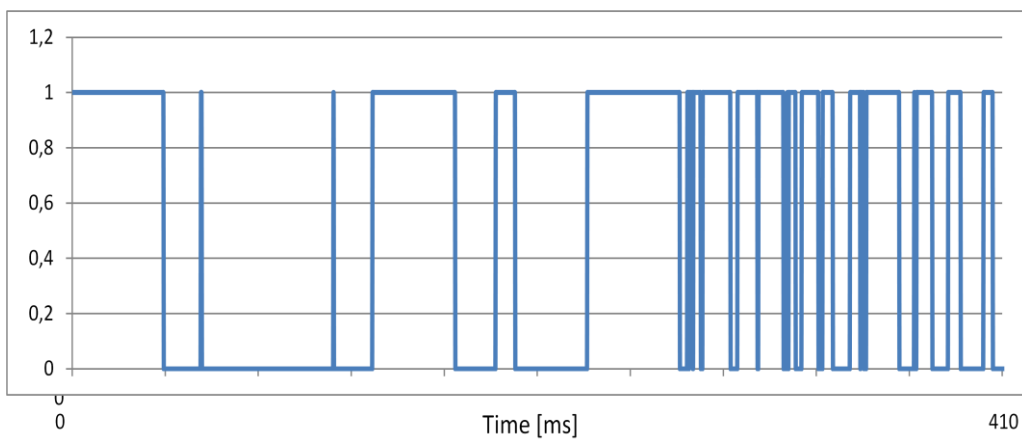


Figure 55 fluidic chip around channel 1, logic analyzer 0.5 V threshold

In Figure 55 the digital marks around channel 1 are visualized by a digital logic analyzer (threshold 0.5 V). The focus points B and C are clearly visible however; the digital mark recognition has difficulties to distinguish the marks in front of channel 1. This result in faulty mark recognition, therefore the channel find routine that was described earlier in this paragraph is used.

To confirm that the laser is positioned at the centre of the channel, a 200  $\mu\text{m}$  transversal scan was made. In Figure 56 can be seen that the PDIC-intensity finds the marks C and D spaced 100  $\mu\text{m}$  apart.

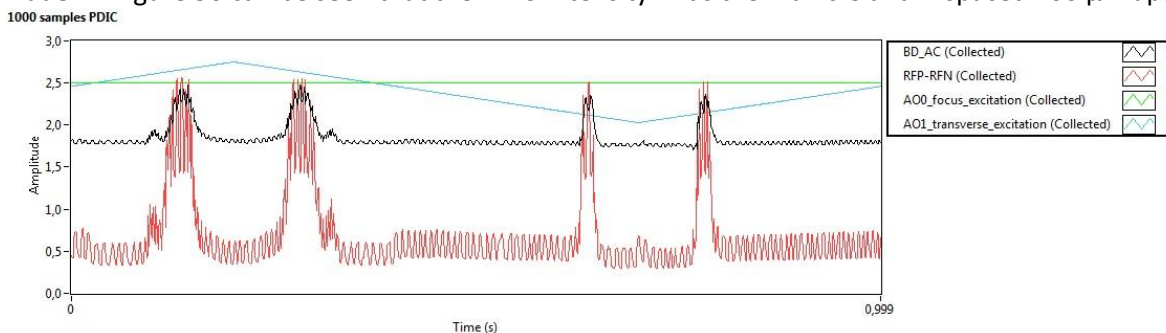


Figure 56 PDIC-FES and PDIC-intensity response, for 200  $\mu\text{m}$  transversal-displacement (1 Hz triangle) 1.5mW laser power

## 10.2 Dark noise, environmental- and leaking light

The dark noise of the MPPC is measured for 0.5/1.5/2.5/3.5 p.e. During the measurement the MPPC was placed inside a dark (light resistant) bag supplied with the MPPC module. All measurements are performed at 21 degrees Celsius and shown in the 2<sup>nd</sup> row of Table 5.

**Table 5 MPPC dark noise and environmental light**

p.e.	Dark noise [kcps] ( inside light resistant bag)	Dark noise + Environmental light [kcps] ( inside detector box with 100x attenuator)
0.5	780	970
1.5	210	240
2.5	50	65
3.5	16	20

The dark noise counted at 0.5 p.e. corresponds well to the 800 kcps specified in the datasheet of the MPPC module.

Next some measurements were performed in the experimental setup; the MPPC was placed inside the fluorescence detector box. The top was covered with the chipholder. Inside the fluorescence detector a 525 nm optical bandpass filter prevents most (< 0.001 %) of the 405 nm excitation light to reach the MPPC. For protecting the sensitive MPPC an additional light attenuator is placed in front of the MPPC, this attenuates the complete light spectrum 100x. Because of the high sensitivity of the MPPC, some of the environmental light from around the experimental setup will be detected by the MPPC, this is shown in the 3<sup>rd</sup> row of Table 5. It can be concluded that compared to the Dark noise the environmental light does not significantly increase the photon count. The 405 nm excitation light that reaches the MPPC is called leaking light. For different laser powers the leaking light detected by the MPPC is shown in Figure 57, Figure 58. During this experiment the laser beam is positioned in the centre of the fluidic channel (no fluorescent particles or solution inside). When the laser is disabled no leaking light is present, and light levels are identical to those in the 3<sup>rd</sup> row of Table 5.

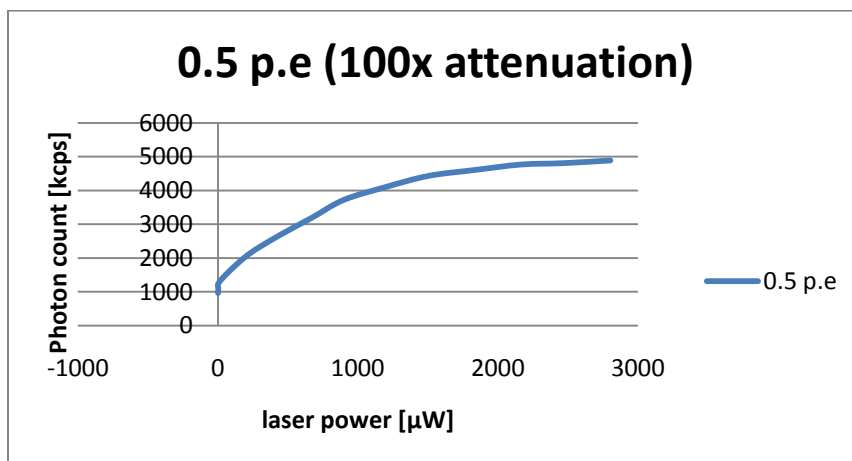


**Figure 57 laser light (405 nm) leaking into the fluorescence detector (0.5 p.e.)**

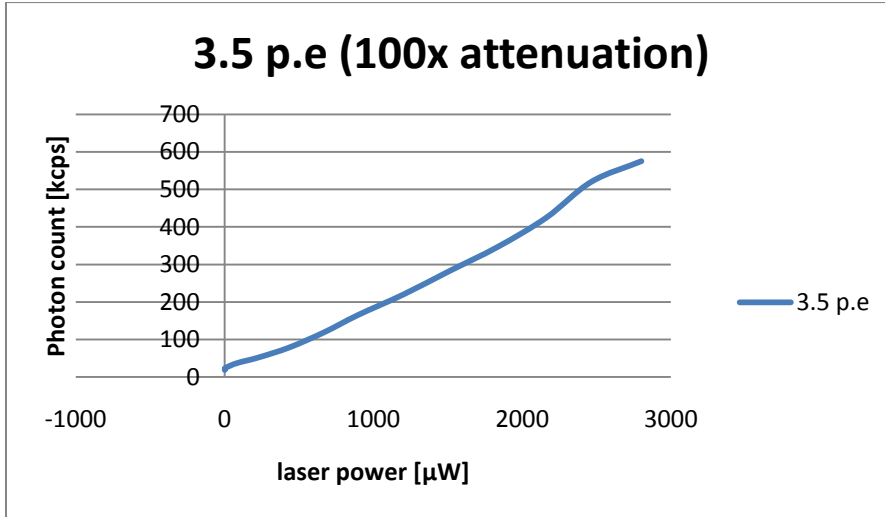


Figure 58 laser light (405 nm) leaking into the fluorescence detector (3.5 p.e.)

A laser excitation power of 1.5 mW results in a photon count of 4435 kcps (0.5 p.e). The leaking light photon count can be determined by subtracting the dark noise and environmental light:

$$4435 \text{ kcps}(\text{total count}) - 970 \text{ kcps}(\text{darkcount} + \text{environment}) = 3465 \text{ kcps}(\text{leaking light count})$$

The number of leaking light photons received by the MPPC (paragraph 5.5.5):

$$n_{i\_MPPC} = \frac{n_{det\_MPPC}}{P_d} = \frac{3465 \cdot 10^3}{0.45} = 7.7 \cdot 10^6 \text{ photons/s}$$

This corresponds to a photon detector incident power of (paragraph 5.5.5):

$$P_d(\lambda) = n_{i\_MPPC}(\lambda) \cdot \frac{hc}{\lambda} = 7.7 \cdot 10^6 \cdot \frac{6.63 \cdot 10^{-34} \cdot 3.00 \cdot 10^8}{405 \cdot 10^{-9}} = 3.78 \cdot 10^{-12} \text{ W}$$

If we assume that all the leaking light originates at the output from the first beamsplitter of the fluorescence detector (Figure 22), the light has travelled through the second beamsplitter, bandpass filter and attenuator. The leaking light is:

$$P_{leaking} = P_d \cdot \frac{1}{A_{beamsplitter} \cdot A_{bandpass\ filter} \cdot A_{attenuator}} = 3.78 \cdot 10^{-12} \cdot \frac{1}{0.1 \cdot 1 \cdot 10^{-5} \cdot 0.01} = 378 \mu\text{W}$$

The leaking 405 nm light has a power of 378 μW, this is one fifth of the total illumination power (1.5 mW).

### 10.3 Beads

Experiments with fluorescent beads are performed by inserting beads suspended in washing medium in (one of) the microfluidic channels. For the  $6\ \mu\text{m}$  beads a concentration of  $3.4 \cdot 10^6\ \text{beads/mL}$  is used and for  $2.5\ \mu\text{m}$  beads a concentration of  $24 \cdot 10^6\ \text{beads/mL}$  is used. To initiate a fluidic flow in the channel, the inlet and outlet are filled with different fluid levels (different volumes). The laser beam is positioned at the centre of the fluidic channel and a measurement is started by scanning the laser beam in the transversal direction (perpendicular to the liquid flow in the channel). For maximum performance the scan frequency is chosen equal to the VCA resonating frequency (65 Hz). During one period, the laser beam passes the channel twice (on both the rising and falling edge). Each period the fluorescence detector is sampled 100 times (50 samples rising edge, 50 samples falling edge). The resolution of the scan is the amplitude of the scan divided by 50.

Figure 59 shows an experiment with  $6\ \mu\text{m}$  beads during a  $200\ \mu\text{m}$  scan. The resolution of this scan is  $200\ \mu\text{m} / 50 = 4\ \mu\text{m} = 4\ \mu\text{m}/\text{pixel}$ . The  $100\ \mu\text{m}$  channel is clearly visible; inside the channel the  $6\ \mu\text{m}$  beads can be seen, because the beads are not completely in focus the diameters seem larger. Each bead is detected three times because of the two sub-beams created by the optical pickup grating (chapter 4). To generate Figure 59 the laser beam had to scan 1000 times across the channel (500 periods). The intensity plots are generated in real-time by Labview.

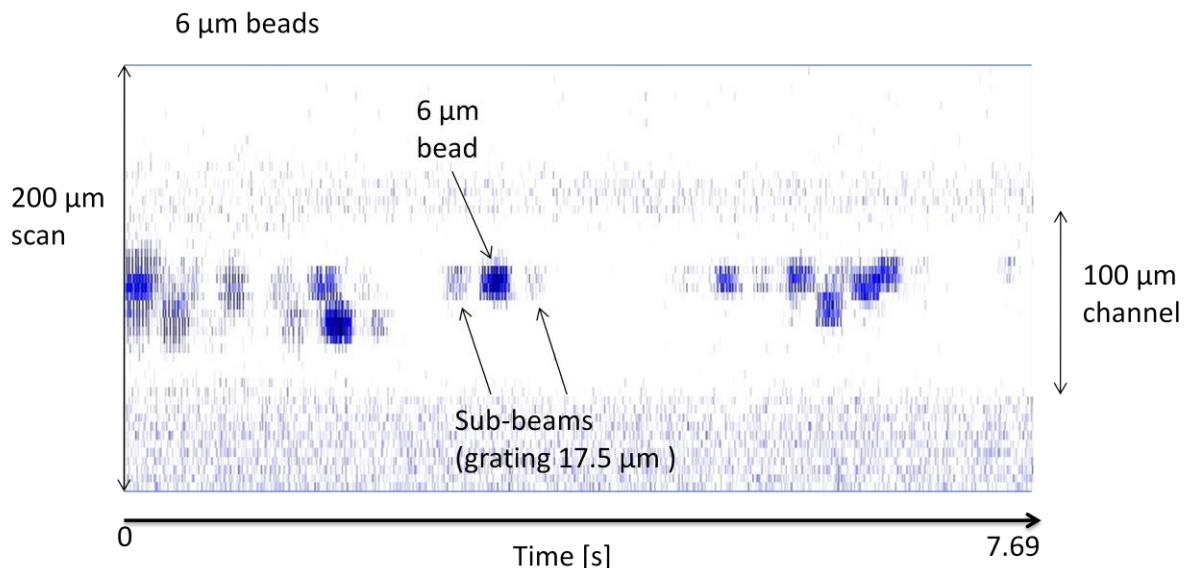


**Figure 59 transversal scan of  $200\ \mu\text{m}$  with  $6\ \mu\text{m}$  fluorescent beads**

The real-time scan of Figure 59 was created by adding two rows of 50 samples per period. Unfortunately, the timing of the fluorescence detector (photon counting) is performed randomly by Labview. Without correcting this timing, the result is a shifted vertical axis and mirrored beads, shown in Figure 60. Because of the random timing, Labview does not know where to start the second row of 50 samples. Therefore the two rows are out of sync and in each row the bead is alternating visible at two different places. Luckily, the timing is only random at start and constant during the scan. The random timing at the start can be corrected in Labview in real-time but has to be readjusted manually every time a new measurement is started. A readjusted scan is shown in Figure 61.

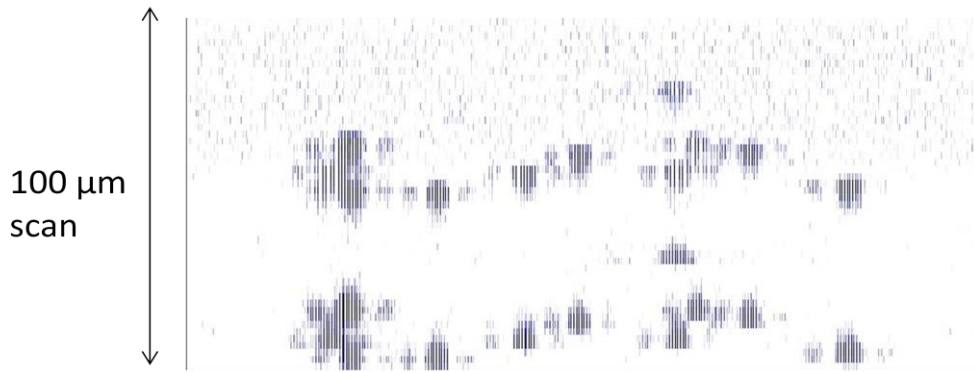


Figure 60 incorrect timing during transversal scan (100 μm) with 6 μm fluorescent beads

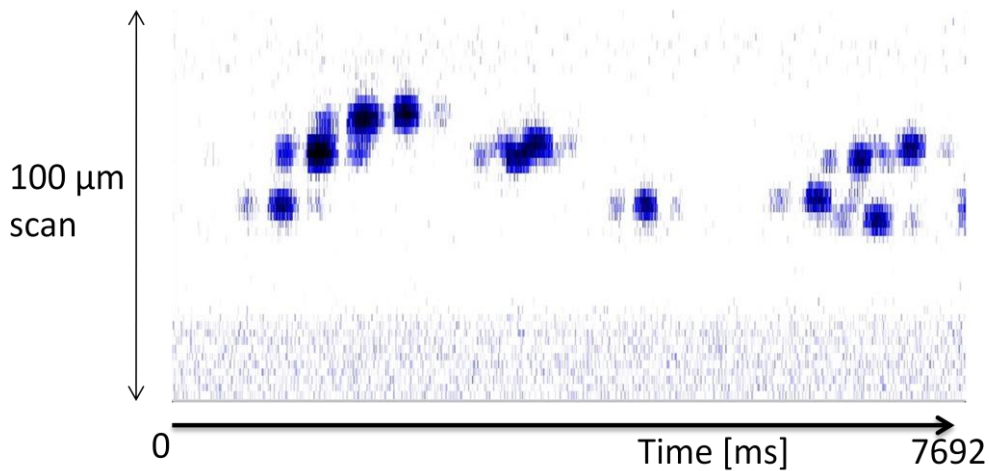


Figure 61 readjusted timing during transversal scan (100 μm) with 6 μm fluorescent beads

The speed of the beads can be calculated by measuring the time between the two sub beams. If the beam is in focus the distance between those two sub beams is 17.5 μm. An advantage of using the sub beams for speed calculations is that the speed determination is independent of the particle size (speed determination only depends on focus). The speed of the individual beads is determined by:

$$V_{particle}[\mu\text{m/s}] = \frac{17.5 \mu\text{m}}{t_{sub\ beam\ 2}[\text{s}] - t_{sub\ beam\ 1}[\text{s}]}$$

One of the 2.5 μm beads detected during a 50 μm scan (Figure 64) is shown in Figure 62. The time between the two sub beams is 1273 ms therefore the speed of this bead is 13.7 μm/s, which is in agreement with optical observations.

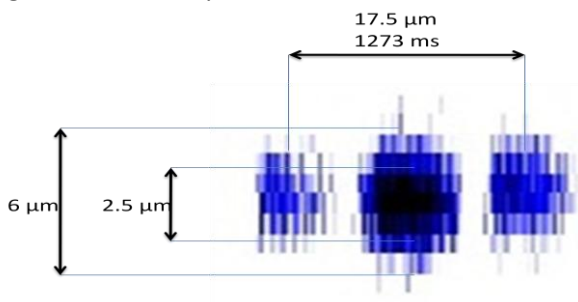


Figure 62 detection of 2.5 μm bead (bead 1 of Figure 64)

The resolution of this scan is  $50 \mu\text{m} / 50 = 1 \mu\text{m} = 1 \mu\text{m}/\text{pixel}$ . If we measure the bead height this corresponds to  $6 \mu\text{m}$ , however for this test  $2.5 \mu\text{m}$  beads were used. This difference is a result of a bead that is not in the focus of the laser. In Figure 63(top) the laser beam is focused on the bead. The Fluorescence light detected by the MPPC will have a plateau of  $2.5 \mu\text{m}$  and two Gaussian shaped borders ( $0.4 \mu\text{m}$  in width), these borders result from the partial illumination of the Gaussian shaped laser beam. In case the laser is not focused on the bead, Figure 63(bottom) the response will broaden and the peak value will be lower. The broadening can be specified using:

$$Z(w) = Z_R \sqrt{\left(\frac{w}{w_0}\right)^2 - 1} \quad (\text{paragraph 3.5})$$

For the bead in Figure 62:  $W = \frac{6 \mu\text{m} - 2.5 \mu\text{m}}{2} = 1.75 \mu\text{m}$ , the out of focus distance ( $Z$ ) of the bead is  $4.7 \mu\text{m}$ .

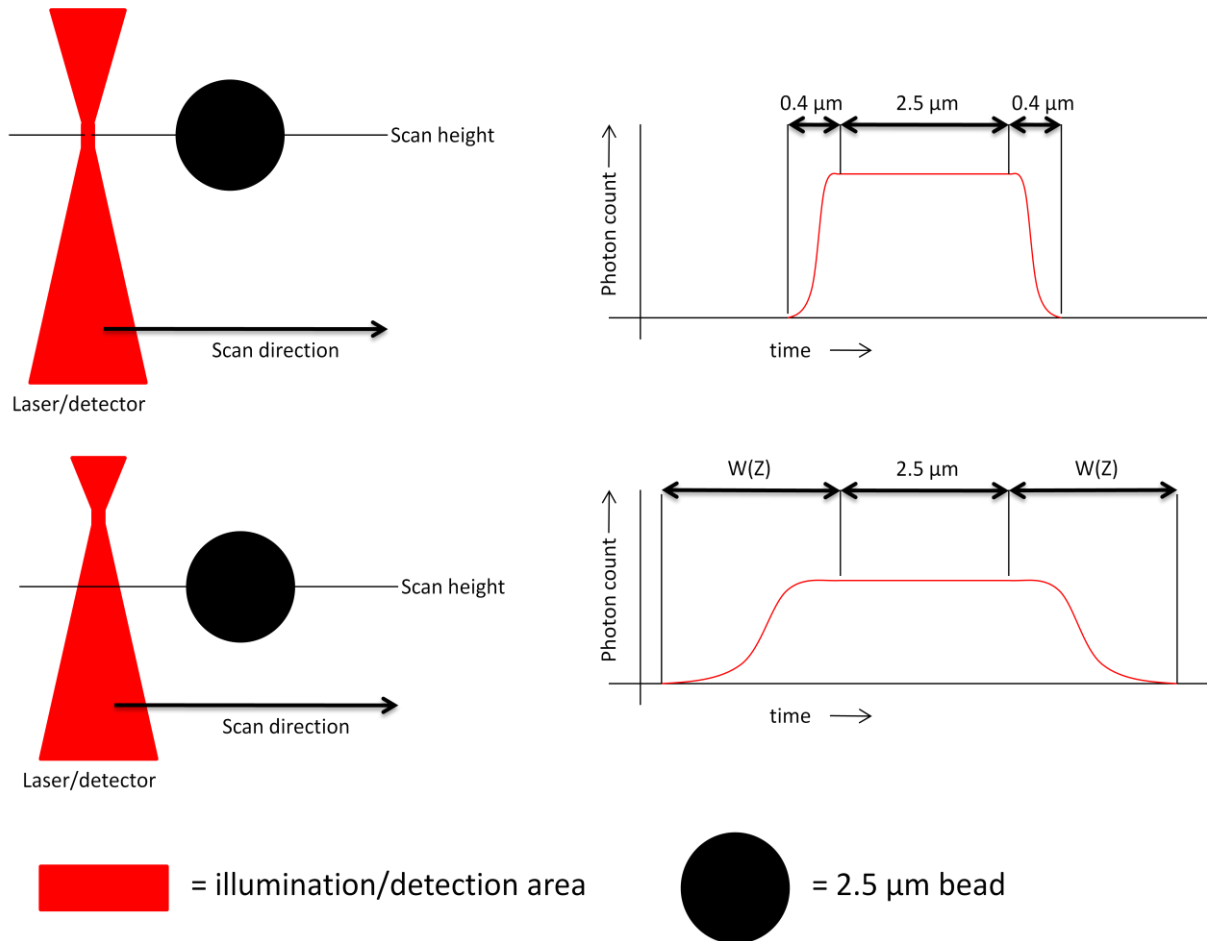


Figure 63 laser is focused on the bead (top), bead is not in focus (bottom)

The following experiment is performed using 2.5  $\mu\text{m}$  beads. A transversal scan of 50  $\mu\text{m}$  at the centre of the 100  $\mu\text{m}$  channel is shown in Figure 64. The resolution of this scan is 50  $\mu\text{m}$  / 50 = 1  $\mu\text{m}$ , from Figure 64 can be seen that this resolution proves to be sufficient to visualize the 2.5  $\mu\text{m}$  beads. The individual beads are numbered from 1 to 11. For each bead the speed and vertical position in the fluidic channel is calculated in Table 5.

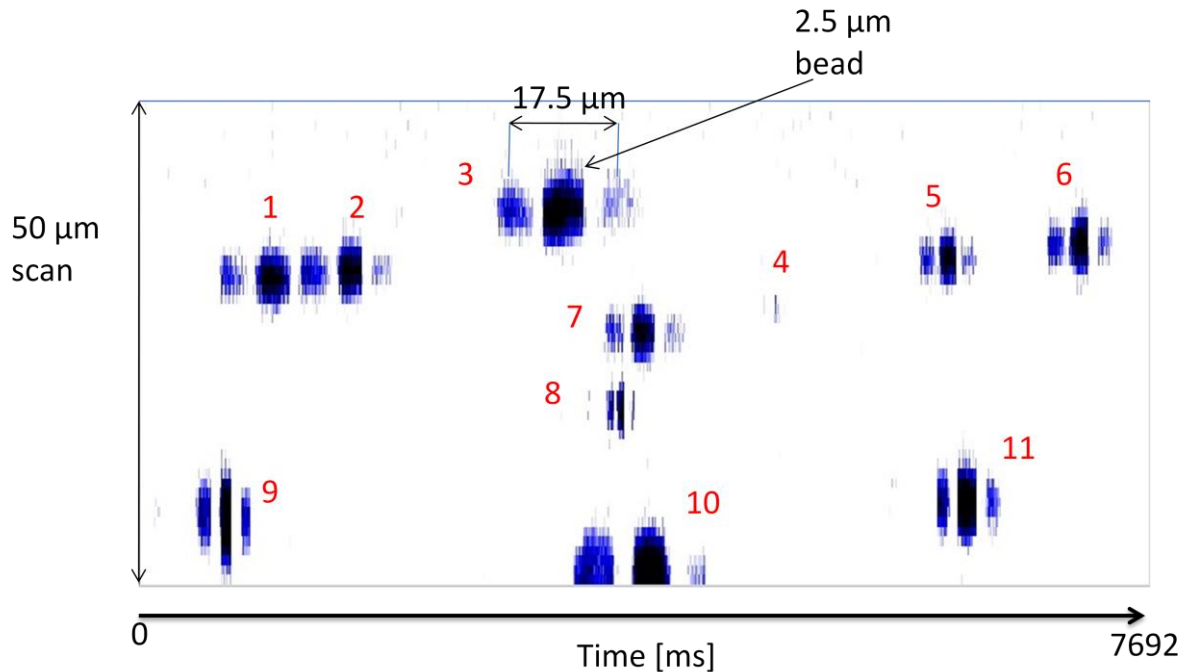


Figure 64 50  $\mu\text{m}$  scan of 2.5  $\mu\text{m}$  beads at the centre of a fluidic channel

Table 6 speed and vertical position of the 2.5  $\mu\text{m}$  beads

Bead number	speed		vertical position		
	time between 1st and 3rd peak [ms]	speed [ $\mu\text{m}/\text{s}$ ]	peak height [ $\mu\text{m}$ ]	w [ $\mu\text{m}$ ]	vertical position [ $\mu\text{m}$ ]
1	1273	13.7	6	1.75	4.7
2	1007	17.4	6	1.75	4.7
3	1591	11	8	2.75	7.5
4	too fast/no focus/noise?				
5	637	27.5	6	1.75	4.7
6	743	23.6	7	2.25	6.1
7	796	22	6	1.75	4.7
8	371	47.2	6	1.75	4.7
9	584	30	11	4.25	11.6
10	1539	11.4			
11	743	23.6	9	3.25	8.9

### 10.3.1 Non fluorescent beads

To prove that the beads experiment performed in paragraph 10.3 are the result of fluorescent emission and not caused by scattered light, experiments with 6  $\mu\text{m}$  non fluorescent beads were performed. During these experiments no fluorescent light was detected by the fluorescence detector. It can therefore be concluded that only fluorescence is measured in paragraph 10.3.

### 10.3.2 Fluorescence absorbtion

The bead experiments in paragraph 10.3 show fluorescence minima when beads are detected. This does not correspond to the theory that fluorescent beads produce more fluorescent light in comparison to non fluorescent parts of the channel. These minima cannot be the results of internal reflections or scattering (paragraph 10.3.1). A possible explanation could be that the MPPC is working in a saturation region (too much leaking light is incident on the MPPC). To verify this theory the leaking light is filtered using an optical lowpass filter, wavelengths < 430 nm are attenuated. Because of the limit amount of time these experiments could not be finished in time.

### 10.3.3 Maximum flow speed

Experiments are performed at the resonance frequency of the transverse VCA, 65 Hz. Time between two successive passes of the laser beam:

$$t_{scan} = \frac{1}{2 \cdot 65 \text{ Hz}} = 7.69 \text{ ms}$$

The detection area is 0.4 μm in width (Figure 65). To detection (part of) a bead:  $t_{scan} < t_{detect}$

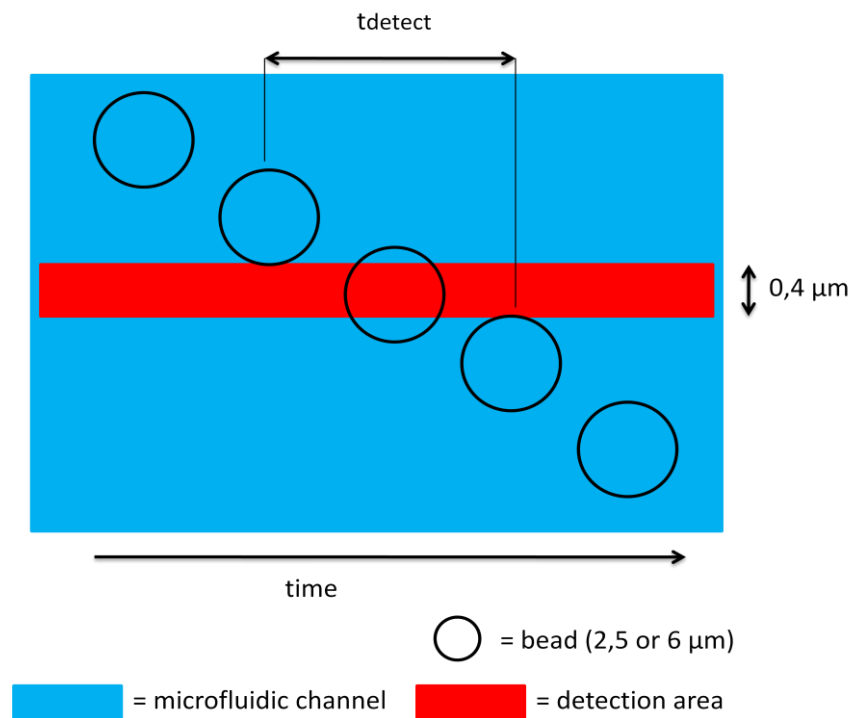


Figure 65 bead detection

The maximum flow speed is:

$$\frac{2.5 \mu\text{m} + 0.4 \mu\text{m}}{7.69 \text{ ms}} = 0.4 \text{ mm/s} \quad (2.5 \mu\text{m beads})$$

$$\frac{6 \mu\text{m} + 0.4 \mu\text{m}}{7.69 \text{ ms}} = 0.8 \text{ mm/s} \quad (6 \mu\text{m beads})$$

Comparing the maximum flow speed to flow speeds measured during bead experiments (Table 6), the μflow can detect beads at flow speed several times higher than currently used. However, this will decrease the accuracy of the speed measurements.

## 11 Conclusion/recommendations

In this chapter conclusions are drawn using the targets specified in paragraph 1.2. Recommendations for future research are also presented.

### 11.1 Conclusion

- An automatic positioning system for finding the on-chip microfluidic channels was successfully developed using on-chip digital marks and an advanced focus system. The three microfluidic channels are automatically located and the laser can be positioned at the centre of a channel within 1 minute.
- Beads of 2.5  $\mu\text{m}$  and 6  $\mu\text{m}$  can be visualized in real-time without problems. Since the resolution of the laser beam is 0.4  $\mu\text{m}$ , beads  $> 0.4 \mu\text{m}$  could be visualized in theory. No experiments with cells have been performed, due to the limited time available. However, it is very likely that cells can be visualized with the same resolution. By using image processing the counting of beads could be automated.
- Real-time 2D images of the microfluidic channel are generated by Labview. In these images the vertical position of the beads (position in the channel width) is visible. Moreover the vertical position of the beads (position in the channel height) can be calculated for similar sized beads. The speed of the beads is another interesting property that can be determined from the 2D images; speed can be determined independent from the bead size.
- Since no experiments with cells were performed, assessing of viability and vitality could not be tested.
- During this thesis all available time was needed for fluorescence measurement, impedance measurements have not been performed. Therefore, no combined fluorescence/impedance measurements can be shown.

### 11.2 Recommendations

In this thesis an automatic positioning system for finding the three on-chip microfluidic channels was developed. An improvement could be made in the sliding mechanism since it requires a lot of space. For a more compact and cheaper solution the slider could be removed and the optical pickup can be mounted in a fixed position. Fixing the optical pickup should not be a problem for alignment of the fluidic chip, since the transverse VCA has a range of 2 mm. By routing multiple channels within a range of 2 mm this would even allow a scan of multiple channels simultaneously.

A complex system of digital marks is used in this thesis, most of the calibration marks are not used at the moment. A simple (single) mark between the channels could already be sufficient for automatic positioning. It is also recommended to add more reflective areas in the digital mark layer, this allows for continuous adjusting the focus instead of using the linear focus profile that's used at the moment.

Another recommendation is to integrate a light scattering detector. Although this detector can only visualize the surface /shape of the particles, this detector enables label free detection. The only change to the current fluidic chip design is the addition of a reflective layer inside the microfluidic channel. The PDIC can be used as a detector for the scattered light. In combination with impedance

spectroscopy this results in a more advanced label free detection. This solution is compact and cheap since no expensive optical filters and MPPC's are necessary.

In this thesis digital image processing has not been used. However for automatic counting of beads, determining the amount of vital/viable cells (using dyes) or calculating the transversal/vertical position and speed of particles, image processing is a requirement.

The  $\mu$ flow uses a DAQ for waveform generation and sampling of analog signals. Originally the tasks of the DAQ were performed by the microcontroller; unfortunately it proved to be difficult to send large amounts of data to the Labview GUI using a microcontroller. In a future design, the microcontroller and DAQ tasks could be taken over by a powerful DSP processor. This would also allow for dedicated signal processing of the measurement data.

-

## References

- ATMEL (2010). "AT91SAM7S128 ". from [http://www.atmel.com/dyn/resources/prod\\_documents/6175s.pdf](http://www.atmel.com/dyn/resources/prod_documents/6175s.pdf).
- Banerjee, A., Y. Shuai, et al. (2008). "High-sensitivity MEMS based on-chip fluorescence detection system: measurement and analysis of ultimate sensitivity limits." 2008 17th Biennial University/Government/Industry Micro-Nano Symposium, Proceedings: 177-182 258.
- Braunl, T. (2008). Embedded robotics: mobile robot design and applications with embedded systems, Springer.
- Corkan, A. and H. Du (1998). "PhotochemCAD: A computer-aided design and research tool in photochemistry." Photochemistry and Photobiology **68**: 141-142.
- Fan, K. C., C. L. Chu, et al. (2001). "Development of a low-cost autofocusing probe for profile measurement." Measurement Science & Technology **12**(12): 2137-2146.
- FertilityScore (2009). "Fertilityscore, male fertility test." from <http://www.fertilityscore.co.uk>.
- Gawad, S., L. Schild, et al. (2001). "Micromachined impedance spectroscopy flow cytometer for cell analysis and particle sizing." Lab on a Chip **1**(1): 76-82.
- Gutmann, A. B. and E. B. Gutmann (1941). "Quantitative Relations of a Prostatic Component (Acid Phosphatase) of Human Seminal Fluid." Endocrinology **28**: 115.
- Hamamatsu. "MPPC S10362-11-100U ". from [http://jp.hamamatsu.com/products/sensor-ssd/4010/4025/S10362-11-100U/index\\_en.html](http://jp.hamamatsu.com/products/sensor-ssd/4010/4025/S10362-11-100U/index_en.html).
- Herman, B. L., J.R. (2010). "Fluorescence Excitation and Emission Fundamentals ". from <http://www.olympusmicro.com/primer/techniques/confocal/fluoroexciteemit.html>.
- Hinterdorfer, P. (2009). Handbook of single-molecule biophysics. New York, Springer.
- Holmes, D., H. Morgan, et al. (2005). "High throughput particle analysis: combining dielectrophoretic particle focussing with confocal optical detection." Biosensors and Bioelectronics **21**(8): 1621-1630.
- Invitrogen (2001). "PeakFlow Flow Cytometry Reference Beads." from <http://probes.invitrogen.com/media/pis/mp14825.pdf>.
- Invitrogen (2006). "CellTrace calcein violet, AM." from <http://probes.invitrogen.com/media/pis/mp34858.pdf>.
- Invitrogen (2009). "LIVE/DEAD Fixable Dead Cell Stain Kits." from <http://probes.invitrogen.com/media/pis/mp34955.pdf>.
- John, A. C. (1993). "The Physics of the compact disc <http://www.physics.udel.edu/~watson/scen103/cd-astig.html>." Physics education **28**.

Katayama, R. and Y. Komatsu (2008). "Blue/DVD/CD compatible optical head." Applied Optics **47**(22): 4045-4054.

Kauffman, J. A. (2000). "Light levels and noise. Guide detector choices." Photonics Spectra: 149-153.

Kauffman, J. A. (2005). "Choosing your detector." OE magazine.

Kostner, S. and M. J. Vellekoop (2007). "Cell analysis in a microfluidic cytometer applying a DVD pickup head." Sensors and Actuators **132**: 512-517.

Kruger, J., K. Singh, et al. (2002). "Development of a microfluidic device for fluorescence activated cell sorting." Journal of Micromechanics and Microengineering **12**(4): 486-494.

Kummrow, A., J. Theisen, et al. (2009). "Microfluidic structures for flow cytometric analysis of hydrodynamically focussed blood cells fabricated by ultraprecision micromachining." Lab on a Chip **9**(7): 972-981.

MatrixMultimedia (2010). "ECIO ARM ". from <http://www.matrixmultimedia.com/datasheets/ECIO-60-2.pdf>.

Melexis (2007). "MLX75012 ". from <http://www.datasheetdir.com/MLX75012+photo-detector>.

Odgaard, P. F. (2004). Feature Based Control of Compact Disc Player. Control engineering. Aalborg, Aalborg University.

Olympus (2009). " Resolution Criteria and Performance Issues ". from <http://www.olympusmicro.com/primer/digitalimaging/deconvolution/deconresolution.html>.

Olympus (2010). "Basic Concepts in Fluorescence." from <http://www.olympusmicro.com/primer/techniques/fluorescence/fluorescenceintro.html>.

R.J.Raterink (2008). Detecting human spermatozoa using electrical conductivity measurements, University of Twente.

Renesas (2003). "M63028/029FP ". from [http://documentation.renesas.com/eng/products/.../rej03f0024\\_m63028\\_29fp.pdf](http://documentation.renesas.com/eng/products/.../rej03f0024_m63028_29fp.pdf).

Segerink, L. I., A. J. Sprenkels, et al. (2010). "On-chip determination of spermatozoa concentration using electrical impedance measurements." Lab on a Chip **10**(8): 1018-1024.

Shimomura, T., C. Izawa, et al. (2008). "A highly sensitive, highly reproducible laser-induced fluorescence detection system with optical pickup." Measurement Science & Technology **19**(8): -.

Sigma-Aldrich. "Fluorescein." from [http://www.sigmaaldrich.com/catalog/ProductDetail.do?D7=0&N5=SEARCH\\_CONCAT\\_PNO%7CBRAND\\_KEY&N4=F6377%7CSIAL&N25=0&QS=ON&F=SPEC](http://www.sigmaaldrich.com/catalog/ProductDetail.do?D7=0&N5=SEARCH_CONCAT_PNO%7CBRAND_KEY&N4=F6377%7CSIAL&N25=0&QS=ON&F=SPEC).

Stoilovic, M. (1991). "Detection OF Semen and BloodStains using Polilight as a Light Source." Forensic Sience International **51**: 289-296.

Torng, J. S., K. C. Fan, et al. (2006). "A genetic approach on the PID control of VCM for auto-focusing laser probe." Progress on Advanced Manufacture for Micro/Nano Technology 2005, Pt 1 and 2 **505-507**: 373-378.

Valleydesign "<http://www.valleydesign.com/borofloat.htm>."

Villarreal, M. R. "Spermatozoa." from [http://en.wikipedia.org/wiki/File:Complete\\_diagram\\_of\\_a\\_human\\_spermatozoa\\_en.svg](http://en.wikipedia.org/wiki/File:Complete_diagram_of_a_human_spermatozoa_en.svg).

WHO (2010). WHO laboratory manual for the Examination and processing of human semen. Cambridge, Cambridge University Press.

Wikipedia (2006). "PID feedback." from <http://en.wikipedia.org/wiki/File:Pid-feedback-nct-int-correct.png>.

Wikipedia (2009). "Gaussian beam waist." from <http://en.wikipedia.org/wiki/File:GaussianBeamWaist.svg>.

Wikipedia (2009). "NA for a lens." from [http://en.wikipedia.org/wiki/File:Numerical\\_aperture\\_for\\_a\\_lens.svg](http://en.wikipedia.org/wiki/File:Numerical_aperture_for_a_lens.svg).

Wikipedia (2010). "Photon." from <http://en.wikipedia.org/wiki/Photon>.

Wikipedia (2011). "Laser Doppler vibrometer."

Yang, S. Y., S. K. Hsiung, et al. (2006). "A cell counting/sorting system incorporated with a microfabricated flow cytometer chip." Measurement Science & Technology **17**(7): 2001-2009.

Yim, V., S. Y. Lee, et al. (2008). Multipurpose DVD Pick-up Scanner for Analysis of Microfluidics and Micromechanical Structures.

Zhang, H. P., C. H. Chon, et al. (2009). "Methods for counting particles in microfluidic applications." Microfluidics and Nanofluidics **7**(6): 739-749.

Zhu, H., O. Yaglidere, et al. (2010). "Cost-effective and compact wide-field fluorescent imaging on a cell-phone." Lab on a Chip **11**(2): 315-322.

# Appendix 1 Schematics

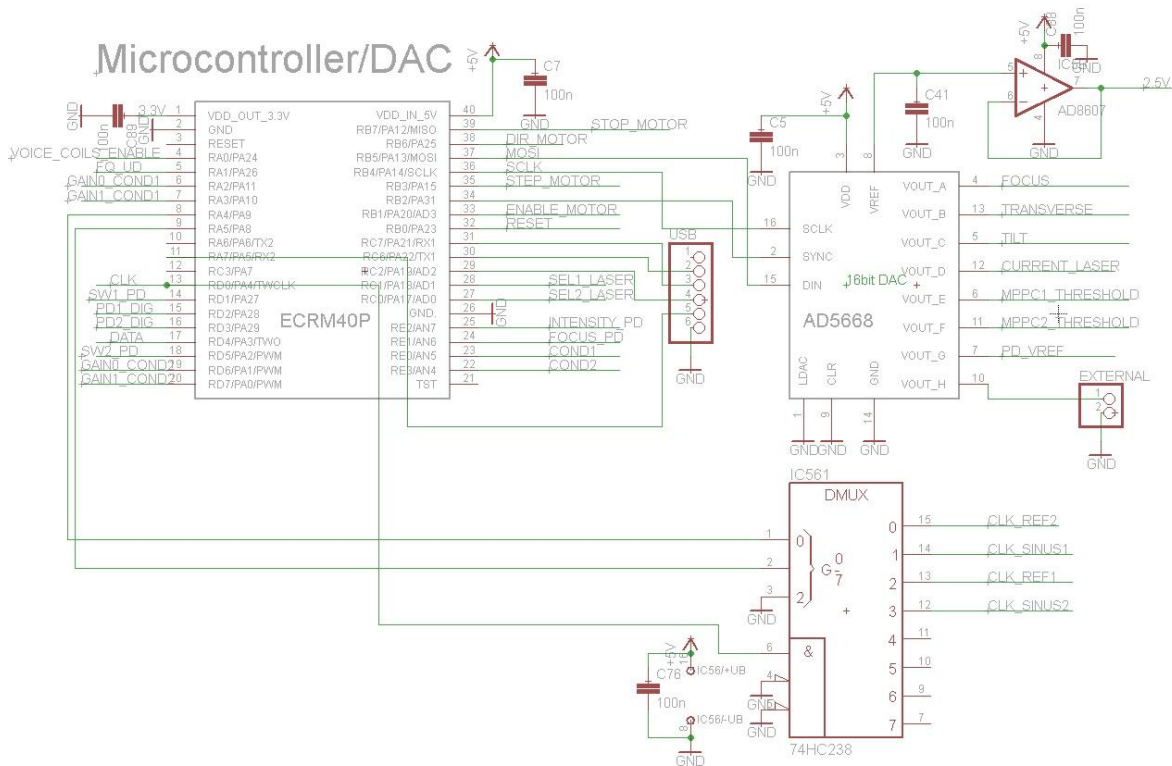


Figure 66 microcontroller and DAC

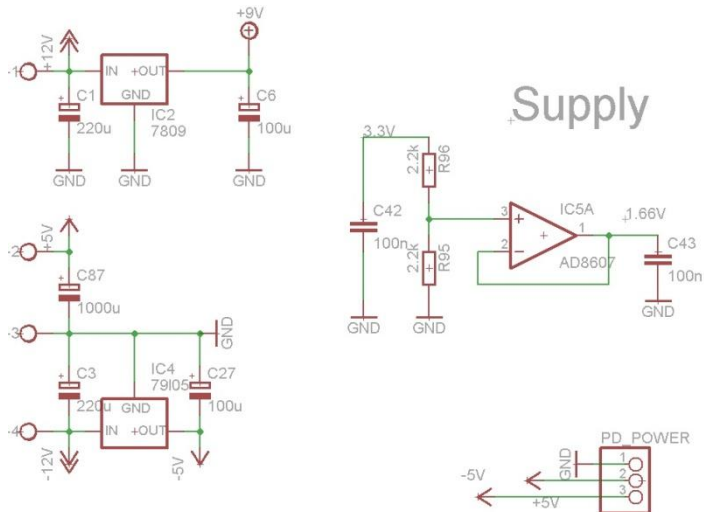


Figure 67 supply

## Appendix 2 PCB's

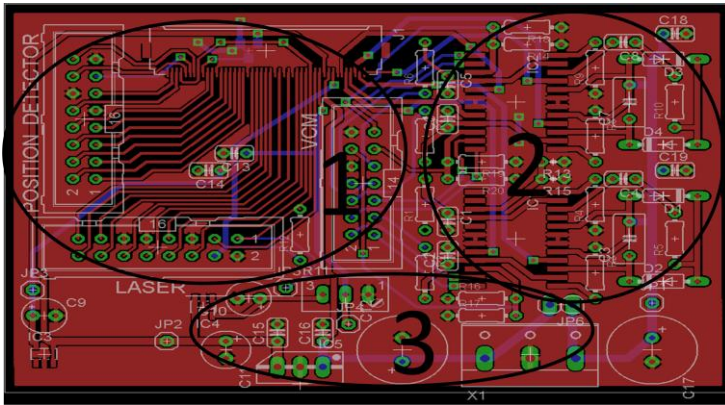


Figure 68 first PCB: optical pickup and Labview interface (1), VCA drivers (2), power supply (3)

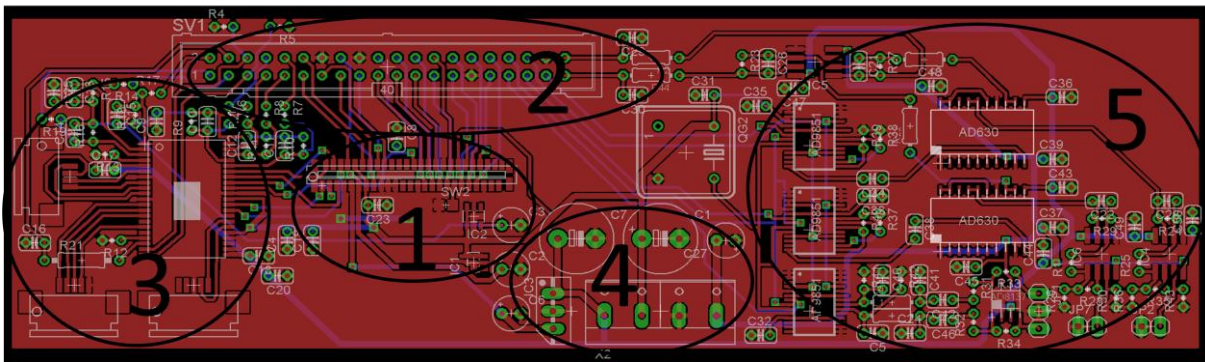


Figure 69 second PCB: optical pickup interface (1), Labview DAQ interface (2), VCA drivers (3), power supply (4), impedance detectors (5)

Appendix 3 Mechanical drawings

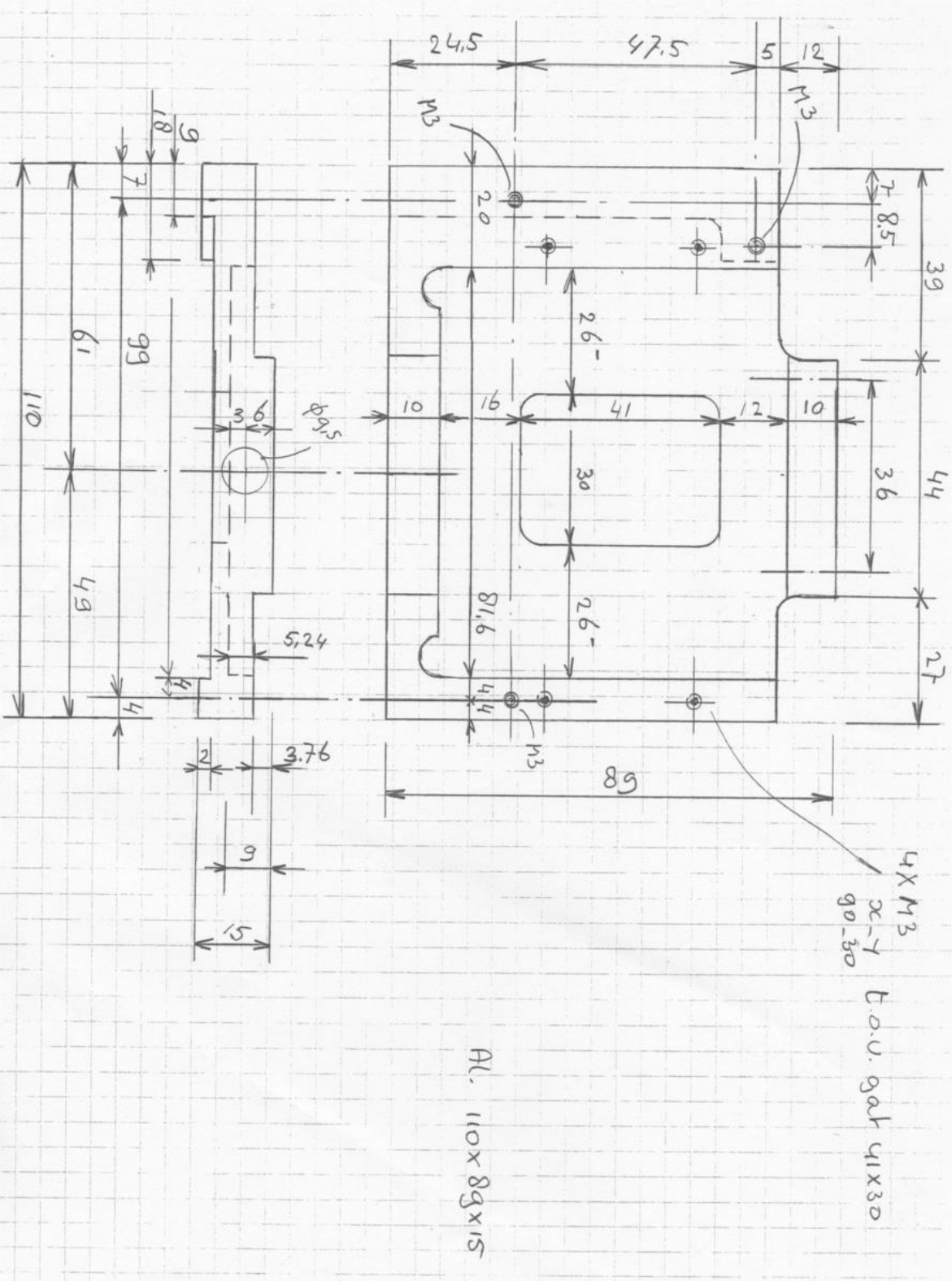


Figure 70 chipholder framework

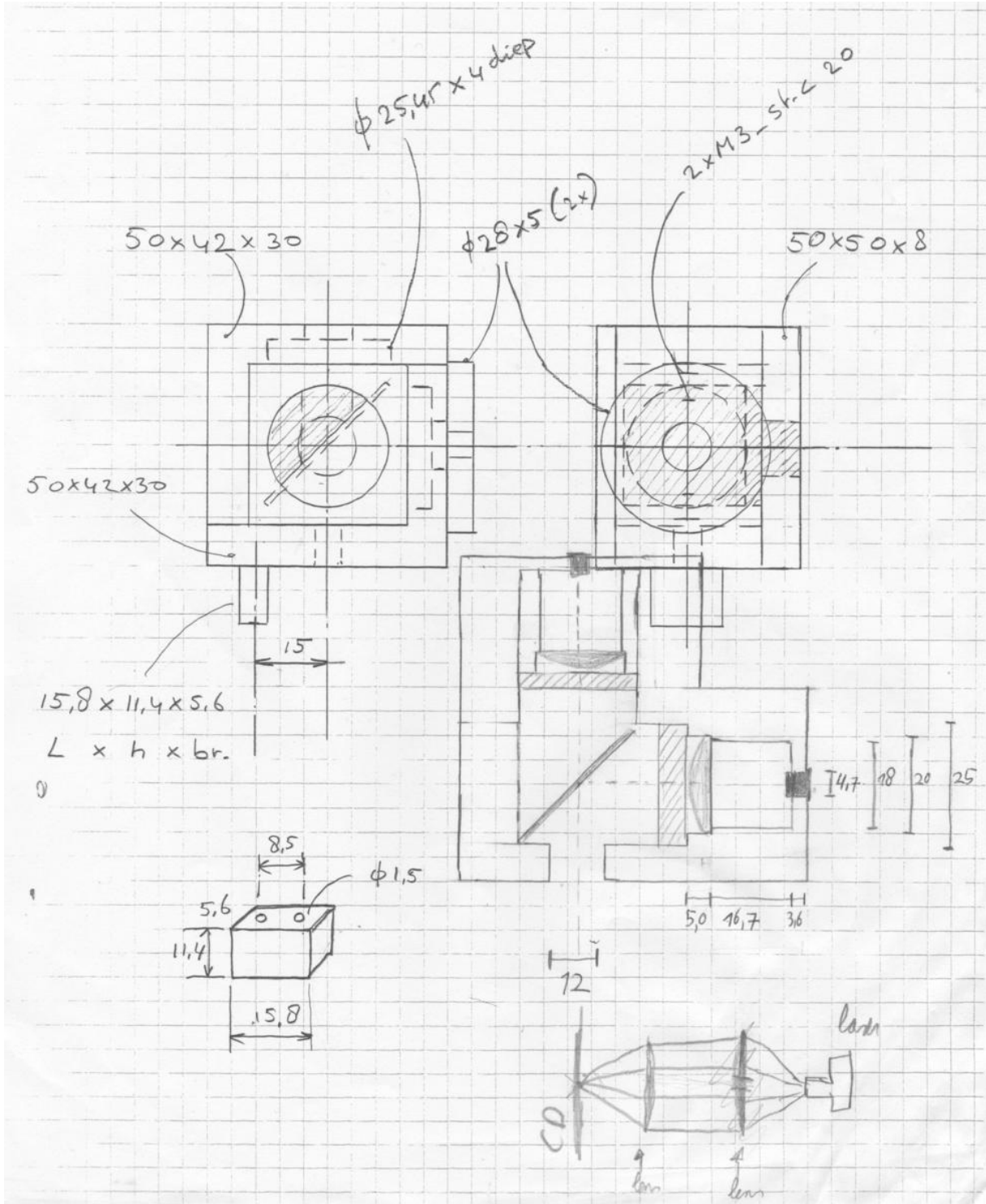


Figure 71 fluorescence detector part 1

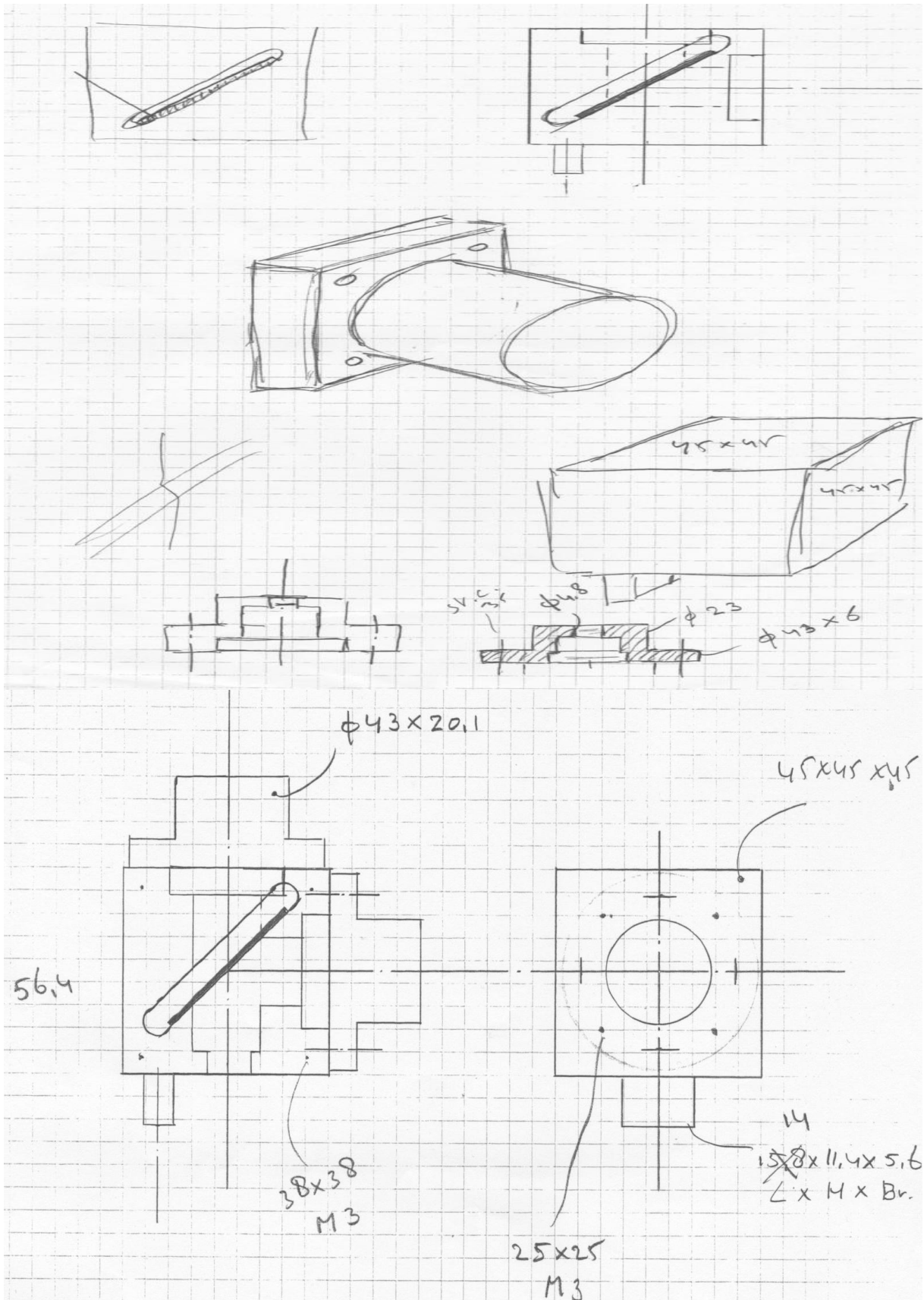


Figure 72 fluorescence detector part 2

# Appendix 4 Microcontroller flowcharts

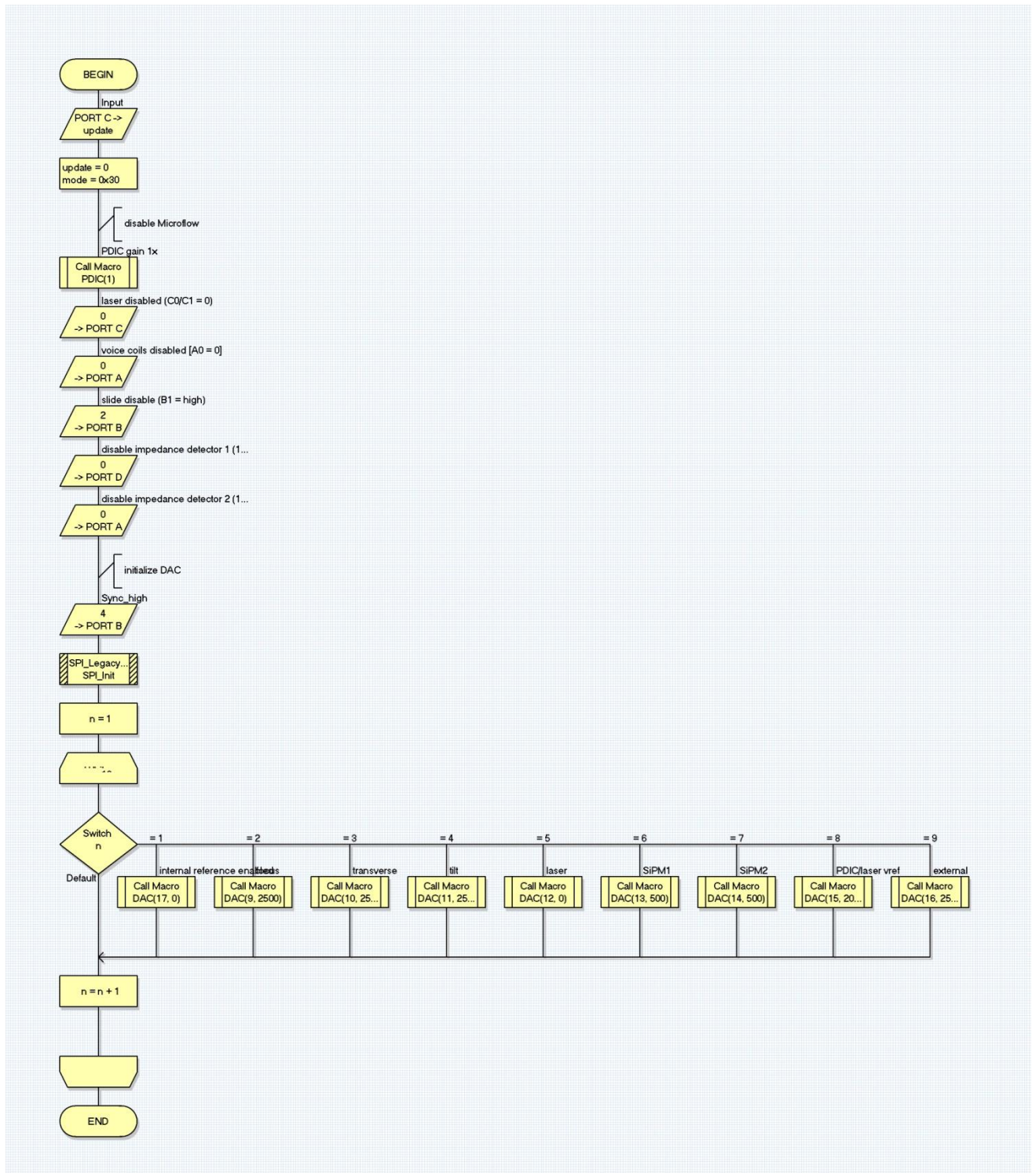


Figure 73 initialize

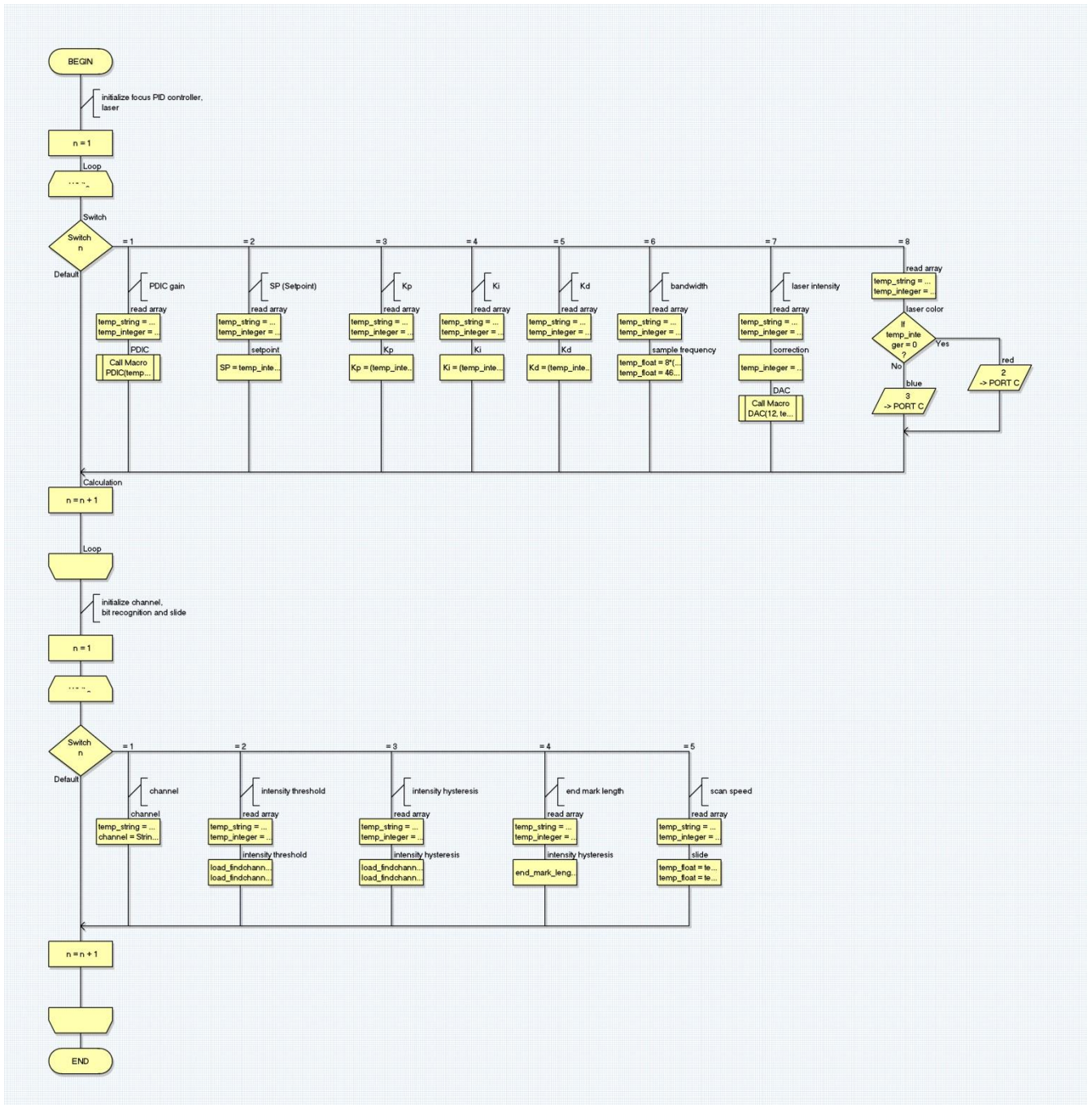


Figure 74 load findchannel

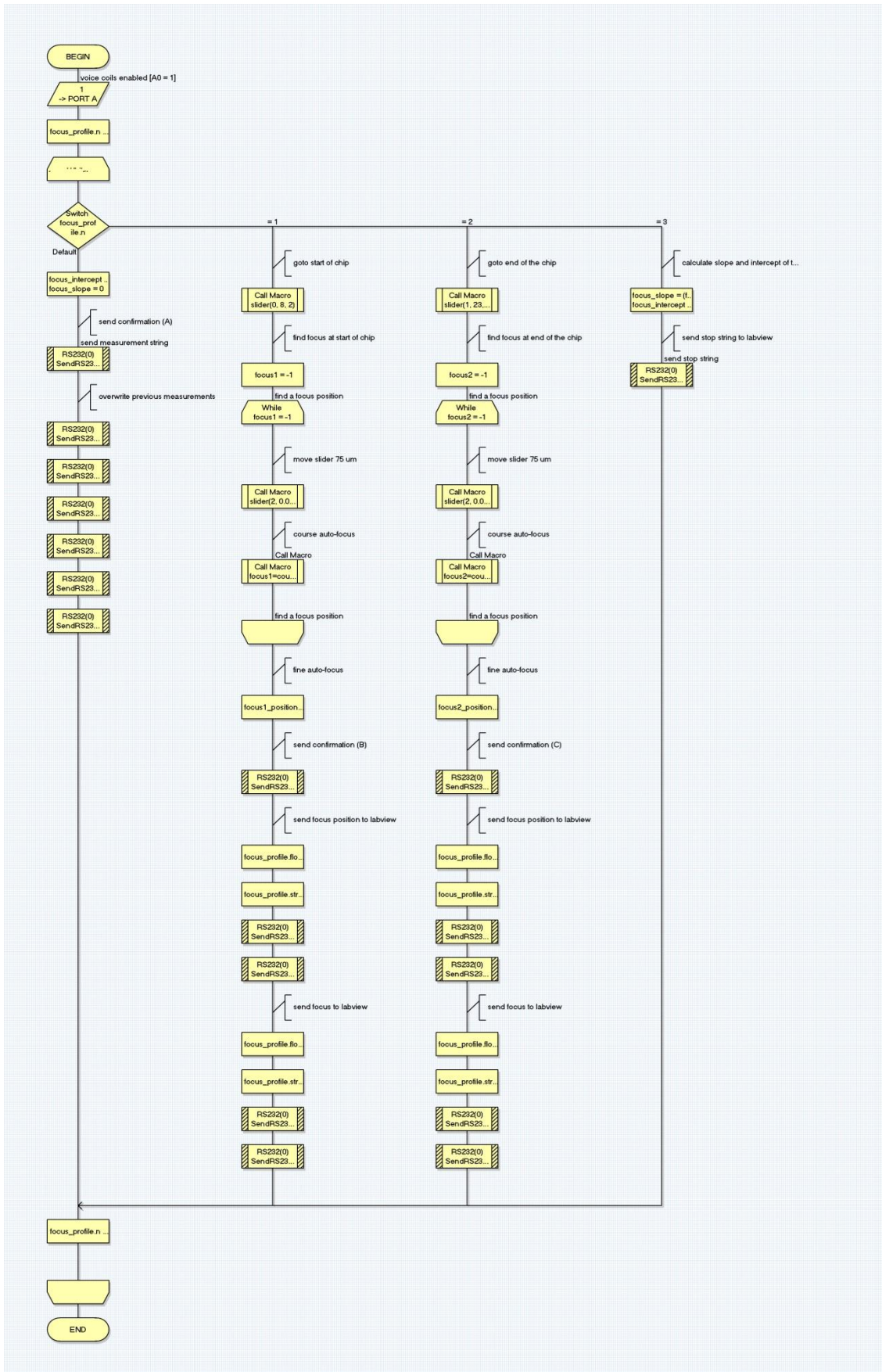


Figure 75 focus profile



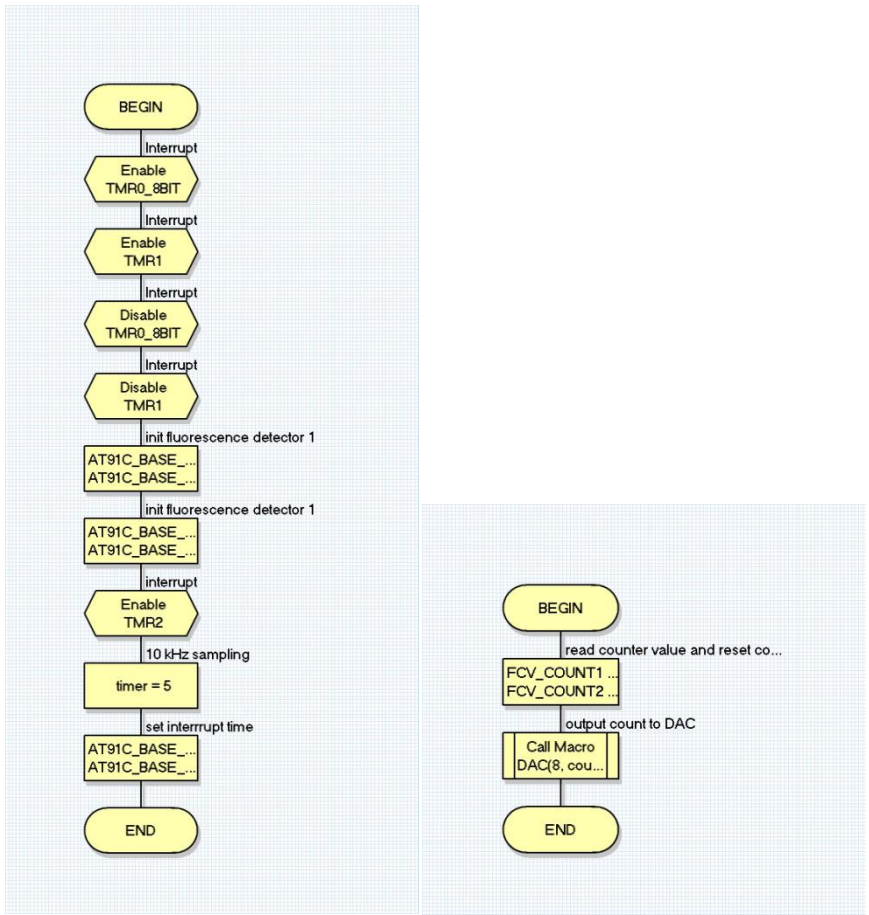


Figure 77 MPPC (left), MPPC interrupt (right)

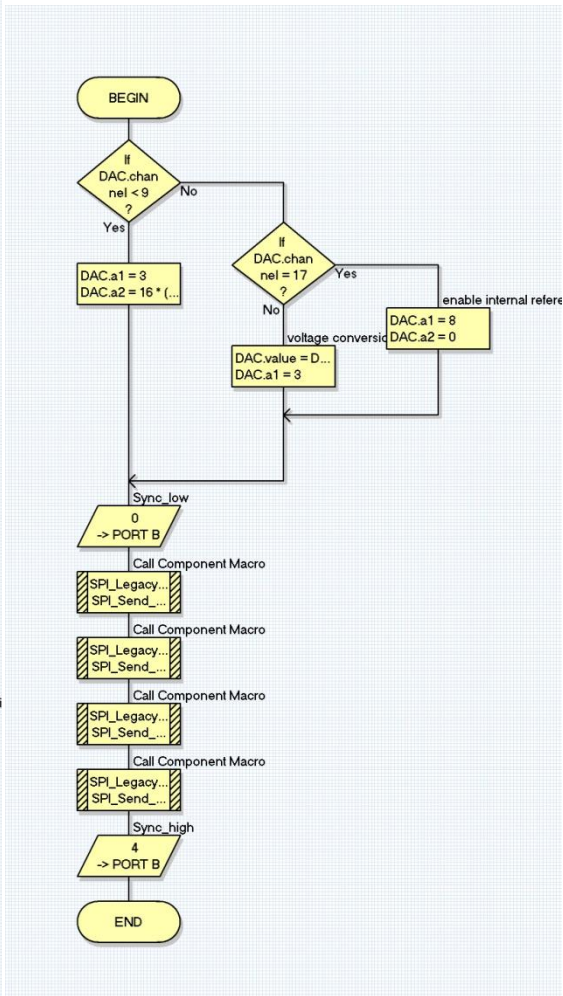
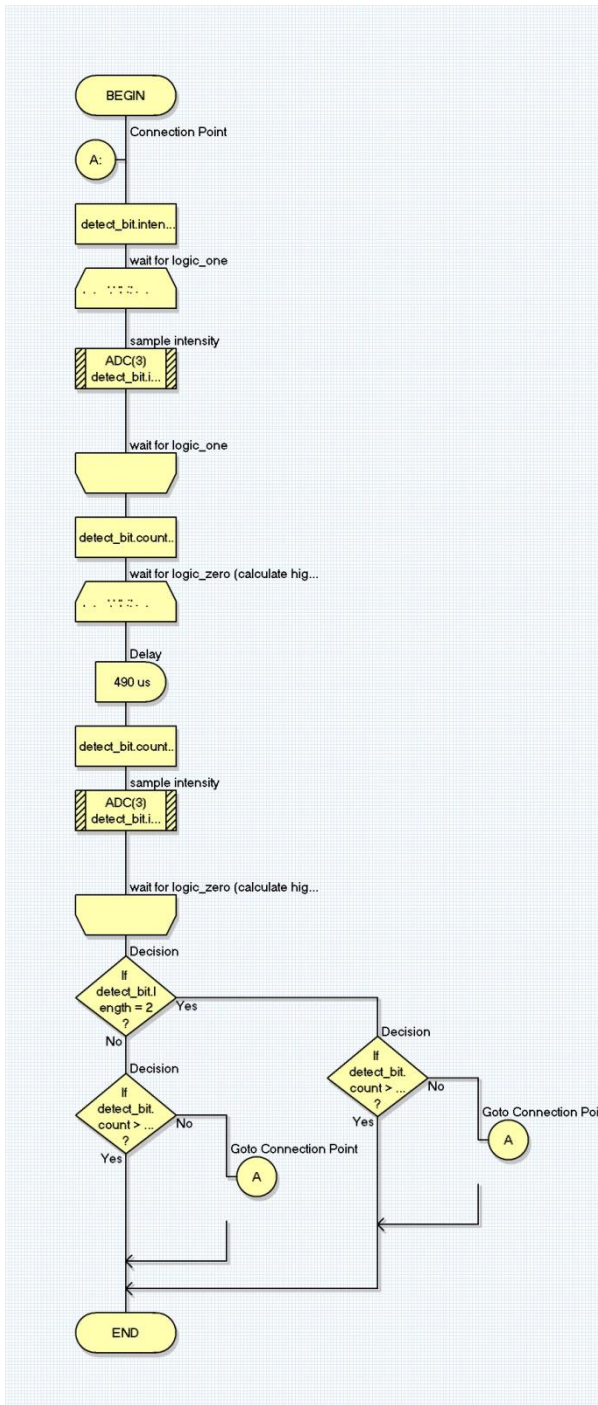


Figure 78 detect bit (left), DAC (right)

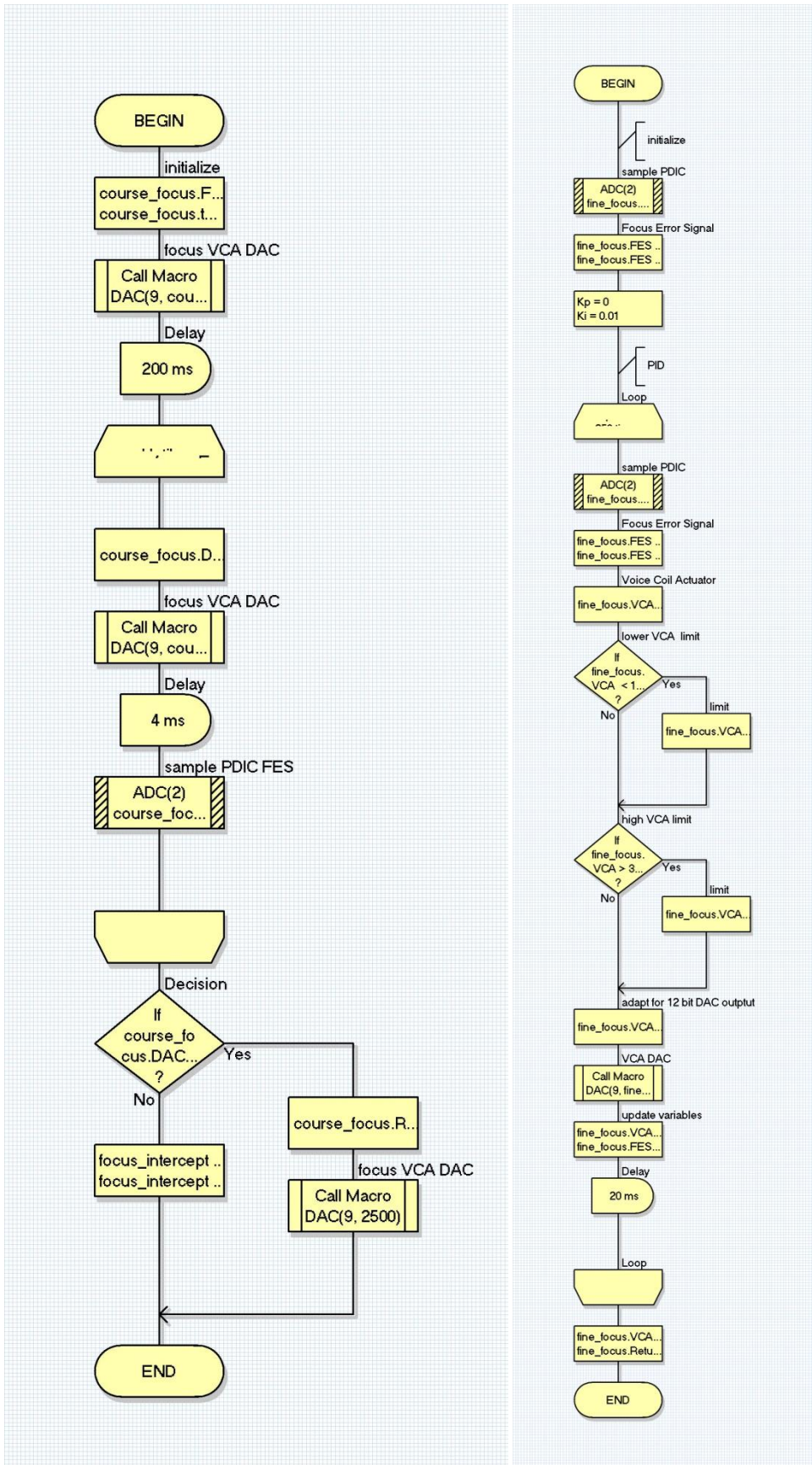


Figure 79 course focus (left), fine focus (right)

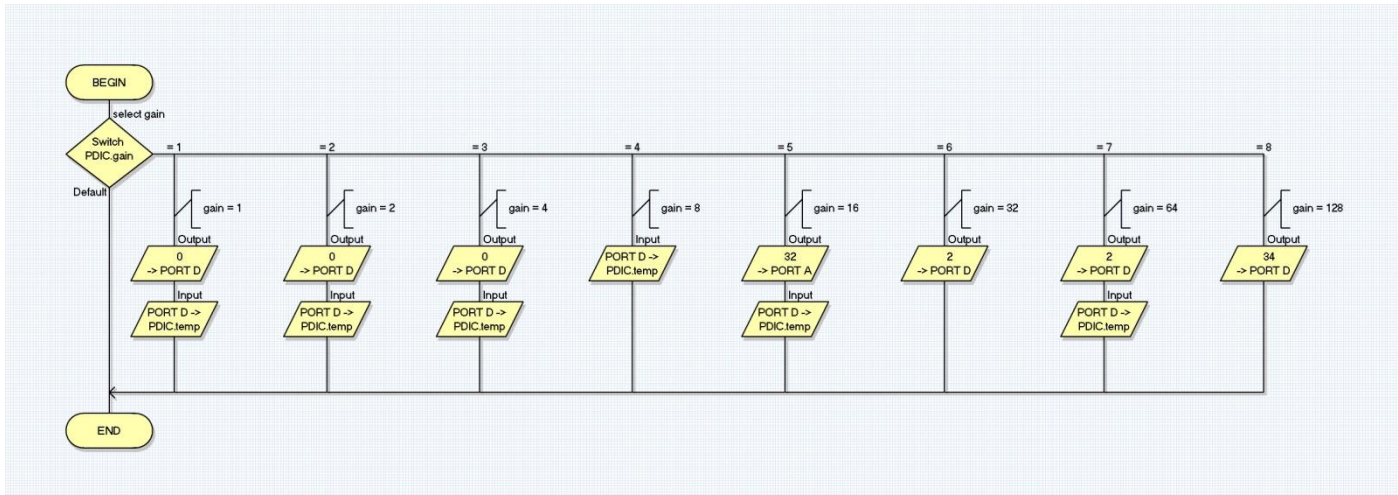


Figure 80 PDIC

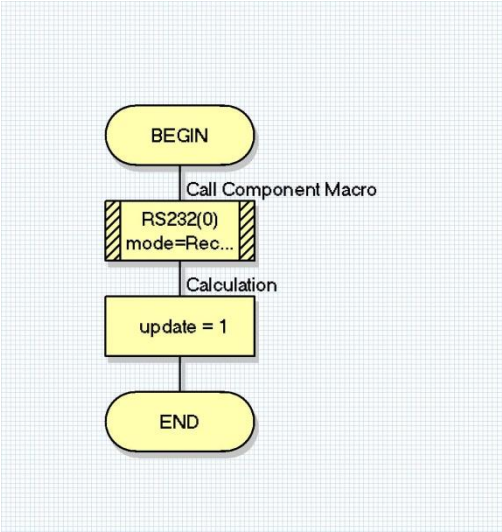
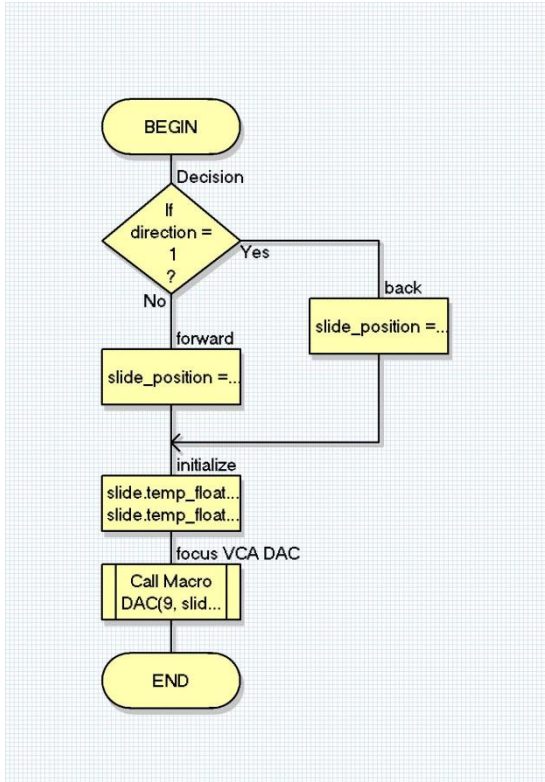


Figure 81 Slide interrupt (left), USART interrupt (right)

## Appendix 5 Wiring

### flatcable optical pickup

pin	device	function	comment
1	VCM	TR-	transverse
2	VCM	T1-	tilt
3	VCM	FO-	focus
4	VCM	FO+	focus
5	VCM	T1+	tilt
6	VCM	TR+	transverse
7	laser	GND	
8	laser	thermistor	
9	laser	9V blue laser supply	
10	laser	5V red/ir laser supply	
11	laser	VREF	reference voltage laser driver 2,5V
12	laser	PDOUT	IV amplifier out, laser power
13	laser	5V laser driver	
14	laser	ENOSC	digital control of RF oscillator
15	laser	SEL2	select IOOUT/enable IC
16	laser	SEL1	select IOOUT/enable IC
17	laser	GND	
18	laser	IR	input current bias 500ohm to ground, laser current
19	laser	GND	
20	wave aberration		
21	wave aberration	GND	
22	wave aberration		
23	wave aberration		
24	wave aberration		
25	wave aberration		
26	position detector	VREF	2.5V reference voltage position detector
27	position detector	GND	
28	position detector	E	
29	position detector	F	
30	position detector	G	
31	position detector	H	
32	position detector	A	
33	position detector	C	
34	position detector	GND	
35	position detector	B	
36	position detector	D	
37	position detector	test	adjustment mode, low(off)?
38	position detector	EN	sleep mode, high(on)
39	position detector	SW0	operating mode
40	position detector	SW1	gain mode
41	position detector	SW2	gain mode
			5V power
42	position detector	VCC	supply
43	position detector	RFN	neg(A+B+C+D)
44	position detector	RFP	pos(A+B+C+D)
45	position detector	GND	

## ECIO\_ARM

pin	function	block	name
1	3,3V output		VDDOUT
2	GND		GND
3	RESET		RESET
4	enable	voice coils	A0/PA24
5	FQ_UD	conductivity	A1/PA26
6	gain0_detector1	conductivity	A2/PA11
7	gain1_detector1	conductivity	A3/PA10
8	DDS-chipselect0	conductivity	A4/PA9
9	DDS-chipselect1	conductivity	A5/PA8
10	TXD0	bluetooth	A6/TXD0
11	RXD0	bluetooth	A7/RXD0
12	CTS	bluetooth	C3/PA7
13	clock	conductivity postition	D0/PA24/TWCK
14	SW1	detector	D1/PA27
15	SiPM 1 output	SiPM	D2/PA28
16	SiPM 2 output	SiPM	D3/PA29
17	data	conductivity postition	D4/PA3/TWD
18	SW2	detector	D5/PA2
19	gain0_detector 2	conductivity	D6/PA1
20	gain1_detector 2	conductivity	D7/PA0
21	TST		TST
22	detector 2 output	conductivity	E3/AD4
23	detector 1 output	conductivity postition	E0/AD5
24	focus output	detector postition	E1/AD6
25	intensity output	detector	E2/AD7
26	GND		GND
27	select2	laser	C0/PA17
28	select1	laser	C1/PA18
29	RTS_bluetooth	bluetooth	C2/PA19
30	TXD1	USB	C6/PA22
31	RXD1	USB	C7/PA21
32	reset	conductivity	B0/PA23
33	enable	motor	B1/PA20
34	sync	DAC	B2/PA31
35	step	motor	B3/PA15
36	SCLK	SPI	D6
37	MOSI	SPI	B5/PA13/MOSI
38	dir	motor	B6/PA25
39	stop	motor	B7/PA12
40	5V input		VDDIN

## cable to DAQ

pin		function
1	unused	
2	GND	GND
3	AO1	transverse-DAQ
4	AI8	transverse-microcontroller
5	GND	GND
6	AI0	focus-microcontroller
7	AO0	focus-DAQ
8	AI1	RFP-RFN
9	AI9	(B+D)-(A+C)
10	GND	GND
		fluorescence 1 (dac channel ext)
11	AI2	
12	AI10	fluorescence 2 (dac channel tilt)
13	GND	GND
14	AI3	impedance 1
15	AI11	impedance 2
16	GND	GND
17	extern	100KHz
18	extern	GND

AI4            A00(focus) excitation  
AI12          A01(transverse) excitation

## DIL switch electrodes

1	electrode3->detector1
2	electrode7->detector1
3	electrode9->detector1
4	electrode10->detector1
5	electrode1->detector2
6	electrode9->detector2
7	
8	sinus2->electrodes2/6
9	sinus2inv->electrodes4/8
10	sinus1->electrode10